DSE - Wind Turbine Wake Visualisation

Design of a system to measure the wake boundaries of a wind turbine and keep track of the wake meandering

DSE Group 1

D. Bakker	4148916	J. Klein	4110692
M. Becker	4152042	L. Koomen	4098730
R. v.d. Brandt	4150562	B. Omarali	4084047
R. Corporaal	4176421	D. Spengler	4062469
J. Janssen	4111516	S. Walraet	4178041

Final Report

Design Synthesis Excercise

TU Delft Delft University of Technology

Aerospace Engineering

July 1, 2014

Summary

This report is the final report of the TU Delft's Design Synthesis Exercise's group 1. It presents T-WRAX (Turbine Wake RAdar in X-band)—an X-band radar system to be mounted on a wind turbine to track its wake's boundaries.

The wind energy market is growing and more wind farms are expected to be built in the future. Wind turbines located inside wind farms influence each other: If a wind turbine is located inside the wake of another turbine upstream, it may experience fatigue loads due to asymmetric loading, reducing its lifetime. Furthermore, it experiences lower wind speeds which lowers its efficiency. Additionally, wakes are not travelling in a straight line but meander. This behaviour is not well understood yet and being able to track meandering boundaries of a wake could help in improving wind farm efficiency in the future. Other solutions for this purpose, such as Laser Imaging Detection And Ranging (LIDAR) and Sonic Detection And Ranging (SODAR), already exist but are either limited to certain operational conditions or are very expensive. The requirements set for the T-WRAX system are that it shall track wind turbine wake boundaries with an accuracy of 1 m, provide a spatial resolution of 10 m and a range of 500 m. The wind speed to be measured shall be at least up to 25 m/s. The continuous operation time shall be at least 12 hours and no modifications shall be made to the wind turbine. Furthermore, use of LIDAR or SODAR technology is not allowed.

In order to design the radar system, a reference wind turbine—the Vestas *V80-2.0 MW*—with a hub height of 70 m and a rotor diameter of 80 m is chosen. The wake is assumed to expand from those 80 m to 160 m and meander to each side by 40 m. The boundary of the wake is defined to be the point where the velocity inside the wake is 95 % of the free-stream velocity.

The work that was performed prior to this report is summarised: several other measurement techniques were considered and used to work out initial design concepts. These were: two designs using aerial devices carrying anemometers located inside the wake, acoustic tomography, radar and smoke imaging—the radar design was chosen after a trade-off.

This initial design was to perform measurements of clear air turbulence, without the need for precipitation like a conventional weather radar. However, after more research, it is concluded that this is not possible for the intended application scenario. Other, comparable, radar systems are the Texas Tech University Ka-band (TTUKa), IRCTR Drizzle Radar (IDRA) and Polarimetric Agile Radar in S- And X-band (PARSAX) systems. Analysing these, it is concluded that an X-band radar system can meet the design requirements.

The resulting design is an X-band radar that uses a Frequency Modulated Continuous Wave (FMCW) signal with a sawtooth sweep from 10 to 10.5 GHz, transmitting power of 50 W and requires at least light fog, equivalent to a reflectivity factor of -28 dBZ, in order to take measurements. The system uses two antennas, one transmitter and one receiver, is expected to have a mass of about 130 kg and a diameter and height of 1.8 m and 3 m, respectively. It has a range of 520 m, spatial resolution of 3.3 m and a temporal resolution of 4 s. Its power consumption is estimated at 1.9 kW. The design is divided into a mechanical, electronics and data processing subsystem. The electronics subsystem is planned to include a power supply connecting to the turbine which has yet to be designed.

An operations and logistics plan suggests how to transport, install and operate the system as well as how to dispose of it at the end of its lifetime. Various options for transporting the system up to the turbine's nacelle are still to be decided on but it is shown that it could be lifted up to the nacelle using a cable system and mounted afterwards. At the end of its lifetime, metal components can be recycled and a method to recycle the radome's wall material is currently in development.

A simulation program written by the authors models the applied theory. The Larsen model is used to model the flow of a static wake which is measured. The simulation shows that, in theory, the wake boundaries can be determined with reasonable accuracy with a range of up to 520 m.

A verification and validation procedure suggests that the system should perform measurements under known conditions and furthermore compare measurement data with proven technology like a LIDAR

system.

The system meets most of the requirements stated except for the requirements on having a continuous operation time of 12 hours, an accuracy of 1 m, not to make modifications to a wind turbine and to be recyclable. The operation time depends on the times at which enough precipitation is present. The accuracy is 4 m and must be traded off with other requirements in order to be met. It is decided with the customer of the system that modifications to the turbine may be made. The recyclability requirement is partially met: electronic components that cannot be recycled will at least be Restriction of Hazardous Substances Directive (RoHS) compliant.

A sensitivity analysis shows that the measurement range can be doubled without having to change components of the system. The sampling rate can be increased but has to be traded off with measurement accuracy, and vice versa. The spatial resolution is better than the required 10 m and can be improved further by lowering the measurement range and accepting more noisy, that is less accurate, data. Higher wind speeds can be measured without problems but they are not expected to be much higher than the designed 25 m/s. A sensitivity analysis of the measurement environment shows that suitable precipitation for measurements is present for about 11 % of the time throughout the year in the Netherlands. Favourable locations for measurements are places with a humid climate. Although larger raindrops are assumed to follow the flow less accurately, they are still assumed to provide accurate information about the wake boundary's location.

A risk analysis shows that the operation of the system has a low risk overall but wind turbine operators may not agree to the currently proposed mounting system. A cost analysis of the system estimates a prototype production cost to be about €25,000.

A plan for future design development suggests that the design finalised and improved by undergoing several iterations. Aspects that still have to be designed are a power supply, software to analyse the measurement data and detailed connections for the mechanical subsystem. The production methods should also be determined.

The system is intended to be mounted on different wind turbines and work under varying configurations. These configurations, as well as the logistics for mounting the system on different turbines, must be developed.

The system itself is not fully recyclable but this is considered unavoidable for a radar device. The operation is assumed to be sustainable since it produces no pollution, and because it is expected to contribute to sustainable development.

In conclusion, the T-WRAX system is deemed feasible for detecting wake boundaries, albeit with some limitations. Radar is currently overlooked for this purpose but the work so far has shown that it is possible and may become more popular in the future, given more research of the concept. The designed system itself will require further development.

Acknowledgements

This DSE final report is now finished, but this wouldn't have been possible without the advice and guidance we received during this project. We would like to thank our tutor, Mr. Bierbooms, for taking the time to guide us thoroughly and give us feedback at every phase of the project. We thank our coaches, Mladen and Jinglang for their tips, advice and critical view on our work. Mr. Schepers, we thank you for your professional insight and practical advice during this project. We would also like to thank Dr. Krasnov for helping us out with the issues we encountered during the design of the radar system, without your thorough explanations and advise it wouldn't have been possible for us to learn how to design a radar system and actually design one within three weeks.

Contents

Summary ii

Acknowledgements iv

List of Abbreviations ix

List of Symbols xi

List of Figures xiii

List of Tables xv

1 Introduction 1

2 Project Motivation and Analysis 2
- 2.1 Project Motivation . . . 2
- 2.2 Analysis of Initial Requirements . . . 2
- 2.3 Reference Frame . . . 3
- 2.4 Reference Wind Turbine . . . 4
- 2.5 Reference Wake . . . 4
- 2.6 Wake Boundary Definition . . . 5

3 Previous Work 6
- 3.1 Measurement Techniques Study . . . 6
- 3.2 Initial Design Concepts . . . 8
- 3.3 Trade-off . . . 10
  - 3.3.1 Trade Method Rationale . . . 10
  - 3.3.2 Trade-off Criteria and Results . . . 11
- 3.4 Initial Radar Design . . . 12

4 Literature Review 15
- 4.1 Wind Turbine Principles . . . 15
  - 4.1.1 Wind Turbine Working Principles . . . 15
  - 4.1.2 Wind Turbine Wakes . . . 15
  - 4.1.3 Wake Meandering . . . 15
  - 4.1.4 Relevance . . . 15
- 4.2 Radar Systems . . . 16
  - 4.2.1 General Principles . . . 16
  - 4.2.2 Differences for Weather Radars . . . 17
  - 4.2.3 Clear Air Turbulence Measurements . . . 18
- 4.3 Similar Applications and Experiences . . . 19
  - 4.3.1 TTUKa Radar . . . 19
  - 4.3.2 PARSAX . . . 21
  - 4.3.3 IDRA . . . 22

5 System Specifications **24**
5.1 Design Process & N^2-Chart . . . 24
5.2 Functional Diagrams . . . 25
5.3 Sizing Equations . . . 26
5.3.1 Received Power . . . 26
5.3.2 Antenna Gain and Beamwidth . . . 27
5.3.3 Signal to Noise Ratio . . . 27
5.3.4 Antenna Rotation . . . 27
5.3.5 Velocity Resolution . . . 28
5.3.6 Number of Measurements . . . 28
5.3.7 Range Resolution . . . 28
5.3.8 Tangential Resolution . . . 29
5.3.9 Distance Frequency Shift . . . 29
5.4 Sizing Results . . . 29
5.4.1 Fixed Characteristics . . . 30
5.4.2 Variable Characteristics . . . 31
5.4.3 Performance Estimation . . . 31
5.5 Antenna Design . . . 32

6 Mechanical Subsystem Specifications **33**
6.1 Payload Overview . . . 33
6.2 Antenna Rotation and Positioner . . . 33
6.2.1 Commercial Available Positioners . . . 34
6.2.2 Torque Calculation . . . 34
6.3 Wind Turbine Tower Vibration . . . 36
6.4 Aerodynamics . . . 36
6.5 Radome Wall . . . 37
6.6 Mounting . . . 38
6.6.1 Influencing Factors . . . 38
6.6.2 Installation Design Options . . . 39
6.7 Structures . . . 40
6.7.1 Structural Design and Dimensions . . . 40
6.7.2 Stability . . . 42

7 Electronics Subsystem Specifications **45**
7.1 System Overview . . . 45
7.2 System Components . . . 45
7.2.1 Control Processor . . . 45
7.2.2 VCO . . . 46
7.2.3 Power Divider . . . 46
7.2.4 Amplifier . . . 47
7.2.5 Power Attenuator . . . 47
7.2.6 LNA . . . 47
7.2.7 I/Q Demodulator . . . 47
7.2.8 Low-pass Filters . . . 48
7.2.9 Data Acquisition . . . 48
7.2.10 Antenna Rotation . . . 48
7.2.11 Weather Conditions Determination . . . 49
7.2.12 Power Management . . . 49
7.2.13 Data Processing and Storage . . . 49
7.3 Subsystem Verification . . . 49

8 Data Processing Subsystem Specifications **51**
8.1 Signal Characteristics . . . 51
8.2 Quadrature Deramping . . . 52
8.3 Low-pass Filter . . . 53
8.4 Windowing . . . 53
8.5 Double Fast Fourier Transform . . . 55
8.5.1 First Fourier Transform . . . 55
8.5.2 Second Fourier Transform . . . 57
8.6 Range and Radial Velocity Determination . . . 57
8.7 Clutter Suppression . . . 57
8.8 Smoothing . . . 58
8.9 Noise Clipping . . . 59
8.10 Wake Boundary Determination . . . 60
8.11 Subsystem Verification . . . 60
8.12 Computational Cost and Data Storage Estimation . . . 61

9 Operations and Logistics **63**
9.1 Operations and Logistics Overview . . . 63
9.2 Operations and Logistics Procedures . . . 63

10 Simulation **66**
10.1 Simulation Operations . . . 66
10.2 Verification . . . 68
10.3 Results . . . 71
10.4 Discussion . . . 71

11 System Evaluation **75**
11.1 System Verification . . . 75
11.2 System Validation . . . 75
11.3 Compliance Matrix . . . 75
11.4 Sensitivity Analysis . . . 77
11.5 Environmental Sensitivity . . . 79
11.5.1 Onshore . . . 79
11.5.2 Offshore . . . 79
11.5.3 Other Geographical Locations . . . 79
11.5.4 Precipitation Measurements Validity . . . 79
11.6 Risk Analysis . . . 80

12 Economic analysis **83**
12.1 Cost Analysis . . . 83
12.1.1 Radar Dishes . . . 83
12.1.2 Mechanical Subsystem . . . 83
12.1.3 Electronics Subsystem . . . 83
12.1.4 Data Processing Subsystem . . . 84
12.1.5 System Operation . . . 84
12.2 Existing Market . . . 84

13 Future Design Development and Integration **86**
13.1 Post-DSE Design and Development Logic . . . 86
13.1.1 Finalise Detailed Design . . . 86
13.1.2 Acquire Materials & Produce System . . . 89
13.1.3 Case-specific Configuration . . . 90
13.1.4 Customise Logistics . . . 91
13.1.5 Operate System . . . 91
13.2 Gantt Chart . . . 91
13.3 Sustainable Strategy . . . 91

13.3.1 Sustainability in Production 91
13.3.2 Sustainability in Operation 92
13.3.3 Contribution to Sustainability 92
13.4 Recommendations 92
13.4.1 Electronic Design Recommendations 92
13.4.2 Mechanical Design Recommendations 92
13.4.3 Data Processing Recommendations 93

14 Conclusion **94**

Bibliography **95**

Appendix A Post DSE Gantt Chart **100**

Appendix B Design Specifications Summary **102**

List of Abbreviations

ABL Atmospheric Boundary Layer. 36

ADC Analog to Digital Converter. 48

ALTAS Autonomous Lighter Than Air System. 9

AZ Azimuth. 34

BOS Background Oriented Schlieren. 6

CESAR Cabauw Experimental Site for Atmospheric Research. 22

CFD Computational Fluid Dynamics. 2, 36, 88, 89

CW Continuous Wave. 17, 21, 22

DARR Delft Atmospheric Research Radar. 21

DOT Design Option Tree. xiii, 8, 9, 38, 39

DSE Design Synthesis Exercise. 2, 33, 75, 86, 88, 91

ECN Energieonderzoek Centrum Nederland. 76

EL Elevation. 34

FEM Finite Element Model. 40, 41, 89

FFT Fast Fourier Transform. xiii, 28, 29, 51, 53–57, 60–62, 68–70, 88

FMCW Frequency Modulated Continuous Wave. ii, xiii, 9, 13, 14, 17, 22, 26–31, 46, 51, 52, 75, 78, 80, 92

GPS Global Positioning System. 10

GS Ground Station. 9

HGS Helikite with Ground Station. 8, 9, 11, 12

HPBW Half Power Beamwidth. 27

IDRA IRCTR Drizzle Radar. ii, 22, 51

IRCTR International Research Centre for Telecommunications and Radar. 22

LIDAR Laser Imaging Detection And Ranging. ii, 2, 3, 9, 75, 84, 85, 94

LNA Low Noise Amplifier. 45, 47, 50, 84

NP Nylon Phenolic. 37, 38

NWI National Wind Institute. 20

OEM Original Equipment Manufacturer. 38, 81, 93

PARSAX Polarimetric Agile Radar in S- And X-band. ii, xiii, 21

PCB Printed Circuit Board. 89

PD&D Project Design & Development. 86, 91

PLL Phase-locked Loop. 46

PPP Precise Point Positioning. 10

RMS Root Mean Square. 48

RoHS Restriction of Hazardous Substances Directive. iii, 76, 91

SNR Signal to Noise Ratio. 27, 30, 31

SODAR Sonic Detection And Ranging. ii, 2, 3, 7, 9, 84, 85, 94

T-WRAX Turbine Wake RAdar in X-band. ii, iii, xiii, xv, 1, 14, 19, 21, 24–26, 30, 31, 46, 51, 53, 75, 76, 83, 91, 102

TTU Texas Tech University. 19

TTUKa Texas Tech University Ka-band. ii, xiii, 8, 20, 21, 78, 84, 85

UAV Unmanned Aerial Vehicle. 8–12

VCO Voltage Controlled Oscillator. 45, 46, 49, 78, 84, 88

List of Symbols

- A — Area
- A — Amplitude
- B — Bandwidth
- C_n^2 — Refractive index structure constant
- C_t — Thrust coefficient
- D — Rotor diameter
- D — Precipitation diameter
- D — Drag
- F — Noise factor
- F — Force
- G — Gain
- G_r — Receiver gain
- G_t — Transmitter gain
- H — Hub height
- I — Moment of inertia
- Ia — Turbulence intensity
- K — Scattering capability constant
- K — Number of samples
- K_{atd} — Conversion constant
- L — Loss
- L — Offset length
- N — Number of chirps
- P — Power
- P_n — Noise power
- P_r — Received power
- P_t — Transmitted power
- R — Resistance
- R — (Measurement) Range
- ΔR — Range resolution
- ΔR_t — Tangential range resolution
- R_f — Flux Richardson number
- T — Torque
- T — Time
- T_c — Chirp time
- T_{target} — Time on target
- U_∞ — Free-stream velocity in x-direction
- V — Velocity
- V_∞ — Free-stream velocity
- V — Voltage
- V — Volume
- V_c — Unit volume
- W — Weight
- W — Window function
- Z — Reflectivity factor
- a — Acceleration
- c — Speed of light
- c_0 — Speed of light
- d — Distance
- e_A — Antenna efficiency
- f — Frequency
- f_D — Doppler frequency
- f_b — Beat frequency
- f_o — Initial chirp frequency
- f_s — Sampling frequency
- k — Boltzmann constant
- m — Mass
- p — Distance to focal point
- r — Particle radius
- r_0 — Radial distance
- s — Path of a curve
- s_R — Received signal
- s_T — Transmitted signal

- t — Time
- u,v,w — Directions of flow (for example)
- v — Velocity
- v_D — Doppler velocity
- w — Width
- w — Weighting function
- x,y,z — Directions in a Cartesian coordinate system
- α — Rotational acceleration
- ϵ — Energy dissipation rate
- η — Target reflectivity per unit volume
- λ — Wavelength of electromagnetic wave
- ω — Rotational rate
- ϕ — Radar elevation angle
- ϕ — Refractive index gradient
- ρ — Density
- σ — Radar cross-section of a target
- τ — Pulse time
- τ — Time delay
- θ — Radar azimuth angle
- $\theta_{\frac{1}{2},t}$ — Transmitter half power beamwidth (also simply referred to as 'beamwidth')
- ξ — Phase difference

List of Figures

2.1 Definition of the wind turbine coordinate system. . . . 3
2.2 Definition of the wake measurement area. . . . 4

3.1 One measurement in the horizontal plane is sufficient to measure the horizontal velocity vector, assuming that it is aligned with the free-stream velocity. . . . 13
3.2 Even for $|V_y| = 0.1V_x$, the assumption introduces a negligible error. Note that near the wake boundaries, the y-velocity is assumed to be even smaller [13]. . . . 13

4.1 Wake meandering is a term for sweeping movements of the wind turbine wake [25]. . . . 16
4.2 Modelling of a weather radar target filled with water droplets [27]. . . . 17
4.3 Rayleigh, Mie and optical scattering region [27]. . . . 19
4.4 Rayleigh and Mie scattering patterns [31]. . . . 19
4.5 One of the Ka-band radars on field [33]. . . . 20
4.6 Wake meandering measured using the TTUKa radar system [35]. . . . 20
4.7 Two examples of a TTUKa doppler radar wake measurement [34]. . . . 20
4.8 Layout of the PARSAX radar on top of the Faculty of Electrical Engineering, Mathematics and Computer Science [37]. . . . 21
4.9 The IDRA system on top of the Cabauw meteorological tower [39]. . . . 22
4.10 IDRA measurement data mapped over a satellite image of the surrounding area [40]. . . . 23

5.1 N^2-Chart for the T-WRAX design process. . . . 24
5.2 Functional flow diagram of the T-WRAX. . . . 25
5.3 Functional breakdown diagram of T-WRAX. . . . 26
5.4 Working principle of the offset gregorian antenna [47]. . . . 32

6.1 Parabola antenna dish geometry. . . . 35
6.2 Vestas V80 [2], the radiator on top of the back of the nacelle obstructs the view of the radar. 38
6.3 DOT of the radar mounting options. . . . 39
6.4 Radome layout schematics. . . . 40
6.5 Forces at the rope/radome connection. . . . 41
6.6 Side view of reaction forces on the legs of the system. . . . 42
6.7 Side view of reaction forces on the legs of the radar mounted on top of the nacelle. . . . 43

7.1 Block diagram of the T-WRAX electronic subsystem. . . . 46

8.1 Data processing algorithm of the T-WRAX system. . . . 51
8.2 A sawtooth wave modulation as used for this FMCW radar. . . . 52
8.3 Magnitude response of the low-pass filter. . . . 54
8.4 Rectangular and Blackmann-Harris window and their corresponding Fourier transform for a windowed sinusoid [73]. . . . 56
8.5 Range-Doppler double FFT processing. . . . 56
8.6 Example of a Doppler spectrum that has been smoothed. . . . 59

10.1 Flow chart of the simulation program. . . . 66
10.2 Spectrogram of the transmitted signal. . . . 67
10.3 Simulation grid used in the simulation. . . . 67
10.4 Example of a Gaussian regression. . . . 68
10.5 Range-speed response pattern. . . . 69
10.6 Radar sweep velocity response. . . . 70

10.7 Results for case 1: $U_\infty = 15$ m/s, $Ct = 0.5$, $Ia = 0.05$, $D = 80$ m, $H = 70$ m. 72
10.8 Results for case 2: $U_\infty = 15$ m/s, $C_t = 0.7$, $Ia = 0.06$, $D = 40$ m, $H = 70$ m. 73
10.9 Wake boundary position case 1. 74
10.10Wake boundary position case 2. 74

13.1 Project design and development logic (detailed design). 87
13.2 Project design and development logic (case specific configuration). 87
13.3 Post-DSE design logic for the electronic system. 88
13.4 Post-DSE work guideline for mechanical subsystem. 89

A.1 Post DSE Gantt chart part 1. 100
A.2 Post DSE Gantt chart part 2. 101

List of Tables

2.1 Top level data requirements. 2

3.1 Mid-term trade-off criteria and weights. 11
3.2 Trade summary table for the primary trade criteria. 12
3.3 Trade summary table for the secondary trade criteria. 12
3.4 Initial radar system design compared with the detailed design, T-WRAX. 14

5.1 Fixed characteristics for T-WRAX. 30
5.2 Variable characteristics for T-WRAX. 31
5.3 T-WRAX performance estimation. 31

6.1 Positioner requirements based on selected antenna. 33
6.2 List of commercial available positioners and their performance. 34
6.3 Results of the moment of inertia estimation. 35
6.4 Relevant material properties [56]. 38
6.5 Mechanical subsystem specifications. 41

8.1 Characteristics of different window functions taken from [39]. 55

11.1 Compliance matrix of the requirements for the T-WRAX system. 76
11.2 Risk Map for the radar system design concept. 82

12.1 Cost-breakdown of the electronics subsystem components. 84

1 | Introduction

Wind energy is a growing market. In the coming years, many new wind parks will be built globally of which a large number will be built offshore. The first wind turbine in a wind farm is subjected to the undisturbed wind flow. If, however, multiple wind turbines are placed together in a wind farm, the turbine upstream will affect the ones downstream. The affected airflow behind a wind turbine is called a wake. In the wake the mean flow velocity is lower than in the surrounding air and the turbulence intensity is higher. If another wind turbine is then placed somewhere in the path of this wake, its efficiency will be lower and the loads acting on it will be higher, leading to an increase in fatigue. For this reason it is important to be able to predict the behaviour of this wake, to optimise the placement of wind turbines in wind farms. To be able to make a good model of the wake behaviour, it is necessary to measure the actual behaviour of wind turbine wakes.

In this report, the design of Turbine Wake RAdar in X-band (T-WRAX), a radar system, is described, that will be used to measure the behaviour of the wind turbine wake. The purpose of this project is to track the meandering of wake boundaries of a wind turbine during a considerable time period at on- and offshore wind farms, using a low-cost, stand-alone, durable and recyclable system. Systems exist already that can perform these measurements, but they are either limited in some way, for example with a low measurement rate, or they are very expensive. In previous work it was concluded that the best method to meet all requirements would be a radar system.

The first chapter in this report describes the problem at hand in more detail and states the project motivation. Secondly a summary is given of the system selection process and trade-off from previous work. Next literature on radar in general and weather radar specifically will be discussed. Then the preliminary sizing of the radar system is described, using simplified equations for the radar system performance. After this preliminary design the mechanical and electronic subsystems are designed in further detail. The processing of the measured radar signal will also be described. After the design of the radar system the usage of the radar system is discussed in further detail. First, the operations and logistics of the complete system are described. Next an evaluation of the performance, risks, sensitivities, verification and validation of the proposed design is given. After that an economic analysis of the current market and the place of the radar system within this market is performed, and lastly a description of the remaining work on the design and construction of the radar system and recommendations for further research are given. Additionally, appendix A presents Gantt charts of the planned procedures beyond the work of this report and appendix B gives an overview of the most important design specifications as well as a technical drawing of the designed system.

2 | Project Motivation and Analysis

This chapter is concerned with defining the problem that is to be solved, and under which requirements it must be done. The motivation for the project is explained in section 2.1. The analysis of initial requirements is given in section 2.2. The reference frame and wind turbine are presented in sections 2.3 and 2.4 respectively. Finally the wake boundary definition is discussed in section 2.6.

2.1 Project Motivation

This project has been undertaken by Design Synthesis Exercise (DSE) group 1, one of 22 groups, as a final project for the Bachelor's in Aerospace Engineering of TU Delft. The purpose of the DSE is to be 'an exercise in which students are given the opportunity to obtain design experience in a multidisciplinary design project' [1]. It was started on April 22nd 2014, and spans 11 weeks under the supervision of Dr. ir. Wim Bierbooms.

The objective of this project is to design a system to measure the wake boundaries of a wind turbine and to keep track of the wake meandering. The system could be a competitive alternative to the more commonly used wake visualisation devices, Laser Imaging Detection And Ranging (LIDAR) and Sonic Detection And Ranging (SODAR), which are expensive. Another one of its purposes would be to provide validation data of Computational Fluid Dynamics (CFD) models of wind turbine wakes and wake meandering. The group's intention is to achieve high-quality measurements, while keeping the system's costs as low as possible.

2.2 Analysis of Initial Requirements

The project tutor Dr. ir. Wim Bierbooms has laid out a series of top level requirements for the measurement device. These were the initial requirements given at the start of the project, before the form of the device was known in any way. These requirements cover data quality and quantity, operational conditions and others. This list of requirements was the initial target for the measurement device. As it took its final form, it was determined that the device was constrained in a way that prevented some requirements from being met. This is explained and justified later in the report in the requirements compliance matrix in section 11.3, after the design has been presented and evaluated.

Firstly, the requirements of the measurements themselves are presented. The wake boundary locations should be measured on rotor hub level. The measurements have to be of a certain quality, and be collected at a minimum amount of locations at a certain rate. Note that the range requirement is for behind the wind turbine facing downstream.

Table 2.1: Top level data requirements.

Criterion	**Requirement**
Range [m]	Up to 500
Spatial Resolution [m]	10
Sampling Rate [Hz]	0.25
Operation time	Minimum 12 hours
Accuracy [m]	1
Maximum data loss [%]	5

The data was initially required to be collected under certain operating conditions and constraints. These are:

- The device should be able to operate on both onshore and offshore wind turbines.
- The device should operate in a free-stream velocity range of 4 m/s to 25 m/s.
- The device should preferably be mobile and applicable to other wind turbines or wind farms.
- The device is constrained to not include modifications to or constructions on the wind turbine.
- The device should have a lifetime of 10 years.

Furthermore, there are general requirements for the device:

- The device should be recyclable.
- The device should be cheap, however the maximum allowable cost is negotiable.
- LIDAR and SODAR should be excluded from this project since they are already developed and are the competitors

2.3 Reference Frame

In order to maintain consistency, an axis system for the wind turbine's wake is defined here. The axis system used throughout this report is a right-handed Cartesian coordinate system, with its origin at the centre of the wind turbine rotor, as shown in figure 2.1. The x-axis points downstream and parallel to the rotor axis, the y-axis points to the right when looking from the upwind direction and parallel to the ground plane, and the z-axis points to the ground and parallel to the turbine tower.

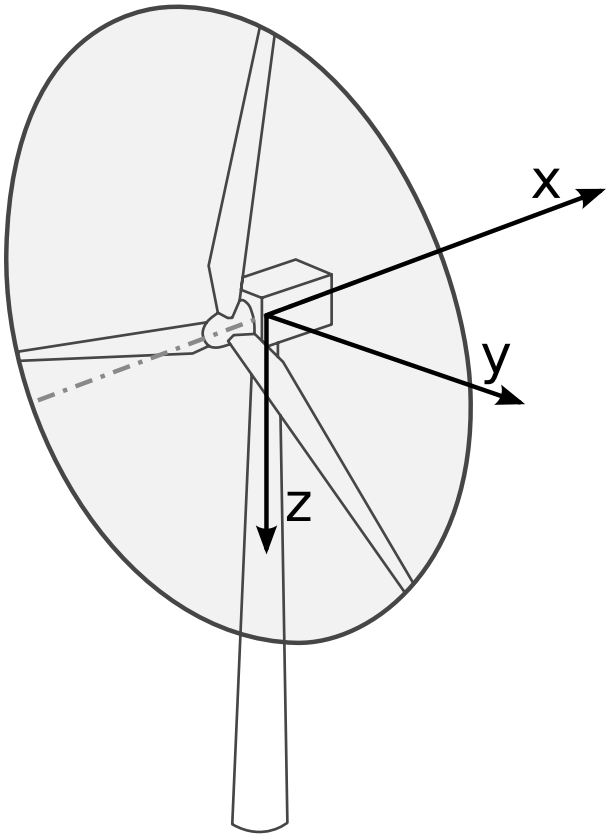

Figure 2.1: Definition of the wind turbine coordinate system.

2.4 Reference Wind Turbine

The wind turbine used for reference in this report is the *V80-2.0 MW* by Vestas. This model has the following specifications [2]:

- Rated power — 2 MW
- Cut-in wind speed — 4 m/s
- Rated wind speed — 14 m/s
- Cut-out wind speed — 25 m/s
- Rotor diameter — 80 m
- Hub height — 70 m
- Nacelle width — 3.5 m
- Nacelle height without the radiator — 4 m
- Radiator height — 1.4 m

2.5 Reference Wake

To track the wake boundary, a measurement area has been defined, which encloses the theoretical wake which is elaborated on in section 4.1. The area is situated on a plane located at hub height (70 m), parallel to the ground, and is further defined in figure 2.2. This reference wake area is used to define the limits which the device must be able to reach in order to find the meandering boundaries.

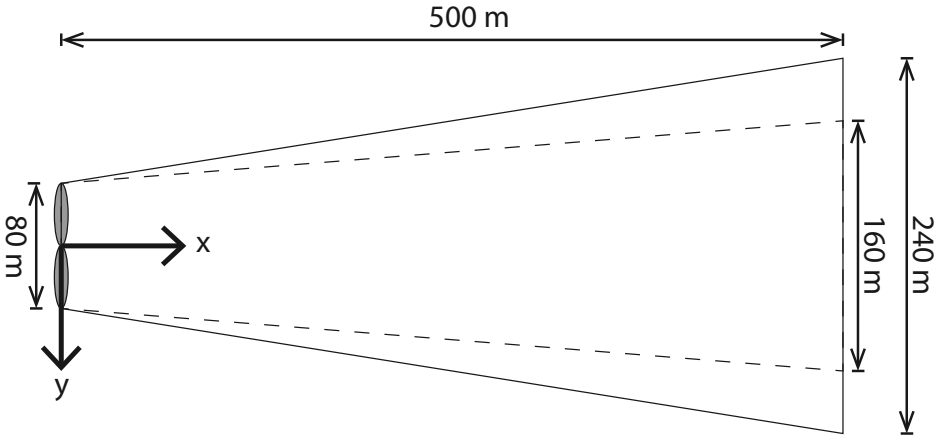

Figure 2.2: Definition of the wake measurement area.

The inner boundaries are the boundaries of the wake without any meandering with the wake expanding from 80 m (1 rotor diameters, or $1D$) to 160 m ($2D$) at the end of the measurement area, in all directions since it has a circular cross-section.

The outer boundaries enclose the meandering wake, with an increased area width of 40 m ($0.5D$) on each side at 500 m downstream. This defines the theoretical measuring area and is used throughout the report. Note that this is based on the assumption that the wake moves exactly in x-direction. In reality, the wind is always at an angle to the x-axis and forces the wake to move slightly sideways.

The radar device will not search the entirety of the wake measurement area, but its swath does at least cover the wake boundaries at rotor hub height.

2.6 Wake Boundary Definition

As a mass of free-stream air moves through a wind turbine, it has a certain velocity and therefore contains kinetic energy. Since part of this energy is mechanically extracted by the rotors, the energy level of the flow is lower, which results in a velocity deficit behind the turbine. The rotation of the blades also induces a rotational motion within the wake behind the rotor, whereas the pressure differences near the blade tip cause additional vortices to be formed there [3]. This causes an increased turbulence intensity behind the turbine with respect to the free-stream flow turbulence intensity [3].

The wind turbine wake is defined as the region behind the wind turbine where there is a velocity deficit compared to free-stream velocity. The velocity data collected by the radar device will be used to determine the wake boundaries. To do so, the boundaries are defined as the point where the wake's velocity is 95 % of the free-stream's velocity. This is, in reality, an arbitrary choice, as wake effects diminish downstream and do not have clearly defined boundaries. Due to the boundary becoming less distinct, the magnitude of the velocity deficit does not decrease in a predictable way when approaching the edge of the boundary. The details on finding the wake boundary through the processing of the data is explained later in this report, in section 8.10.

3 | Previous Work

Earlier in the project of visualising the wake of wind turbines, a mid-term report presenting the work completed until that point was made. It is a precursor to this report and its purpose was to perform a preliminary feasibility study on various measurement techniques, form initial design options from feasible measurement techniques and select one in a trade-off. Section 3.1 presents results of the measurement techniques study. The techniques of particle imaging, active acoustic measurement, radar and mechanical measurement were deemed feasible and considered as basis for initial design options which are given in section 3.2. The design trade-off is presented in section 3.3 and finally the initial radar design is presented in section 3.4.

3.1 Measurement Techniques Study

The project was approached by brainstorming for various types of measurement techniques that could be appropriate for locating wind turbine wake boundaries. Their principles were researched and previous applications were studied, so that a statement could be made on the feasibility of the technique. The ones that were deemed to have potential were used for the initial design options. The measurement techniques studied were schlieren and shadowgraph imaging, light scattering, particle imaging, passive and active acoustical techniques, mechanical measurement techniques, mechanical boundary tracking and radar.

Schlieren Imaging

The principle of schlieren imaging is to visualise density variations of a medium using the light that passes through it. Light rays that pass through the turbulent air are refracted and deflected, and a lens setup can image the pattern formed by the light. This is most commonly applied to supersonic flows or flows with large temperature variations. A new schlieren-based system, Background Oriented Schlieren (BOS), has the benefit of being easier to apply on a large scale, and requiring fewer precisely aligned components. However, for a wind turbine, under optimal conditions the amount of refraction caused by the medium is an order of magnitude too small, even for a very sensitive schlieren systems [4]. Therefore, on an unconventional and very large scale, neither traditional schlieren nor BOS were deemed feasible.

Shadowgraphy

Shadowgraphy uses a similar principle as Schlieren imaging, except that the refracted light pattern is projected onto a screen, instead of using a lens setup. The refraction of light will create areas with lower light intensities, and these shadows can be analysed to determine flow information of the medium. Shadowgraphy was found to be even less sensitive than Schlieren, and was also left unconsidered for the initial design options [5].

Light Scattering

The study on the light scattering measurement technique found that it was only conducted on singular points in velocity flows, not on large scales. The principle is to observe light scattered by particles and their movement. The light source can be either natural light or lasers. Besides it only being used on a small scale, the study in the mid-term report also found that a high installation accuracy is required to filter out unwanted light sources [6, 7]. For these two reasons light scattering was deemed unfeasible.

Particle Imaging

Partice imaging has already been established as a flow measurement technique in aerodynamics. Particles, chosen to be neutrally buoyant so that they closely follow the flow, are seeded into a flow and photographed.

Generally pulses from a laser sheet are used to illuminate a specific (cross-sectional) area, which is captured with a camera. Evaluating a series of images can give information about the speed and direction of the flow. This is most commonly applied to small test sections under 1 m^2 in size. Conventional particle imaging is not possible due to short range of lasers, but a study was found demonstrating that it was possible at a range of 7.8 km using natural light [8]. With a sufficient amount of seeded particles, it was deemed that particle imaging of the wake had potential.

Acoustic - Passive

Passive acoustical techniques generally rely on sound produced by the measured object itself. In the mid-term report the technique of conventional beamforming using a microphone array was studied. The time delay between microphones of a sound source can be analysed to determine the source's incidence angle. Eventually more arrays could be used to determine it's 2-D and 3-D location. This technique has been used to visualise powerful airfoil tip vortices, or aircraft wakes, but never wind turbine wakes. Wind turbine wakes have a large range of frequencies which are not well researched, so it was found to be unclear if the boundary would be sufficiently distinguishable from the frequencies of sound emitted from the free-stream. It was deemed highly improbable that wake boundaries could be properly visualised using this technique.

Acoustic - Active

Active acoustic measurement techniques pump the flow with a controlled and known sound. The technique considered is to have a microphone and sound source on opposite ends of the measurement area. The time it takes for a sound with a specific frequency to cover the distance between the two points is measured. Since sound waves travel through fluids at a speed which is the sum of the local speed of sound and the local flow velocity component in the direction of wave propagation, a difference in speed of the medium will result in a difference in the propagation time between the microphone and the sound source [9]. This technique will be able to measure changes in mean velocity and temperature along the path between the receiver and the transmitter. Some error is introduced by variations in local speed of sound, but replacing the transmitter and receiver with a transducer and measuring propagation time in both directions eliminates this. From measurements over multiple ray-paths, post-processing techniques may be used to produce a velocity field. A sufficiently large amount of transducers are required to adequately produce this velocity field, which was determined to be a limiting factor. However, in the literature study a possible solution using acoustic tomography was found in a paper by Rogers et al. [10]

Acoustic - Doppler Effect

A third acoustic technique was studied, analysing the Doppler effect on a transmitted sound signal. SODAR is based on the backscattering of acoustic pulses sent in one or more directions measured by directional microphones on the ground, with three different directions being required in order to obtain a fully three-dimensional velocity profile. When an acoustic pulse emitted meets particles or fluctuations in the refractive index of air, its energy is scattered in all directions, with some of it in the direction of the microphone. However, the measurement volume for SODAR is usually very big compared to other measurement techniques, this is why most SODAR systems are used to measure mean wind rather than for instantaneous measurements. It is also sensitive to misalignment errors, which causes wind speed measurement errors. It was however deemed feasible to be used in an initial design option.

Radar

Radar uses radio waves to detect objects and determine their range, altitude, direction and speed. A transmitter emits pulses of radio- or micro waves in predetermined directions. Any object in their path reflects tiny portions of the waves' energy back to a dish or antenna that is located at the same site as the transmitter. The radar system measures the travel time of the reflected wave from the transmitter to the object and back which, using the travel speed of the wave, can be used to determine the distance to the object. Objects that are moving away or towards the radar system in the radial direction will cause a slight shift in the frequency of the reflected radio waves, this is known as the Doppler effect. Past examples of radar's usage showed that it has been used extensively in atmospheric measurements, and

that the effect of light precipitation and rain was detectable. It was therefore determined that the velocity deficit area of a wind turbine could be measured. An example is a Texas Tech University research project [11], an experiment using a Ka band radar, named the Texas Tech University Ka-band (TTUKa), with a frequency of 38 GHz. This Ka band radar had a high measurement resolution and range of several kilometres. It was very expensive, but since a simpler radar device would be sufficient for measuring at a range of 500 m and in only one plane, radar was deemed a feasible measurement technique.

Mechanical Measurement

Mechanical measurement of the flow was also studied. Several types of anemometers—wind speed sensing instruments—were evaluated and compared. Anemometers measure from within the flow, and only at the point at which they are placed. They can use several different principles to measure: drag on deflection plates, pitot tubes, the cooling effect of airflow on a hot wire and others. It was found that in previous cases, anemometers have been used on weather masts and weather balloons. Experiments had also been conducted using several Unmanned Aerial Vehicles (UAVs) with high mobility carrying multiple anemometers. Special attention should be given to the wind speed range, which affects the feasibility of different UAVs and anemometers. A fleet of cheap and fully autonomous UAVs carrying anemometers could be a feasible option to determine the flow field and with it the wake boundaries. Autopilot software would be required to keep the UAVs at all measurement points behind the turbine, while still following the wake meandering and yawing of the turbine. All of this could be accomplished and therefore result in a feasible option.

Mechanical Boundary

A boundary tracking system employs an idea of using a self stabilising floating device connected to a ground station that uses the velocity gradients at the wake boundary for passive control. The floating part of the system is designed as a helikite, with a helium balloon to keep the device buoyant and hub height at any wind speed, and aerodynamic wings to steer and stabilise the device. When the device moves from the free-stream into the wake boundary it experiences a loss in stream-wise velocity, a negative azimuthal velocity, and a negative radial velocity. With a specialised aerodynamic design, the device can be pushed out of the boundary, whereafter it will attempt to reinsert itself, effectively balancing on the boundary. Movements in $x-$ and z-directions are then controlled by moving the ground station. The disadvantage of the system is that it requires a unit at every designated measurement location, and that production is complicated since every unit must be tailored to a local velocity gradient that varies downstream. This measurement technique is also quite sensitive to tip vortices from the rotors, and atmospheric fluctuations. Therefore the mid-term's literature study determined that some elements of passive boundary tracking may be combined with other measurement techniques, but a passive boundary tracking device seems unfeasible.

3.2 Initial Design Concepts

Five design options were produced in the mid-term report: smoke imaging had been derived from particle imaging, acoustic tomography as a form of active acoustics, radar, and both a Helikite with Ground Station (HGS)- and UAV-based mechanical measurement system. Design Option Trees were created and a form for the system was selected. Each system was then designed in more detail and first-order estimates were made of its specifications. As part of the initial design, the operations and logistics of the system were outlined. An analysis of the potential risks that could affect the system was made and compiled in a risk map. The flexibility of the design solution was analysed by studying how its specifications were affected by changes in the requirements in the sensitivity analysis. A cost analysis gave an estimate of the cost breakdown, and its sustainable impact was taken into account in the sustainable development strategy section of the initial design. The design options will be briefly summarised in this section, the full version can be found in the mid-term report [12].

Mechanical Measurement System - HGS

The design option of an HGS tracks the boundary by measuring the streamwise velocity and following the $0.95V_\infty$ strip of the flow. It consists of a helikite (UAV) and a ground station (Ground Station (GS)) connected by a chord. The UAV mass is 1 kg with 1.5 m wingspan, has a wing surface area of 1.05 m^2 and a balloon volume of 0.4 m^3. The helikite UAV control is done via movement of the GS and chord length. Along with the HGS an alternative installation approach was investigated, which followed from the Design Option Tree (DOT). In contrast to the ground based system, the Autonomous Lighter Than Air System (ALTAS) UAV has to remain in its desired position at the wake boundaries by only using its flight controls and is therefore autonomous. The lighter-than-air UAV carries anemometers and hovers at the wake boundaries.

The main sensitivity issues arise if accuracy and sampling rate requirements become stricter as the system dynamics would have to be reconsidered. Some considerations that were found for this design options sustainability were that the batteries used are potentially harmful and may leak in a crash, and that if a diesel engine is used for propulsion, it would be pollutant. The former can be mitigated by protecting the battery and ensuring that is recoverable, and in the latter case the engine type is not fixed and may also be electrical. The estimated production cost of a single unit is €400. The full system of 100 units costs €40,000. A twelve hour operation of the full system is €4,544.

Mechanical Measurement System - UAV

This design option differed from the HGS design as this system uses 100 fixed-wing UAV units that are flown in a certain trajectory instead of hovering at the boundary location. The mass of a single unit is about 3 kg with a wingspan of 2 m. The UAVs carry anemometers in order to measure the velocity deficit from which the wake boundaries can be deduced. This is accomplished by having measurement segments on which each UAV is moving in y-direction while measuring the x-component of the wake's velocity. As this kind of operation requires more power, all units could periodically fly back to base to recharge/refuel.

This concept was found to be highly dependent on the trajectory, because it influences the range, endurance, accuracy, resolution and measurement frequency. Main sensitivity drawbacks result from a change in resolution requirements as new trajectories have to be designed. Furthermore, the unit can only travel at a certain speed, so there is a limited feasible sampling rate range.

In terms of sustainability the same principles apply as for the HGS. The costs were estimated to be €400 for production and about 4 €/h for operation of one unit, giving an estimated total cost of €44,800 for production and operation of 100 units for 12 hours.

Electromagnetics and Acoustics using the Doppler Effect

Early on in the development of this initial design concept, three different forms of remote sensing using the Doppler effect were considered. These were radar, LIDAR and SODAR, and although LIDAR and SODAR were disallowed as a general requirement in section 2.2, similar devices based on the same principle were considered. It was found early on that radar was the best choice due its high potential for range and accuracy.

The proposed Doppler-based design concept consists of an Frequency Modulated Continuous Wave (FMCW) radar system, placed on top of the wind turbine nacelle. It measures wind velocity in the horizontal hub plane, but only in the radial direction originating at the hub. This was, however, determined to be sufficient to find the locations of the wake boundaries, with an additional assumption that the radial wind velocity component could be used to determine the wind speed in free-stream direction. It was initially thought that the wind velocity field could be measured in all types of weather conditions. The transmitted radio power was calculated to be 30 W, the approximated system weight 100 kg, and the dish diameter 3 m.

Radar was found to be slightly polluting during production and disposal, but due to the small amounts of material used, the environmental impact was determined to be minimal. The environmental effects during the operation of radar are negligible. The costs for the entire system and assembly were estimated to be around €15,000, not including any installation costs and operational losses due to installation.

Acoustic Tomography

An acoustic tomography system consists of 1–3 UAVs flying around the wake, a large amount (50 ± 15) of microphones placed on the ground/sea, and a ground station. The UAV generates sound that is picked up by all microphones and stored on small data storage systems. Post-processing is used to generate an approximate flow-velocity field from the propagation time of the sound waves.

The system appeared to be rather sensitive to errors in the position and velocity data, making it the dominant factor in its accuracy, therefore a specialised Precise Point Positioning (PPP) Global Positioning System (GPS) system is used to obtain position accuracy in the order of centimetres. The microphone arrangement and the flight path of the UAV would have to be thoroughly analysed and optimised because they determine the location and spacing of the measurement points. Furthermore, the frequency of the sound emitted by the UAV was found to have an influence on the amount of atmospheric attenuation and therefore the maximum detection range.

The acoustic tomography design was found to be relatively sustainable due to its modest energy usage and use of recyclable materials, with a long lifetime. The total production cost of the system was approximated to be €22,000 using a state-of-the-art UAV.

Smoke Imaging

The smoke imaging system utilises relatively few elements and is quite straightforward. A smoke machine is placed on the nacelle to seed the wake with particles, which is then photographed by a pair of cameras placed on opposites sides of the wake. Images of the wake captured in rapid succession can be analysed in post-processing to determine its velocity field. This is determined by the changes in light intensity in the images, and from the velocity field the boundaries are found from velocity deficits.

It can scale relatively well with changes in the top-level requirements and may be improved by using cameras at more locations. A better spread in x-direction would improve the resolution and accuracy of the images. Having cameras placed at different heights or at different y-axis positions will capture velocity field components of more planes, due to the changing view angle. This would lead to a better 3-D mapping of all the wake's boundaries. This would come at an increase in production and operation costs, especially for the camera vehicles.

The smoke imaging systems strong point is its simplicity of using particles to make the flow visible, and can be realised using off-the-shelf components. Therefore, low development costs and a high probability of success are expected. A preliminary cost analysis yielded an estimate of €25,000 with an hourly operating cost of €135. Its weak points, however, were the short operation time and the need to inject material into the flow with every use. This also makes the system less sustainable.

3.3 Trade-off

After creating design concepts as explained in [12], a decision was made on which of these concepts was the most feasible one for the final design. A trade-off was performed and reported upon in the Mid-Term report [12]. This section summarises the trade-off procedure and results.

3.3.1 Trade Method Rationale

Generally, it is very common to include all possible design solutions in order not to overlook potentially useful and innovative options. However, since entirely different measurement techniques are available, only the ones that were regarded as feasible after the initial literature study were developed into design options and included in this trade-off.

For the actual trade-off, the traditional method of scoring each of the options against weighted criteria was used. A numbered scale from 1 to 10 was used for both the weight factors and scores. These criteria, their weight factors and scoring norms were carefully established and agreed before the actual trade-off was executed.

Finally, the scores of the design concepts were evaluated by the team. A decision was made whether the best scoring concept really is the best concept and shall therefore be implemented or if the trade-off method needs to be adjusted in some way.

3.3.2 Trade-off Criteria and Results

In order to perform the trade-off, different trade criteria were determined and split into a primary and secondary category. The primary category includes the most important requirements and encompasses the criteria with the highest weights attached to them. The secondary criteria serve as a means to tip the scales in case two design options score very similar on the primary criteria. Criteria are assigned weights ranging from 1 to 10. Primary criteria are those with weights ranging from 6 to 10 while secondary criteria weights range from 1 to 5. Every design concept is assigned a score for each criterion, where the best scoring concept is given a score of 10, and the others are scaled to this.

The primary and secondary criteria and their weights are presented in table 3.1.

Table 3.1: Mid-term trade-off criteria and weights.

(a) Primary criteria.

Criterion	**Weight**
Accuracy	9
Agility	7
Operational Reliability	7
Resolution	8
Safety	8
Sustainability	8

(b) Secondary criteria.

Criterion	**Weight**
Data flexibility	2
Development cost	5
Production cost	5
Upkeep cost	5
Mobility	3
Probability of success	5
System complexity	5

After assigning scores to each of the design concepts, for each of the criteria, trade summary tables were made combining this information, see tables 3.2 and 3.3. Note that a higher grade means a more favourable performance on that criterion. For example, a higher 'Production cost' grade indicates a lower production cost. Furthermore, due to our inability of accurately determining the performance of the design options in an absolute scale, they are expressed as relative values from 1 to 10. This means that the option we consider best scores 10 points and all the other options receive a grade relative to that. Every design should however score acceptably on each criterion. Scoring dramatically on one of the criteria causes a design concept to be excluded, regardless of the overall score. This was however not expected to happen since these issues should have been discovered during the feasibility analysis already.

From table 3.2 showing the trade-off table for the primary criteria, it was shown that radar wins by a large margin of 115 points followed by smoke imaging, UAV mechanical system, acoustic tomography and HGS mechanical system all within a range of 70 points. On all primary criteria, radar scored the highest. The possible accurate smoke imaging system suffers from a poor sustainability score together with both mechanical systems which were expected to either have high power or helium usage. The acoustic tomography system as well as the HGS mechanical system have a low agility score since they have many components stationed on the ground or sea that could be difficult to move with the changing wind direction. The systems that received a low safety grade did so because they either have devices moving inside the wake that could break loose and hit other wind turbines or because of possible safety hazards for people operating the system in case of smoke imaging.

Since the radar system only consists of one component that can be mounted on the nacelle, it received the best grade for agility. Furthermore, its power consumption is relatively low and injects no objects into the stream, which awarded it the best grade for sustainability and safety.

The secondary criteria trade-off also results in radar having the highest score, but by a smaller margin. The simpler design concepts score higher on development cost and probability of success. However, radar also gets the best score for many criteria here. This secondary trade-off was intended to be used in the case of the primary trade-off having a non-definitive result. Since this was not the case, it is not very relevant. It is, however, noteworthy that the two trade-offs show similar results with radar winning both and smoke imaging emerging as an alternative.

In order to test the robustness of the trade-off, several different weight distributions along the criteria were tested to simulate changing customer preferences. However, since radar scored the highest on all primary criteria, it becomes clear that it would win in all of these scenarios. It was therefore concluded

Table 3.2: Trade summary table for the primary trade criteria.

Trade-off criterion	Accuracy	Agility	Operational reliability	Resolution	Safety	Sustainability	Score
Weight factor / Design solution	9	7	6	8	8	8	
Smoke Imaging	9	8	8	8	7	5	345
Acoustic Tomography	7	5	7	7	6	7	300
RADAR	10	10	10	10	10	10	460
HGS Mechanical System	6	5	7	7	5	6	275
UAV Mechanical System	8	9	6	7	5	6	315

that radar would be the winning design concept to be further developed, based on the results of the trade-off.

Table 3.3: Trade summary table for the secondary trade criteria.

Trade-off criterion	Data flexibility	Development cost	Production cost	Upkeep cost	Mobility	Probability of success	System complexity	Score
Weight factor / Design solution	2	5	5	5	3	5	5	
Smoke Imaging	6	10	10	4	7	4	7	208
Acoustic Tomography	9	5	6	6	10	2	5	168
RADAR	10	6	8	10	7	8	10	251
HGS Mechanical System	4	9	4	5	4	10	3	175
UAV Mechanical System	5	7	5	3	5	9	2	155

3.4 Initial Radar Design

In the Mid-Term report, a conceptual design for the radar system was presented. This system eventually ended up winning the trade-off, see section 3.3 and [12]. In this section, the results of this initial design are presented and discussed.

Mounting

In order to be able to cope with yawing and have a system which performs desirably well both on- and offshore, the design choice was made to mount the radar on the wind turbine nacelle. However, one problem does arise with mounting a radar on top of the nacelle. A radar can only measure velocity in radial direction. For the purposes of measuring the wake boundaries, the velocity in streamwise direction is required. This would mean that two radars would be required at hub height to measure the full horizontal velocity vector. From this the streamwise component could then be derived and the velocity deficits could be used to define the boundary.

This issue could however easily be resolved by using one assumption for the flow field: It is assumed that the velocity component in horizontal tangential y-direction can be neglected with regards to the stream-wise velocity. Using this assumption, only one velocity measurement from the hub is required to obtain the stream-wise velocity at a certain point, see figure 3.1.

Obviously, this assumption still requires sufficient validation. While a more thorough validation should be done on a larger scale, results from previous experiments can be used to do a first order validation. In [13], Medici shows some measurements done in the wake of a wind turbine model. Although this is a small scale experiment, it can at least give a hint of the nature of the flow field behind the turbine. Especially near the wake edges, which is the region of interest for this project, the ratio of both speeds $|V_y|/V_x$ never exceeds 5 %. In the entire horizontal plane at hub height, this ratio does not seem to exceed 10 %, which is still very acceptable for this project. In figure 3.2, the error introduced due to this assumption is shown for this ratio being 10 %. As can be seen, when the angle ϕ between the measurement direction and the x-direction increases, the error tends to increase but remains very small even for larger values for ϕ than might be required for this project.

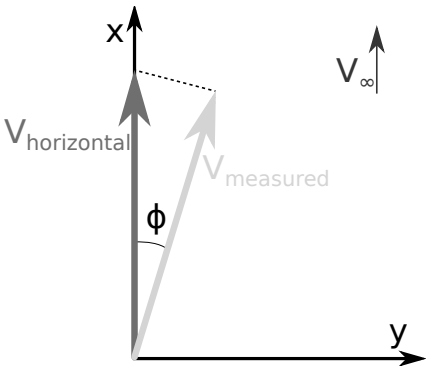

Figure 3.1: One measurement in the horizontal plane is sufficient to measure the horizontal velocity vector, assuming that it is aligned with the free-stream velocity.

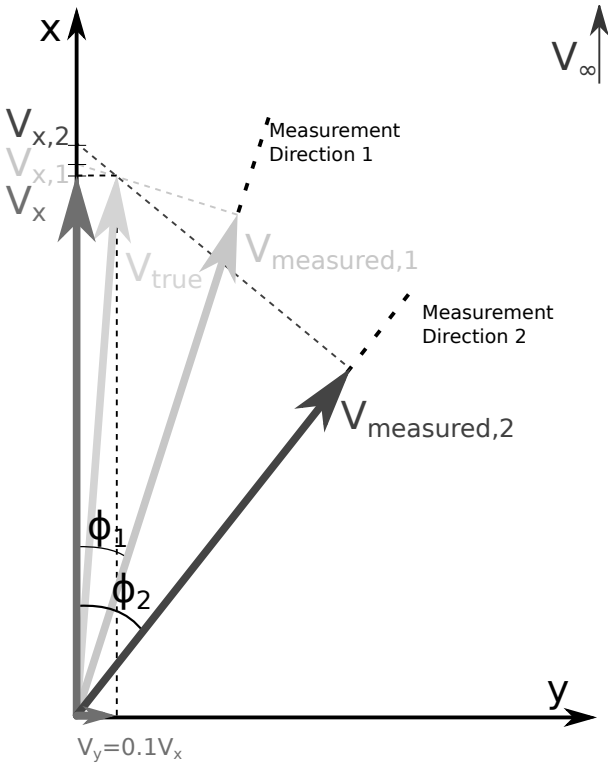

Figure 3.2: Even for $|V_y| = 0.1V_x$, the assumption introduces a negligible error. Note that near the wake boundaries, the y-velocity is assumed to be even smaller [13].

Radar type

Over the years, many different types of radar systems have been developed. All radar system are based on the principle that radio waves are reflected by objects. This reflected signal is received by an antenna and its signal strength, propagation time and frequency shift due to the Doppler effect give information about the object's size, location and velocity. There are three radar types that are most commonly used as weather radar and for atmospheric measurements. Due to its ability to work without a blind spot and higher accuracy, FMCW radar will be used for this project. During the initial design an estimate was made for the optimal frequency band, since this can be a major cost driver for components. The frequency band for the initial design was estimated to be the S band, which lies in between 2 and 4 GHz [14].

Design Details

Many different types of radar antennas are used, of which the two most common types are the parabolic dish antenna and the array antenna. Mainly due to its complexity and cost, the array antenna was discarded and the choice was made to design a system with a single dish antenna with a circulator to make it suitable for both receiving and transmitting. The dish diameter required was estimated at 3 m, which was determined by the required beamwidth and limited by the size of the nacelle on which it had to be mounted and its weight.

Transmission power is determined by the range and the signal to noise ratio required. Based on this, the transmission power required was estimated to be 30 W. From a reference antenna [15] with a similar dish size, the system mass is estimated at 100 kg.

In order to estimate the costs of the system, costs of components were analysed. A total system cost of €15,000 was deemed a reasonable first order cost estimation. It should be kept in mind that this cost estimate only contains the costs for the physical components and assembly — development costs and man hours are not included.

The costs of installing the radar system on top of a wind turbine are not negligible. The system must be lifted to the top of the nacelle, should be fixed to the nacelle in some way and power must be provided. Once the system is placed on top of the turbine, however, it can stay there indefinitely. It is even possible to operate the radar system continuously: Depending on whether it is scientifically interesting to do so, the radar system could spend its entire lifetime on top of the same wind turbine, thereby limiting the installation costs to only once.

Further design development

During more detailed design phases, several changes were made to the initial design, see the remainder of this report. The most important changes are presented in table 3.4

Table 3.4: Initial radar system design compared with the detailed design, T-WRAX.

Design parameter	**Initial design**	**Detailed design**
Radar type	FMCW	FMCW
Antenna type	Parabolic dish	Parabolic dish
Transmitting and receiving antenna	One dish with insulation	Separate dishes
Tranmitting antenna dish diameter	3 m	1.5 m
Receiving antenna dish diameter	3 m	0.6 m
System weight	100 kg	132.4 kg
Transmitted power	30 W	50 W
Radar range	500 m	520 m
Cost estimation	€15,000	€24,324

4 | Literature Review

In this chapter, the relevant results from the literature review are presented. Section 4.1 covers wind turbine wakes, after which the important results from radar literature are presented in section 4.2. The chapter ends with a section 4.3 covering examples of radar applications that are relevant for this project.

4.1 Wind Turbine Principles

This section elaborates on the problem analysis presented in chapter 2. The principles of wind turbines, wind turbine wakes and wake meandering are presented, after which the relevance of this project is presented.

4.1.1 Wind Turbine Working Principles

At a very basic level, the working principle of a horizontal axis wind turbine is as follows: A mass of air is moving with a certain velocity and therefore contains kinetic energy. Part of this energy is mechanically extracted from the flow by the blades' rotation, which is then transformed into electric energy using a generator [16]. Since energy is extracted from the flow, the energy level of the flow after the turbine is lower, resulting in a velocity deficit behind the turbine. The rotation of the blades also induces rotational motion within the flow behind the rotor, whereas the pressure differences near the blade tip cause additional vortices to be formed there [17]. This explains an increased turbulence intensity with regards to the free-stream flow turbulence intensity behind the turbine [18, 19, 20].

4.1.2 Wind Turbine Wakes

The wind turbine wake is defined as the region behind the wind turbine where the velocity is lower than the free-stream velocity [19]. This velocity difference introduces a shear layer, which causes air not passing through the blades to get mixed with the wake. The region of mixing will spread both inwards and outwards, making the width of the wake increase downstream. However, the wake also becomes shallower, causing the wake effects to diminish downstream. Energy contained in turbulent eddies cascades into smaller and smaller eddies to eventually be dissipated into heat. The average velocity increases due to extra energy from the undisturbed air. The largest velocity deficits and turbulence intensities in the wake are found after 1–2D, close to the horizontal axis of the wind turbine [19, 20]. In a free-stream flow with a high turbulence intensity, flows will mix more rapidly and wake effects will decay closer to the turbine [13].

4.1.3 Wake Meandering

The term wake meandering is used for large scale wind turbine wake movements, see figure 4.1. While the time-averaged properties of a wake are already extensively studied, wake dynamics are observed but not fully understood at this moment [21]. Two possible explanations are generally considered. One suggestion is that meandering is caused by large-scale eddies in atmospheric turbulence [19, 22]. The second suggestion is that a wind turbine behaves similarly to a bluff body in a flow, causing periodic vortex shedding [20, 13, 23, 24].

4.1.4 Relevance

With its cumulative capacity increasing approximately 20 % per year [16], wind is more and more establishing itself as an important source of electrical energy. A wind turbine is a machine which converts wind power into electricity.

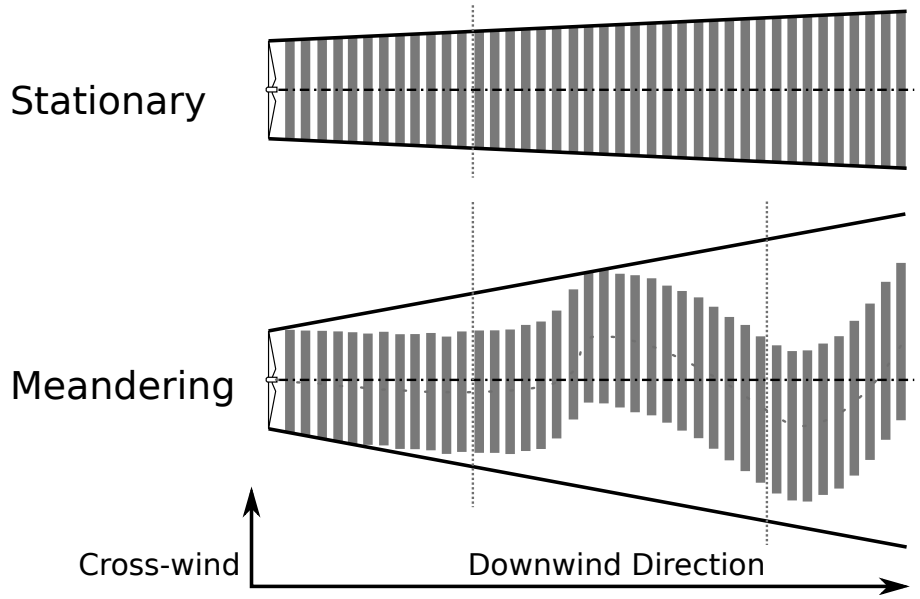

Figure 4.1: Wake meandering is a term for sweeping movements of the wind turbine wake [25].

During the development stages of modern wind energy, the first wind farms began to emerge. Locations of interesting wind resources are limited to certain places. Placing multiple turbines into these areas yields a higher energy output per unit area. On top of that, repair and maintenance equipment can be more concentrated, resulting in an additional cost reduction [18]. Wind farms do not just consist of multiple wind turbines placed close to each other, depending on the size wind farms can have their own electrical distribution, roads, data collection, support personnel etc. Wind farms do however have the disadvantage that upstream wind turbines induce wake effects on downstream turbines, resulting in additional fatigue loads and a lower power output for downstream wind turbines [18]. For these reasons, the ability to predict these wake effects is of high importance.

4.2 Radar Systems

This section presents a review of the literature read about radar. Since radar is a relatively well-researched concept, whole books containing a lot of basic information are available. One of those is Skolnik's 'Introduction to Radar Systems' [26], which most of this section's first part is reviewing. The second part treats specifics about weather radar systems and the third part treats the topic of measuring clear air turbulence, which our final design is not capable of after all.

4.2.1 General Principles

As the name suggests, radar is a system to detect and range targets and it uses radio waves to do so. It is able to determine an object's range, altitude, direction and speed. A transmitter emits pulses of radio- or microwaves, travelling at the speed of light, in predetermined directions. Any object in their path reflects tiny portions of the waves' energy back to an antenna dish that is located at the same site as the transmitter. The radar system measures the travel time of the wave from the transmitter to the object and back which, using the travel speed of the wave, can be used to determine the distance to the object. Radar signals are best reflected by materials of high electrical conductivity such as metals, sea water or wet lands.

Radars that make use of the Doppler shift are called Doppler radars. Objects that are moving away or towards the radar system will slightly change the frequency of the emitted radio waves, which is caused by the Doppler effect. This frequency shift is caused by the objects velocity in radial direction from the antenna.

As opposed to using a pulsed signal, it is also possible to transmit a Continuous Wave (CW) signal. This has the advantage that the signal power is spread out more evenly and leads to requiring less expensive hardware. Also, the obtained measurement data is in the frequency spectrum instead of measuring over time which leads to higher range resolutions using FMCW radar systems. While unmodulated CW signal radars can detect the Doppler shift, they are unable to determine range since the pause in between pulses, which lets a pulsed radar determine a time difference between transmitted and received signal, is not present in CW. To mitigate this limitation, CW signals are commonly modulated in the frequency range resulting in FMCW signals.

FMCW radars can detect both the distance to an object as well as its Doppler shift. An incoming signal is compared to the currently transmitted signal. The measured frequency difference, called beat frequency, gives information about the distance of the measured object as well as its Doppler shift. An FMCW radar does not actually measure the time difference between a transmitted and a received signal but only the frequency difference. This is discussed in more detail in section 8.1.

The basic radar equation, as, for example, found in Skolnik's book [26], is

$$P_r = \frac{P_t G_t G_r \lambda^2}{(4\pi)^3 R^4} \sigma \tag{4.1}$$

which relates the received power P_r to the transmitted power P_t and various factors. These are the gain of the transmitting- and receiving antenna G_t and G_r, respectively, the signal wavelength λ, the distance to the target R and the radar cross-section σ. σ describes the reflective area of a target and is dependent on its size, shape and material properties. This equation serves as a good starting point for designing and sizing radar systems.

4.2.2 Differences for Weather Radars

Instead of detecting relatively large objects like aircraft or seacraft, weather radars detect weather by evaluating the signal echos received from precipitation in the air like water droplets.

Since there can be millions of droplets in an area of observation, they are grouped together to count as one target within a certain region. This is illustrated in figure 4.2. θ and ϕ represent the width and height related to the azimuth and elevation angle, respectively. The radial length is denoted by the range resolution ΔR.

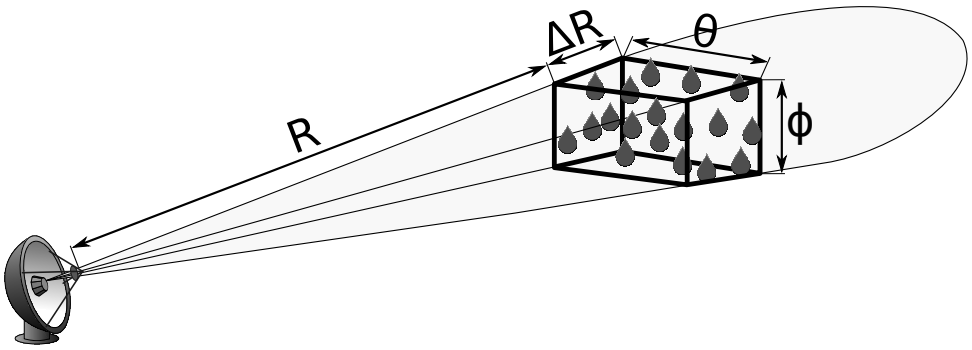

Figure 4.2: Modelling of a weather radar target filled with water droplets [27].

The average radar cross-section σ of a target volume now becomes the sum of individual radar cross-sections and can be expressed as follows [28]:

$$\bar{\sigma} = \sum_j \sigma_j = \frac{\pi^5 |K|^2}{\lambda^4} \sum_j D_j^6 \tag{4.2}$$

K is a complex number related to the scattering ability of a material, for example water, and D is an individual particle's diameter. The average reflectivity of a target area can be expressed as

$$\bar{\eta} = \frac{\bar{\sigma}}{V_c} \tag{4.3}$$

where V_c is the unit volume. Knowing that

$$\sigma = V\bar{\eta} \tag{4.4}$$

with V being a target's volume that, according to Probert-Jones [29], can be expressed as

$$V = \frac{\pi\theta\phi R^2 \Delta R}{8\ln(2)} \tag{4.5}$$

where ϕ, again, is the elevation angle. We can now rewrite the standard radar equation (4.1):

$$P_r = \frac{P_t G_t G_r \lambda^2}{(4\pi)^3 R^4} \cdot \frac{\pi\theta\phi R^2 \Delta R}{8\ln(2)} \cdot \frac{\pi^5 |K|^2}{\lambda^4} \frac{\sum_j D_j^6}{V_c} \tag{4.6}$$

The last term in equation (4.6) is of great importance in radar meteorology and called the reflectivity factor, denoted by the symbol Z:

$$Z = \frac{\sum_j D_j^6}{V_c} \tag{4.7}$$

Its unit is $\mathrm{mm}^6/\mathrm{m}^3$ and it is related to the amount of precipitation present in a unit volume. It is commonly represented in the decibel scale as dBZ and can be seen on weather radar measurement maps. Literature and websites provide lookup tables for the relation between dBZ and rainfall rates [30]. Similar to equation (4.1), equation (4.6) and the dBZ relation are used to design and size weather radars.

It should be noted that the equations in this section only hold true if the size of precipitation relative to the signal's wavelength fulfils

$$r \leq \frac{\lambda}{10} \Leftrightarrow D \leq \frac{\lambda}{5} \tag{4.8}$$

where r is the particle's radius. This is also illustrated in figure 4.3 that shows the required particle size for Rayleigh, Mie and optical scattering. In other words, it is important to have the particles induce Rayleigh scattering as this results in more energy being scattered backwards than is the case for Mie scattering, which is mostly forwards (figure 4.4).

4.2.3 Clear Air Turbulence Measurements

A radar system does not necessarily require precipitation in order to measure flow velocities. Flow that is turbulent enough causes a local gradient in air density that can refract electromagnetic waves. In 1969, Ottersten [32] presented the advances that have been made in that field. He shows that there is a refractive index structure constant C_n^2 that can be expressed as

$$C_n^2 = a^2 \epsilon^{2/3} \frac{\left(\mathrm{d}\varphi/\mathrm{d}z\right)^2}{\left(\mathrm{d}u/\mathrm{d}z\right)^2} \frac{1}{1 - R_f} \tag{4.9}$$

where a^2 is a constant related to the flow's circulation, ϵ is the flow's energy dissipation rate, φ the flow's refractive index gradient, u the flow's horizontal velocity component, z the vertical direction and R_f the flux Richardson number, which, according to Ottersten, approaches 0 in strong turbulence. He also shows that C_n^2 relates to the radar reflectivity η in the following way:

$$\eta \approx \frac{0.38 C_n^2}{\lambda^{1/3}} \tag{4.10}$$

It is important to realise that clear air turbulence measurements require very sensitive antennas and are typically performed on large scale for profiling wind behaviour in skyward direction up to several thousand metres. In a conversation with Dr. Krasnov[1], he told us about a wind profiling radar used in Cabauw that received much stronger echos from a nearby highway, due to the antenna signal's sidelobes pointing in that direction, than the actual desired signal response from the clear air turbulence.

[1] Dr. Oleg A. Krasnov is a research scientist at the TU Delft. He is part of the Microwave Sensing, Signals and Systems department at the faculty of Electrical Engineering, Mathematics and Computer Science. On Thursday the 5th of June 2014, two members of our group had a conversation with him to learn more about radar and get his opinion on the feasibility of our design ideas at that point.

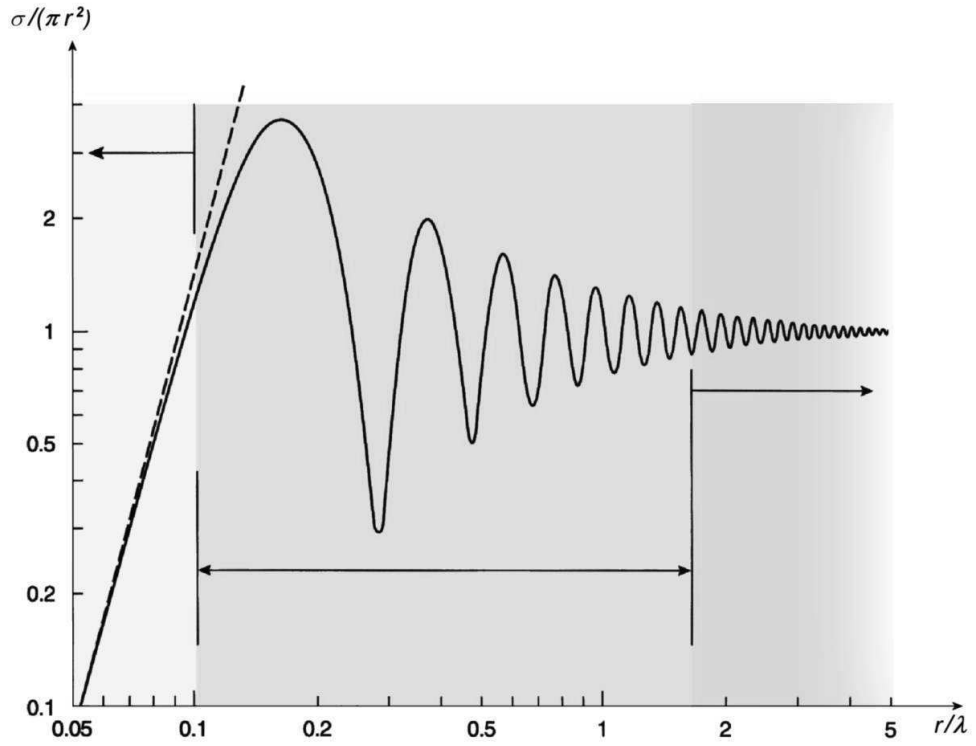

Figure 4.3: Rayleigh (green, left), Mie (red, middle) and optical (blue, right) scattering region in the relation between radar cross-section and wavelength [27].

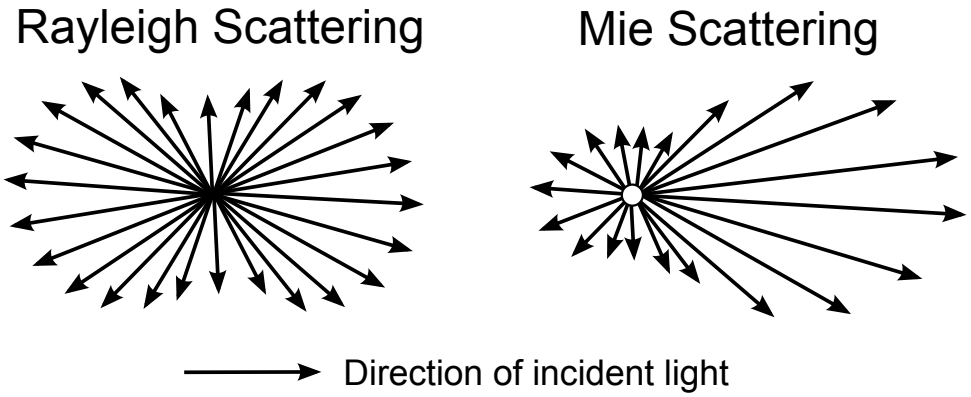

Figure 4.4: Rayleigh and Mie scattering patterns [31].

4.3 Similar Applications and Experiences

During the literature, several papers were found on similar radar systems that were of interest. They considered applications and experience were related to T-WRAX, and were therefore studied. Three different radars and why they are relevant are studied, and their use as reference radars is reported.

4.3.1 TTUKa Radar

Texas Tech University (TTU) developed a Ka-band mobile doppler radar system for full mapping of a wide spectrum of atmospheric phenomena. This made it useful both for the atmospheric science and the engineering community [33]. The radar system consists of dishes mounted on trucks to increase mobility,

see figure 4.5.

These high resolution, high frequency radars are designed with high sensitivity and resolution of data collected, allowing a study of fine-scale atmospheric motions as well. The radar is designed with a large dome around it for protection. The TTUKa radars are a technology which has been proven in measuring large scale flows in wind farms [34]. After initial tests, the National Wind Institute (NWI) measured wind flow across an entire wind plant using the TTUKa radar system. The results of two wake measurements around a wind turbine are shown in figure 4.7, where the wake can be clearly distinguished. Measurements on wake meandering have also been performed, of which the results are shown in figure 4.6.

Figure 4.5: One of the Ka-band radars on field [33].

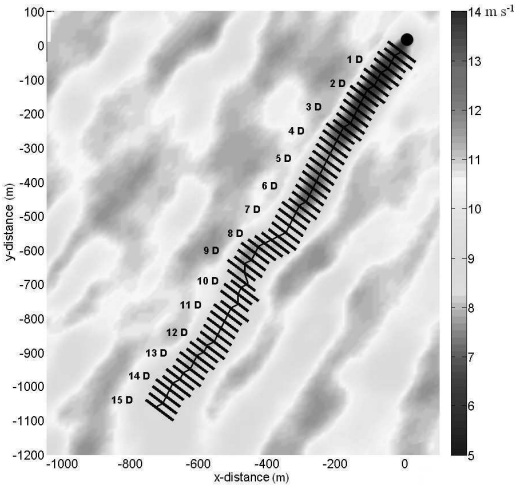

Figure 4.6: Wake meandering measured using the TTUKa radar system [35].

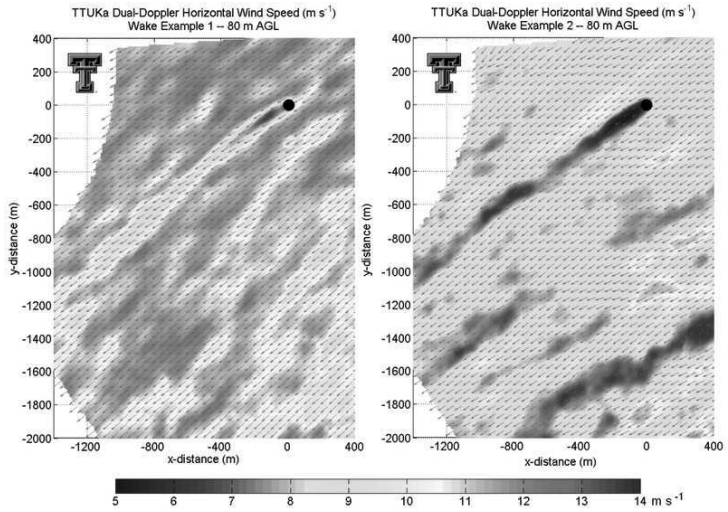

Figure 4.7: Two examples of a TTUKa doppler radar wake measurement [34].

Since the TTUKa is a radar device used to measure velocity fields around wind turbines and wind parks, making it a very useful reference radar for this project. However, some differences exist with the radar designed in this project.

- The TTUKa radar is designed to measure the entire 3-D velocity vector field. For this project, vertical velocities are not required.

Figure 4.8: Layout of the PARSAX radar on top of the Faculty of Electrical Engineering, Mathematics and Computer Science [37].

- The TTUKa can measure a complete measurement volume. The region of interest for this project is only in the horizontal plane.
- While S- or X-band are sufficient for the purpose of this project, the TTUKa radar uses Ka-band radar. This however drives costs up dramatically.
- The radar designed for this project requires a range of 500–600 m. Depending on the weather conditions, the TTUKa radar has a range somewhere around 30 km.

In conclusion, the TTUKa radar can be considered a reference radar and can be considered a proof of concept for measuring wind turbine wakes with radar technology.

4.3.2 PARSAX

The Polarimetric Agile Radar in S- And X-band (PARSAX) is a Doppler polarimetric radar that simultaneously transmits and receives radio waves in orthogonal directions, and can operate in both the S-and X-band. It is an improvement and successor to the Delft Atmospheric Research Radar (DARR). Similar to our radar device, PARSAX is located at an elevated position, at 92 m on the roof of the Faculty of Electrical Engineering, Mathematics and Computer Science of TU Delft.

PARSAX allows the processing of the horizontal and vertical components of both of the back-scattered signals, leading to an improved resolution. It's resolution is fine enough that it is used to track development of water cloud droplets [36]. The waveforms of the signals are generated digitally, providing the useful flexibility of being able to choose different types of waveform [37]. It is also flexible in that it can operate in two bands: in the S-band version it is centred at 3.315 GHz, and in X-band between 9.6 and 10 GHz [38]. It has been designed to operate with a CW signal with bandwidth of 50 MHz for a range resolution at close range of 3 m. The transmitting and receiving antenna are separate, with the receiver being 2.12 m in diameter and the transmitter 4.28 m, they can be seen in figure 4.8[37].

To conclude, PARSAX is similar to our designed radar system in that it is designed for atmospheric remote sensing, and uses a similar radar layout. Since the antenna was designed for a range resolution of 3 m, it has a very similar bandwidth of 50 MHz [38] as compared to our 45 MHz. This supports our range resolution calculation and bandwidth choice explained later in section 5.3.6. Likewise the choice to use a CW signal for PARSAX supports the claims that CW signals are appropriate for achieving improved sensitivity. However PARSAX varies in that is a very adaptable system, that can output multiple signal types and operate at different frequency bands. It proves useful as a reference radar, and demonstrates the X-band is appropriate for a weather radar with requirements similar to ours for small particle detection. More importantly it has proven to be a source for contacting experts, as a key collaborator on the PARSAX project, Dr. O. A. Krasnov, has provided advice on the design of T-WRAX.

4.3.3 IDRA

In 2007, the International Research Centre for Telecommunications and Radar (IRCTR) built a weather radar system at the Cabauw Experimental Site for Atmospheric Research (CESAR) called IRCTR Drizzle Radar (IDRA). Figueras i Ventura [39] discusses the design and working principle of this radar in his thesis. The IDRA system is designed to measure occurences of drizzle and light rain in the atmosphere. It uses a CW signal at a carrier frequency of 9.475 GHz (X-band) which is frequency-modulated to give a sawtooth pattern. The system has two radar dishes, one transmitter and one receiver, is mounted on a tower at 213 m height as shown in figure 4.9 and has a rotational speed of 1 rpm. The TU Delft repository website for the IDRA system [40] provides real-time measurement data as shown in figure 4.10.

Figure 4.9: The IDRA system on top of the Cabauw meteorological tower [39].

The thesis also presents an example of clear air scattering measurements performed by the IDRA system. However, it concludes that the measured responses mostly are due to birds and insects, which further supports our decision to not design our system for clear air turbulence measurements.

In conclusion, the IDRA system has similarities to our radar system, namely that it uses an X-band FMCW signal and can operate at similar maximum range and range resolution settings to our system. Furthermore, it is also designed to observe light precipitation and is mounted on a tower well above ground level. The fact that IDRA performs its job well for observing precipitation but is unable to properly detect clear air turbulence is valuable knowledge for our design approach.

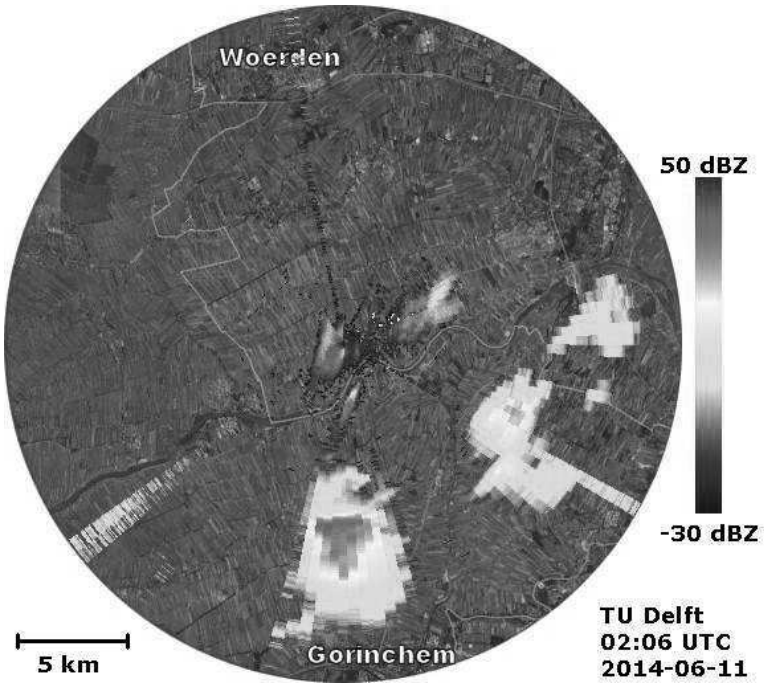

Figure 4.10: IDRA measurement data mapped over a satellite image of the surrounding area [40].

5 | System Specifications

In this chapter the calculation of the basic parameters for the design of the radar system is discussed, one could call it the preliminary sizing of the radar. First, the N^2-chart is given in section 5.1 that describes the order of operations in the design process. Next, the functional diagrams of the radar system are discussed in section 5.2, then the detailed equations used in the sizing are explained in section 5.3, and finally the results of the preliminary sizing are given in section 5.4. Additionally the antenna design is discussed in section 5.5. The antenna price is given in section 12.1.1.

5.1 Design Process & N^2-Chart

In order to design a radar system, it is necessary to understand in which sequence the design parameters are determined and which parameters are subjected to iterations. The N^2-chart illustrating this process is given in figure 5.1.

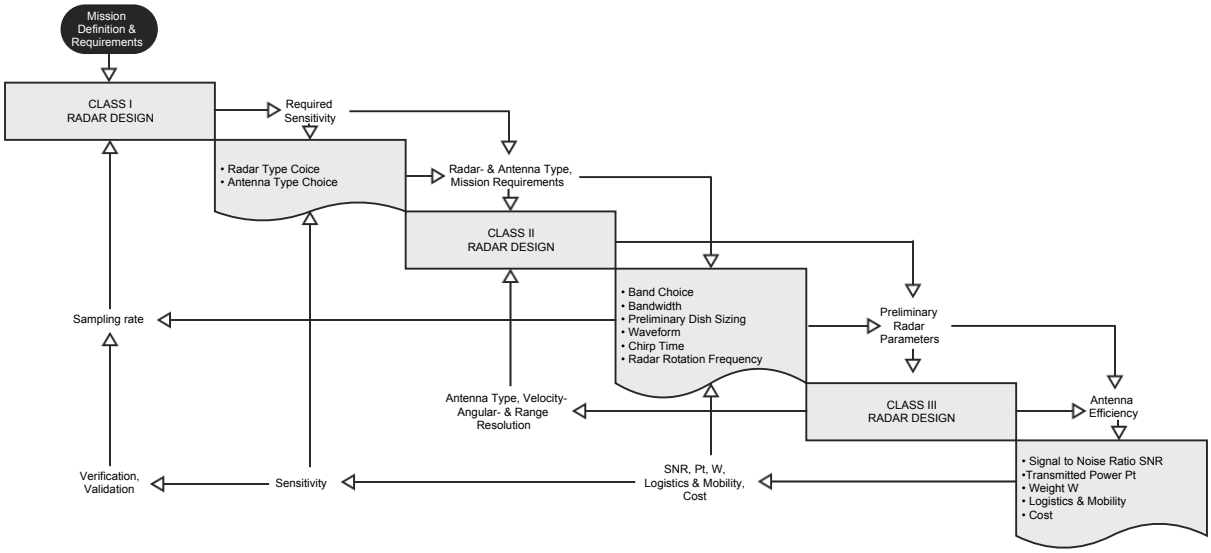

Figure 5.1: N^2-Chart for the T-WRAX design process.

The design process consists of three design classes. In the first design class, it is determined which type of radar system and antenna will be used to fulfil preferably all of the mission requirements. This choice is based on the sensitivity that is required to detect the target of interest.

With the radar system and antenna types known, the second design class will determine preliminary system parameters mainly based on the mission requirements on spatial resolution, angular accuracy and the velocity range. These parameters are highly interrelated which is why they have to be determined at the same time. For example, changing the velocity resolution of the radar system would require a change in band choice, dish size, chirp time and radar rotation frequency. For every single mission requirement, there will be one optimum set of system parameters. However, in order to fulfil all of the requirements, the system parameters need to be carefully assessed with respect to each other.

After a set of system parameters has been determined, the third design class will determine the final design specifications such as its signal to noise ratio, transmitted power, weight, cost, logistics and mobility. Therefore, this last phase of the design process covers both the mechanical and electronics design to fit all of the system parameters into one single device.

Of course, this design approach is not a one way process: several iterations are done along the way. After the second design phase, a sampling rate has been determined which needs to be evaluated. If the sampling rate turns out not to meet the requirements of the first design phase, a different set of system parameters has to be determined.

At the same time, the velocity, range and tangential resolution need to be evaluated with respect to their required values. Of course, it is not always possible to achieve a set of system parameters that fulfils all of the mission requirements but, by the use of iteration, a best possible set must be determined.

Lastly, after the final design class, specifications such as weight and cost are known. It is trivial that, if the weight is too high to be carried by the wind turbine or if the cost is too high for the customer, the design has to be altered. Most importantly, it has to be checked whether the signal to noise ratio that has been determined achieves a sufficient sensitivity to detect the target of interest.

5.2 Functional Diagrams

To give an overview of the functionality and usage of the radar system, a functional flow diagram and a functional breakdown diagram are given. The functional flow diagram is given in figure 5.2.

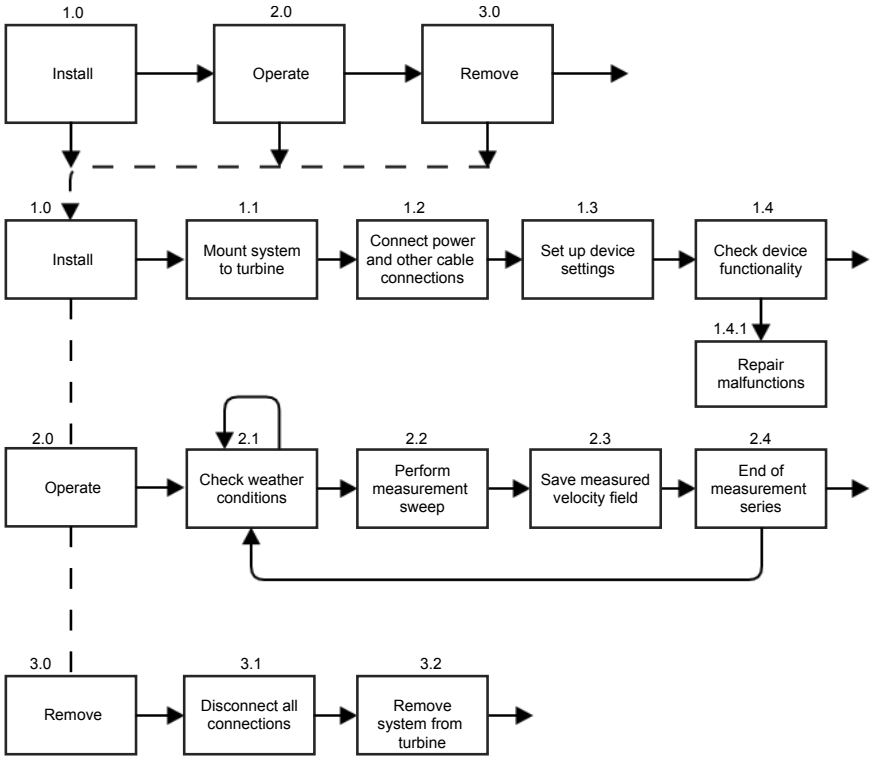

Figure 5.2: Functional flow diagram of the T-WRAX.

The usage of the radar system can be divided in three steps: installation, operation and removal. During the installation phase, the radar system is mounted on the turbine nacelle, power is provided to the system, the system settings for the specific location are set and the system is tested. If any malfunctions are found, they should be repaired. If not, the operation of the system can start. During operation, the radar system checks the weather conditions. If they are suitable for measurements, measurements will be acquired. If not, the system will wait. Once the required measurements have been performed, the system can be disconnected and removed. The functionality of the radar system can also be illustrated using a functional breakdown diagram. The functional breakdown diagram is given in figure 5.3.

The functionality of the radar system can be divided in three sections: providing power, performing the measurements and interpreting the measurement results. Providing power consists of receiving power in some way and distributing it to the system components. Performing measurements consists of a

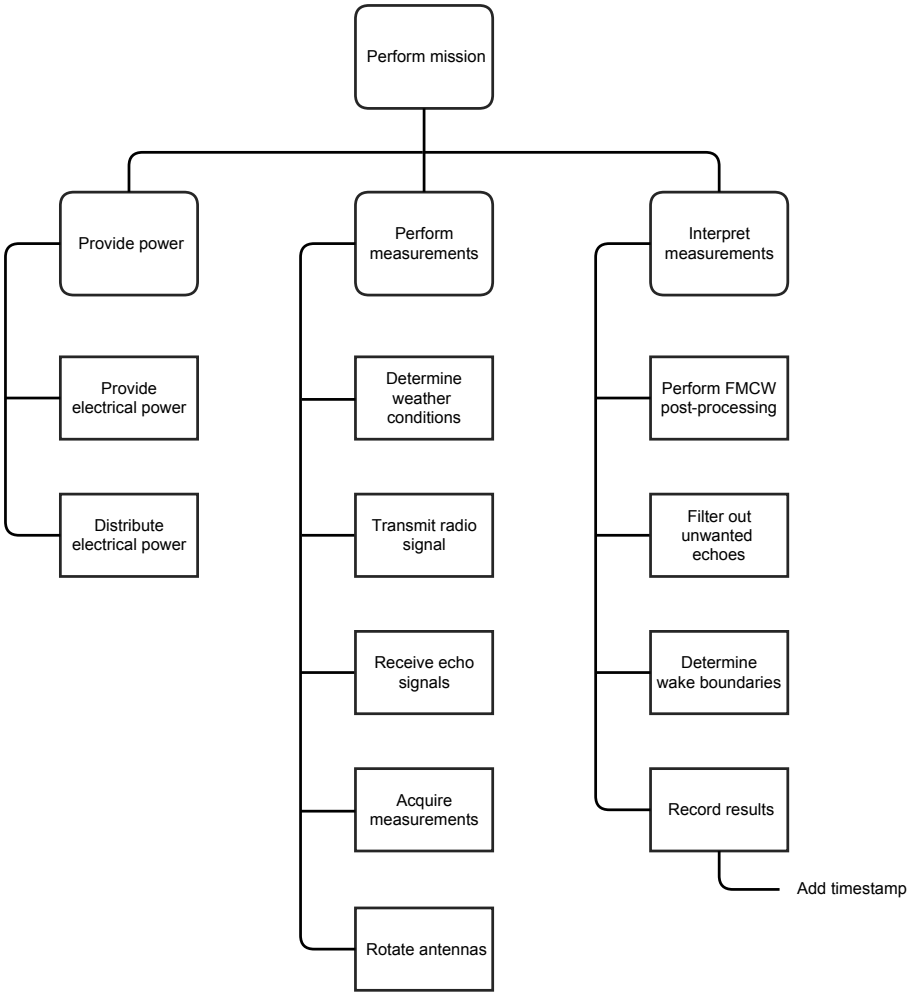

Figure 5.3: Functional breakdown diagram of T-WRAX.

function that determines whether the weather conditions are suitable for acquiring measurements, the transmitter and receiver radar subsystems, a data acquisition function and a functionality to rotate the antennas. The interpretation of the measurement results consists of the standard FMCW post-processing, the filtering of unwanted echoes such as ground clutter or other wind turbines, the determination of the wake boundaries from the measured velocity field and the recording of these results.

5.3 Sizing Equations

A radar is a complex system where a large number of design variables influence a large amount of system performance specifications. Designing a radar system is an iterative process, which makes at least the design process similar to that of an aerospace design. In this section, all aspects of the preliminary sizing of the radar system are given, including equations.

5.3.1 Received Power

For the received power by the radar system directly at the dish, a slightly modified version of the radar equation (see also equations (4.1) and (4.6) in section 4.2) is used, taken from [41],

$$P_r = \frac{P_t G_t G_r \lambda^2 \theta^2_{\frac{1}{2},t} \Delta R}{512 \ln(2) \pi^2 R^2} \eta \tag{5.1}$$

where P_t is the transmitted power, G_t and G_r are the transmitter and receiver antenna gains, respectively, λ is the signal wavelength, $\theta_{\frac{1}{2},t}$ the transmitter antenna half power beamwidth, ΔR is the range resolution, R is the measurement range and η is the effective radar cross section per m^3 of a distributed target, like precipitation.

The received power is an important design variable since the sensitivity and the complexity of the radar system directly depend on it. The higher the received power, the simpler the receiver system will be, but that might require a decrease in sensitivity or increased complexity elsewhere.

5.3.2 Antenna Gain and Beamwidth

The gain and beamwidth of an antenna are difficult to estimate because every part of the antenna design influences them and most of these effects are difficult to accurately model. A sufficiently accurate model, however, is that the antenna gain is given by the equation from [42]:

$$G = \frac{\pi^2 D^2 e_A}{\lambda^2} \tag{5.2}$$

where D is the antenna diameter and e_A is the antenna efficiency. The effects of the dish design are included in the efficiency factor and values for this factor can be taken from reference antennas with a similar design. The only design variable for the antenna gain is then the dish diameter.

The beamwidth of a dish antenna is not an absolute boundary of the angles at which the radio beam propagates. This beam will be the strongest in the straight direction and will decrease in strength towards the sides of the dish. The beamwidth of a dish antenna is usually defined as the angle at which half of the transmitted signal strength is still available—the Half Power Beamwidth (HPBW) $\theta_{\frac{1}{2},t}$. This can be estimated by the relation from [43]:

$$\theta_{\frac{1}{2},t}[deg] = \frac{70\lambda}{D} \tag{5.3}$$

5.3.3 Signal to Noise Ratio

The design Signal to Noise Ratio (SNR) of the radar system determines the sensitivity of the radar, that is, the minimum reflectivity that the radar can measure at the maximum range. It is defined as the received power divided by the noise power and expressed in dB. The received power is given in equation (5.1) and the noise power is given by the standard temperature noise equation

$$P_n = kT_nBF \tag{5.4}$$

where k is the Boltzmann constant, T_n is the system temperature, or noise temperature, B is the bandwidth of the system and F is the receiver noise figure of the radar system which accounts for additional noise generated in the amplification stages. The bandwidth of the radar system therefore largely determines the signal to noise ratio, just as the variables of the received power equation.

5.3.4 Antenna Rotation

To be able to accurately measure a target with a FMCW radar, an important factor is the time on target. FMCW makes use of a Fourier analysis to measure the range and velocity of targets and this Fourier analysis requires a certain amount of measurements to perform the analysis on. The target of interest should be in the measurement path for the complete measurement time of one Fourier series, otherwise the results will not make sense. The time on target can be computed using the relation

$$T_{target} = \frac{\theta_{\frac{1}{2},t}}{\omega} \tag{5.5}$$

where T_{target} is the time on target and ω is the rotational rate of the antenna. This time on target should always be larger than the product of the time of one frequency sweep multiplied with the number of sweeps that are processed together in the Fourier analysis. This is the first driving factor in the rotational speed of the antenna. Other considerations are measurement accuracy in cross-radial direction, where multiple partially overlapping measurements can be used to accurately interpolate the velocity field in this direction, and the time it takes to take one wake measurement. During the rotation of the antenna, the wake moves and if the rotation takes too long, the wake might have moved unacceptably far.

5.3.5 Velocity Resolution

The velocity resolution that the radar system can differentiate is dependent on many parameters. Radar obtains the Doppler velocity information by observing the phase variation between consecutive sweeps. The phase variation of the response of a scatterer at a distance R_0 and moving at a constant velocity from one sweep to the next is the following:

$$\phi(R_0) = 2\pi f_D T_c \tag{5.6}$$

where f_D is the Doppler frequency and T_c is the chirp time. Therefore, by performing a Fast Fourier Transform (FFT) at a particular range cell along N chirps, the Doppler velocity can be retrieved.

The phase has an unambiguous range between 0 and 2π. Therefore, the maximum unambiguous Doppler frequency is

$$f_{Dmax} = \pm\frac{1}{2T_c} \tag{5.7}$$

which means that the maximum unambiguous Doppler velocity is:

$$v_{Dmax} = \pm\frac{\lambda}{4T_c} \tag{5.8}$$

with wave length λ. Now that the velocity measurement range is known, the Doppler velocity resolution can simply be determined by the number of resolution cells in the frequency spectrum of the FFT which equals N chirps:

$$\Delta v_D = \frac{2v_{Dmax}}{N} \tag{5.9}$$

From here, to determine what the velocity resolution is, the chirp time T_c and the number of chirps N need to be known. The chirp time can simply be determined by solving equation (5.8) for T_c using the required velocity range of up to 25 m/s and the band frequency used. The last unknown variable, N, will be determined in the next section. Keep in mind that in order to achieve a velocity measurement range of 25 m/s one has to consider both negative and positive velocities so effectively the velocity range will be from -25 m/s up to 25 m/s.

5.3.6 Number of Measurements

To determine N, an important relation has to be understood: N multiplied with the chirp time T_c determines the time during which a FFT is performed on the measurement data. This time must be smaller than the time on target T_{target} from equation 5.5 in order not to integrate over two different targets:

$$NT_c \leq T_{target} \tag{5.10}$$

Solving this relation for N determines the maximum amount of chirps over which a FFT can be performed. Keep in mind that most FFT algorithms can only be performed in increments of numbers with a base of 2, that is, of numbers of the form 2^n. The reason for this is because the algorithm works much more efficient with base-2 numbers which decreases the processing time significantly. This means that the number of chirps that are included within one FFT must be rounded down to the next base-2 number that is lower than the maximum amount of chirps as determined above. So, for example, for a maximum amount of chirps of 150, one could choose N to be, say, 128 or 64 but not 256 or higher.

5.3.7 Range Resolution

The range of a FMCW radar system is calculated using the beat frequency f_b. According to the Nyquist criterion, the maximum beat frequency that can be unambiguously measured is half of the sampling frequency f_s. Therefore, the maximum unambiguous range is determined by the sampling frequency:

$$R_{max} = \frac{c}{2}\frac{T_c}{B}\frac{f_s}{2} = \frac{c}{2B}\frac{K}{2} \tag{5.11}$$

where c is the speed of light, K is the number of samples and B the bandwidth. In the same way as for the velocity resolution the range resolution can now be determined from the frequency spectrum obtained

from the FFT. The only difference is that the number of resolution cells is equal to $K/2$ since a real valued signal results in a symmetric frequency spectrum from which just one half is required. Therefore, the range resolution is determined by

$$\Delta R = \frac{c}{2B} \tag{5.12}$$

where c is the speed of light. As can be seen, the range resolution is merely dependent on the bandwidth of the used signal.

5.3.8 Tangential Resolution

The tangential resolution depends on both the beam width and the rotation angle over the measurement integration period. The tangential resolution based on the beamwidth can be determined as follows:

$$\Delta R_t = \theta_{\frac{1}{2},t} R \tag{5.13}$$

where $\theta_{\frac{1}{2},t}$ is the beamwidth and R is the corresponding range. As can be seen, the tangential resolution becomes worse with range. The additional error in the tangential resolution due to the rotation of the radar system can be determined using

$$\Delta R_{t,err} = \omega T_c K R \tag{5.14}$$

where ω is the rotation rate of the antenna, T_c is the chirp time, K is the number of samples and R is again the corresponding range. In order to determine the total tangential resolution one cannot simply add both ΔR_t and $\Delta R_{t,err}$ since multiple measurements can be interpolated to achieve a better resolution. However, the maximum theoretical resolution is equal to the error introduced by the rotation of the antenna.

5.3.9 Distance Frequency Shift

The Frequency shift of the received signal due to the travel time can be calculated using the relation from [44],

$$\Delta f = \frac{2RB}{T_c c} \tag{5.15}$$

5.4 Sizing Results

As indicated in the N^2-chart, the first step is to determine the minimum required sensitivity of the radar system. It is possible to measure turbulence in clear air using a radar system, but this will require a very sensitive radar system. Preliminary calculations and advice from Dr. Krasnov, as explained in section 4.2.3, showed that interference from the turbines and the ground or sea would make those clear-air measurements close to impossible, even with a highly advanced and expensive radar system. It was found that the presence of fog or low hanging clouds gives a sufficiently strong radar echo to be able to measure in these conditions. All precipitation types stronger than fog, like drizzle, rain, snow or any other form of precipitation, will then be easily detectable. The design dBZ value for the radar system, based on [45], is -28 dBZ.

The second decision to be made is the radar type. For detecting weather targets, two radar types exist: pulse radar and FMCW radar. A pulse radar is the classic radar where a short radar pulse is transmitted and the radar then waits for the received echoes. A FMCW radar, instead, transmits a continuous radio signal that is constantly changed in frequency within a certain bandwidth. The advantages of FMCW are that the transmission power can be significantly lower and the sensitivity of the receiving part is better, because after the Fourier analysis is performed on the received signal, the actual measurement results are only placed in a small number of Fourier frequency bins while the noise power is spread over the complete frequency range. This improves the signal to noise ratio significantly. Further, the effects of bandwidth are different for pulsed radar and FMCW radar. A pulse radar requires a bandwidth that is inversely proportional to the pulse width, which means that it requires a larger bandwidth for close ranged target detection and a smaller bandwidth for long range detection. An FMCWradar has the

opposite requirements: The shorter the range, the smaller the frequency difference between transmitted and received signal and the less bandwidth is required. The less the bandwidth, the smaller the receiver noise energy that the target energy needs to exceed for reliable detection. In this regard, FMCW radars are inherently capable of having a better target detection at close range than pulse radars and worse at long ranges. However, for the radar system to be designed, only close range target detection is of interest. The biggest advantage of FMCW radar in comparison with a pulse radar is its range resolution. The theoretical resolution of a pulse radar is dependant on its pulse width. A pulse width of 100 ns (which already is very small) results in a range resolution of 30 metres. For FMCW radar, there is no lower theoretical limit. Rather, the resolution is dependent on the bandwidth and can be as low as 1 m. For these reasons, a FMCW radar system is selected.

The following design characteristics can be divided in two groups: fixed characteristics and variable characteristics. The fixed characteristics depend on design parameters that must be fixed in the design and can not be changed once the system has been built. The variable characteristics are basically software settings of the radar system and the post-processing. These settings can still be changed after the system has been built, even during operation, to for example adapt the system to different weather conditions. With these characteristics an estimation of the performance of the system in the worst case condition, during only fog, is made.

5.4.1 Fixed Characteristics

From the received power equation (5.1), it was determined that the attenuation between the transmitted and the received signal will be 192 dB. An inherent problem with FMCW radar system is that some of the transmitted power will leak directly to the receiver. This is not a major problem, since the signals of interest in the received signal are different in frequency than the leakage signal so they will still be detectable, but the leakage signal should not saturate the data acquisition device. The dynamic range of data acquisition devices is usually 100 dB, which means that the leakage signal should not be more than 100 dB stronger than the received signal. Using the attenuation of 192 dB, the isolation between the transmitter and the receiver should then be at least 92 dB. To achieve such a large isolation, a system with two antennas, one for transmitting and one for receiving, is necessary. The fixed characteristics of the radar system are summarised in table 5.1.

Table 5.1: Fixed characteristics for T-WRAX.

Characteristic	**Value**
Frequency band	X-band, 10–10.5 GHz
Transmitter antenna diameter	1.5 m
Transmitter antenna beamwidth	1.4°
Receiver antenna diameter	0.6 m
Antenna efficiency	0.75
Receiver noise figure	1.5 dB
Transmitter power	50 W
Measurement range	520 m

The selected frequency band of the radar system is the X-band, where the officially assigned frequency band ranges from 10 to 10.5 GHz. A higher frequency gives a smaller antenna size, but the echo from weather targets is weaker. Radar components for higher frequencies than X-band are usually also more expensive, since X-band is commonly used nowadays and components for higher frequencies need to be manufactured with higher precision. It was therefore decided that X-band would be a good trade-off. The dish size of 1.5 m is needed mainly to make sure that the beam is thin enough to still be able to achieve a high enough accuracy in the cross-radial direction at the maximum range. The antenna efficiency of 0.75, taken from [46], is assumed as the antenna efficiency of this system. The receiver noise figure of 1.5 is a common assumption. The transmitter power is mainly driven by the required SNR, which should, in the worst case, be 10 dB. Since the SNR is also largely dependent on the measurement range, the required range of 500 m is used for sizing the system. The maximum distance between the radar system and the edge of the wake at 500 m downstream is 520 m.

5.4.2 Variable Characteristics

To be able to size the radar system, a set of variable system characteristics was selected for the worst case of a dBZ value of −28 dBZ. These characteristics are given in table 5.2.

Table 5.2: Variable characteristics for T-WRAX.

Characteristic	**Value**
Bandwidth	45 MHz
Chirp length	0.3 ms (for 25 m/s freestream)
Maximum frequency shift	520 kHz
Measurement integration period	19.2 ms
Rotational rate	22.5 °/s
Frequency sweep	Sawtooth

The bandwidth is selected as a trade-off between the SNR, which gets lower with a larger bandwidth, and the resolution. The range resolution is the measurement resolution in radial direction. The chirp length was calculated using equation (5.8). The maximum frequency shift that will occur in the radar system is at the maximum range of 520 m and the maximum measurable velocity, 25 m/s. The frequency shift due to the velocity is 1667 Hz from equation (5.7) and the frequency shift due to the distance is 520 kHz from equation (5.15). The total maximum frequency shift, and therefore the maximum beat frequency, is thus 521.7 kHz. Using the required time on target and the preferred velocity resolution, the integration period—the time of measurements over which the Fourier analysis will be integrated—was established at 20 ms. The rotational rate of the antenna system is set at 22.5 °/s, which makes the time to sweep the complete wake 4 s, as given in the requirements. For a FMCW radar, the frequency of the transmitted signal must be modulated. The selection of a modulation pattern has an effect on the post processing. A sawtooth sweep consists of a rising linear frequency sweep, followed by a jump to the starting frequency after which this pattern is repeated. This sweep pattern is commonly used since it is simple to process, especially for radar systems that look at distributed targets such as rain [39].

5.4.3 Performance Estimation

Using the characteristics explained above, the expected system performance can be calculated. The result of these calculations is given in table 5.3.

Table 5.3: T-WRAX performance estimation.

Characteristic	**Value**
Range resolution	3.3 m
Velocity resolution	0.75 m/s
Blind range	50 m
Sweep time	4 s
Tangential resolution	up to 4 m

The requirement on the resolution in downstream direction is 10 m, but since the radar system must measure the wake boundaries at an angle close to the turbine, the range resolution must be better than this. A value of 3.4 m is assumed to be sufficient. It is difficult to get a good velocity resolution because a better velocity resolution requires a longer measurement integration period which either decreases the resolution in cross-radial direction or increases the sweep time. A velocity resolution of 0.75 m/s was assumed to be sufficient. Due to the masking of close range measurements—caused by transmitter leakage and the measurements of the wake boundary close to the radar being at a large angle, which induces inaccuracies—the first 50 m of data will be ignored. The time to sweep over the full wake will be 4 s. The maximum achievable tangential resolution was determined to be 4 metres at maximum range using equation (5.14).

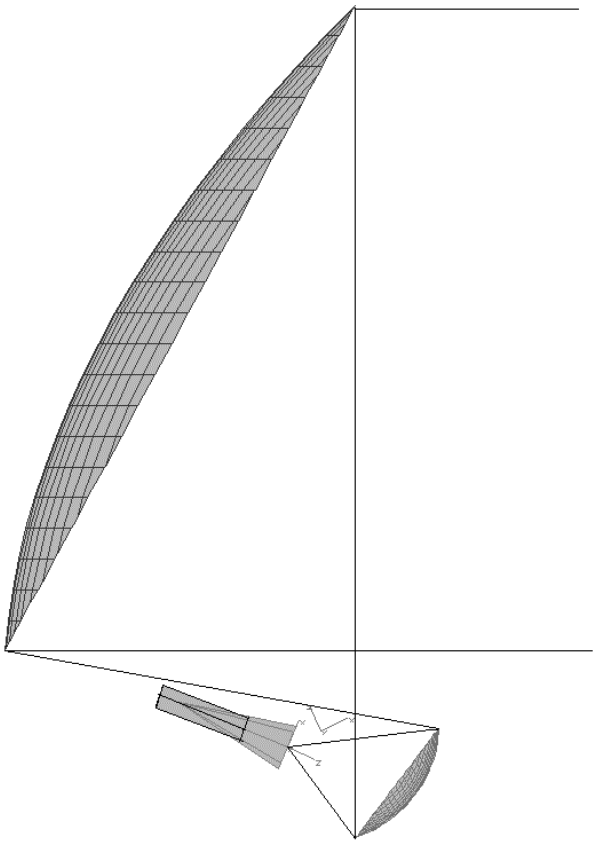

Figure 5.4: Working principle of the offset gregorian antenna [47].

5.5 Antenna Design

An important part of the design of a radar system is the design of the antenna(s). Usually, a custom designed antenna is used for a radar system to make it suit the needs of the system as close as possible. Designing an antenna is however a very complicated task and therefore beyond the scope of this report. Reference antennas can however be used to give an accurate indication of the antenna cost and weight. To achieve the selected antenna efficiency of 0.75, an offset gregorian antenna type is required. An offset gregorian antenna consists of two reflectors, a small concave one to spread the radio signal across the main reflector and the concave main reflector. An offset antenna means that the antenna itself and the small reflector are placed outside of the aperture of the main reflector, to prevent those parts from blocking the signal. The offset gregorian antenna is illustrated in figure 5.4.

Comparable reference antennas were found from Anderson, [48] and [49]. These are a 0.6 m and 1.8 m diameter antenna with an offset feed. They are not gregorian, but the manufacturer already gives an efficiency factor of 0.7–0.75. The weights are 6 kg and 32 kg.

6 | Mechanical Subsystem Specifications

This chapter discusses the mechanical aspects of the radar design. The overview of the radar antennas is given in section 6.1. The radar antennas are mounted on a positioner which allows horizontal rotation, this is explained in section 6.2. The effect of the wind turbine tower vibration is discussed in section 6.3. The velocities around the nacelle and the aerodynamics of possible radome shapes are discussed in section 6.4. The material choice of the radome wall is explained in section 6.5. An overview of the mounting possibilities and the design option tree is given in section 6.6. The final layout and structure of two radar system configurations is discussed in section 6.7. The risk analysis of the mechanical system is discussed in section 11.6. The cost analysis of the mechanical subsystems is explained in section 12.1.2. The manufacturing post-DSE procedures are given in section 13.1. The subsystem recommendations can be further found in section 13.4.2

6.1 Payload Overview

Table 6.1 gives a summary of the requirements and specifications of the payload based on the selected antennas (see section 5.4.1). The weight of the antennas is based on [50].

Table 6.1: Positioner requirements based on selected antenna.

Parameter	**Value**
Rotation range	90°
Rotation speed	22.5 °/s
Design wavelength (λ)	3 cm
Beamwidth	1.4°
Antenna 1 (transmitter) diameter	1.5 m
Antenna 1 focal point distance (p_1)	0.9 m
Antenna 1 width	0.16 m
Antenna 1 weight (m_1)	40 kg
Antenna 2 (receiver) diameter	0.6 m
Antenna 2 focal point distance (p_2)	0.4 m
Antenna 2 width	0.06 m
Antenna 2 weight (m_2)	10 kg

6.2 Antenna Rotation and Positioner

The selection of an appropriate antenna positioner depends mainly on the selected antenna's size and mass. Technical requirements considered are pointing accuracy/resolution, rotation velocity/acceleration, mechanical stability/robustness, delivered torque, weather operation performance and controllability. Other selection parameters are size, mass, durability and costs. In this section, an overview of commercial available positioners will be given, the required torque of the rotation engine is calculated and an estimation on the size and mass of the positioner is made.

6.2.1 Commercial Available Positioners

There are multiple types of positioners with different axis systems; the most common types are Elevation (EL)-over-Azimuth (AZ) and AZ. Depending on the alignment requirements of the antenna a selection can be made. In table 6.2, an overview of commercial available positioners can be found.

Table 6.2: List of commercial available positioners and their performance.

System	Mass [kg]	Size (H×W×D) [m]	Maximum Payload [kg]	Rotation Accuracy [°]	Max. rotation velocity [°/s]	Deliverable Torque [Nm]	Type
ORBIT AL-4012S	40	-	45.5	0.04	20	120	EL/AZ
ORBIT AL-4016S	150	1.01×0.4×0.4	120	0.04	20	200	EL/AZ
ORBIT AL-4034D	2100	-	1400	0.03	15	5750	EL/AZ
FLIR PTU-D300E-EX	13.5	-	40.5	0.006	22	-	EL/AZ
FLIR PTU-D100E	9.1	0.3×0.2×0.2	11.3	0.0075	-	120	EL/AZ
ORBIT FR AL-160-1	10	0.14×0.14×0.14	23	0.03	9	70	AZ
ORBIT FR AL-260-1	11	0.16×0.16×0.16	45	0.03	9	60	AZ
ORBIT FR AL-360-1	20	0.20×0.20×0.20	136	0.03	9	120	AZ
ORBIT FR AL-4269-1	52	0.57×0.26×0.26	45	0.04	15.6	124	EL/AZ
ORBIT FR AL-4270-1	52	0.57×0.32×0.32	91	0.03	12	207	EL/AZ

The radar system will be horizontally aligned as explained in section 6.7.2. This means only AZ rotation is required for the flow visualisation in a horizontal field. Most commercial positioners for antennas have EL and AZ alignment, they are also included in table 6.2 in case they better fulfil the requirements.

6.2.2 Torque Calculation

The deliverable torque is based on the the required rotation acceleration and the moment of inertia of the rotating payload. Assuming that the mass is evenly distributed over the antenna dish area, the moment of inertia I can be calculated with

$$T = I \cdot \alpha \tag{6.1}$$

and the torque T with

$$I = \int r^2 \, \mathrm{d}m = \rho \int r^2 \, \mathrm{d}A \tag{6.2}$$

For these, α is the rotational acceleration, m is the mass, r is the mass distance from the rotation axis, ρ is the density (kg/m^2) and dA is the surface area.

The shape of the parabola (see figure 6.1a) can be found with

$$y^2 = 4 \cdot p \cdot x \tag{6.3}$$

where y and x are the Cartesian coordinates of the parabola and p is the distance between the focal point and the centre of the parabola. For the preliminary estimation, the weight of the antenna will be equally divided over the area of the parabola A. The density ρ, or mass per area, can be calculated by using the area relation of a circle with the line length s of the parabola as radius.

$$s = \int_0^{D/2} \sqrt{1 + [f'(y)]^2} \mathrm{d}y = \int_0^{D/2} \sqrt{1 + \left[\frac{\mathrm{d}}{\mathrm{d}y} \cdot \frac{y^2}{4p}\right]^2} \, \mathrm{d}y = \int_0^{D/2} \sqrt{1 + \frac{y^2}{4p^2}} \, \mathrm{d}y \tag{6.4}$$

$$A = \pi s^2 \tag{6.5}$$

$$\rho = \frac{m}{A} \tag{6.6}$$

The distance r from the antenna surface dA to the rotation axis depends on the parabolic shape of the antenna dish, the offset and angular position; it can be calculated with

$$r = \sqrt{[y \cdot \sin(\theta)]^2 + \left[L + \frac{y^2}{4p}\right]^2} \tag{6.7}$$

where y is the Cartesian coordinate that represents the radius of the antenna circle, θ is the parabola circle angle, L is the offset from the rotation axis and p is the focal point distance from the centre of the parabola. Figures 6.1b and 6.1c give a geometric overview of the relation.

The calculation of the moment of inertia around an axis for an antenna dish becomes:

$$I = \int r^2 \mathrm{d}m = \rho \int r^2 \mathrm{d}A = \rho \int_0^{2\pi} \int_0^{D/2} ([y \cdot \sin(\theta)]^2 + \left[L + \frac{y^2}{4p}\right]^2) y \; \mathrm{d}y\mathrm{d}\theta \tag{6.8}$$

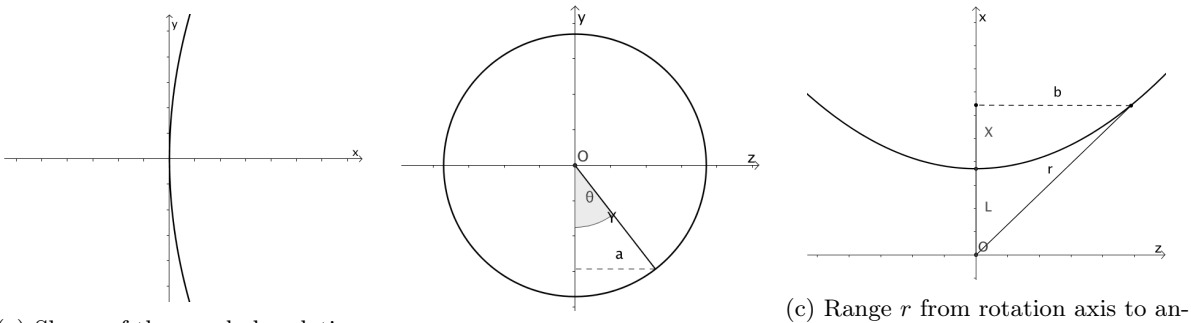

(a) Shape of the parabola relation. (b) Antenna dish frontal cross-section. (c) Range r from rotation axis to antenna section.

Figure 6.1: Parabola antenna dish geometry.

Torque Estimation

To make a preliminary estimation of the required torque, the parameters listed in table 6.1 will be used. The calculated results are listed in table 6.3.

Table 6.3: Results of the moment of inertia estimation.

Parameter	**Unit**	**Antenna 1**	**Antenna 2**
s	m	0.771	0.307
A	m^2	1.87	0.30
ρ	$\mathrm{kg/m}^2$	21.4	33.3
I	$\mathrm{kg\,m}^2$	5.6412	0.2233

For an angular acceleration of 40 $^\circ/\mathrm{s}^2$, the required torque becomes

$$T = (I_1 + I_2) \cdot \alpha = (5.6412 + 0.2233)\ \mathrm{kg\,m}^2 \cdot \frac{40^\circ \pi}{180^\circ} \frac{\mathrm{rad}}{\mathrm{s}^2} = 4.09\ \mathrm{Nm} \tag{6.9}$$

To verify this value, it can be compared to the required torque for a cylinder dish with the same mass, diameter and angular acceleration rotating around an axis:

$$T = I \cdot \alpha = \frac{m \cdot r^2}{4} \cdot \alpha = (\frac{40 \cdot 0.75^2}{4} + \frac{10 \cdot 0.3^2}{4})\ \mathrm{kg\,m}^2 \cdot \frac{40^\circ \pi}{180^\circ} \frac{\mathrm{rad}}{\mathrm{s}^2} = 4.08\ \mathrm{Nm} \tag{6.10}$$

It can be seen that the verification value is (almost) the same as the calculated required torque.

Positioner specifications

Based on the requirement from table 6.1 and required torque in the range of 7 Nm, it can be seen that *ORBIT FR AL-260-1* from table 6.2 fits the requirement and its characteristics can be used as a reference for further design.

Verification

After the radar platform has been build, a test can be conducted to make sure that the required rotational rate can be met. Furthermore, an endurance test can be done to ensure the system will continue to work over its lifetime. Since the antenna positioners are off the shelf components, they are already validated by the manufacturer and their specifications are known. However, during the system integration test the accuracy of the positioners will be validated again.

6.3 Wind Turbine Tower Vibration

According to [51, 52], the wind turbine nacelle horizontal peak acceleration (caused by vibration) is in the order of 1 m/s^2 and the peak displacement in the order of 0.1 m. This acceleration may influence the accuracy of the radar measurements. The velocity deficit in the flow is calculated with the Doppler shift method. The velocity of the wind turbine nacelle also creates a doppler shift, which is an unwanted effect. To find the velocity difference created by the nacelle acceleration, the time of one measurement must be known; this can be calculated with

$$\Delta t = \frac{2d}{c} = \frac{2 \cdot 500 \text{ m}}{3 \cdot 10^8 \text{ m/s}} = 3.3 \cdot 10^{-6} \text{ s} \tag{6.11}$$

where d is the maximum measurement distance and c is the speed of light.

The maximum velocity difference created by the nacelle acceleration can now be found

$$\Delta v = a_{max} \cdot \Delta t = 1 \text{ m/s}^2 \cdot 3.3 \cdot 10^{-6} \text{ s} = 3.3 \cdot 10^{-6} \text{ m/s} \tag{6.12}$$

where a is the acceleration of the nacelle. The calculated velocity difference is magnitudes smaller than the velocity difference that will be measured in the flow field; this means that the doppler shift created by the nacelle vibration can be neglected.

The peak displacement of 0.1 m can cause small range errors. If necessary, this can be corrected in post-processing. The mechanical solution will not compensate for this displacement.

6.4 Aerodynamics

According to reference wind turbines [2] the nacelle width and height are usually in the range of $0.04D$ to $0.06D$. From [3], it can be found that the streamwise velocity at given y/D at $x/D = 0.5$ can range from $0.3V_\infty$ to $0.6V_\infty$. Thus it is assumed that the streamwise velocities on top and at the sides of the nacelle are the same. whereas below and behind the nacelle, the streamwise velocities are considerably lower due to shadows of the tower and the nacelle, respectively. Radial and azimuthal velocities are relatively small and are neglected at the current design stage.

From [53], some aerodynamic constants can be picked:

- Drag coefficient of a sphere: 0.47 (at Reynolds number from 10^3 to $5 \cdot 10^5$)
- Drag coefficient of a cylinder: 1.2 (at Reynolds number from 10^3 to $5 \cdot 10^5$)
- Drag coefficient of a cylindrical cone: 0.7 (for structures in Atmospheric Boundary Layer (ABL))

The radome is designed as a combination of cones and spheres. The precise estimation of the drag coefficient would require the use of CFD, which is outside the scope of the report. Therefore, it is decided to use the cylinder drag coefficient to model the drag. The corresponding reference area is a rectangle resulting from the radome's maximum width and height. Note that the actual drag is expected to be less so the given design will be stiffer than required.

In [53], the shielding effect is described: In case of two bodies placed one behind the other the drag of the second one is usually smaller than in free flow, because of reduced dynamic pressure within the wake of the first body.' If a cylinder is placed behind another one the drag coefficient reduces from 1.17 in free stream to approximately 0.3 at x/D from 3 to 8. At x/D from 0 to 2, the drag coefficient even becomes negative because suction behind first cylinder. Thus, if the radome is installed behind the nacelle or behind the tower, the drag will be considerably lower.

6.5 Radome Wall

Purposes of a radome are [26]:

- Protect the radar dish from rain, snow, hail, sand, salt spray, insects, animals, UV damage, and wide temperature fluctuations
- Shield the radar dish from wind, provide stability

The general requirements on the radome are:

- Provide low signal loss at given bandwidth
- Do not raise the sidelobe level significantly
- Provide a low antenna noise temperature
- Not cause boresight (direction of maximum antenna gain) to shift

Note that this report will only use the signal loss as the driving criteria. When the electromagnetic wave hits the dielectric wall, a part of the signal is reflected back and the rest is transmitted. In order to minimise the impact to the radiation pattern and insertion loss, the reflection should be reduced. This is achieved by minimising the dielectric constant of the radome wall by choosing appropriate materials and layout. Radome walls are often designed with regards to signal wavelength λ. There are multiple radome wall layouts available that are used in various material combinations, values are taken from [54] and [55]:

- Electrically thin wall - Uses extremely thin walls—less than 0.1λ. The transmission of power is usually in the range of 70–80 % range. From [55]: '...signal reflections at the free-space/dielectric boundary are cancelled out by out-of-phase reflections from the dielectric/free space boundary on the other side of the dielectric material'.
- Half-wave wall - The radome wall thickness is made 0.5λ. Similarly to the thin-wall, the reflected signals are cancelled. Additionally, the half-wave wall also provides more structural strength. The transmission power exceeds 84 %.
- Full-wave wall - Similiar to half-wave except for additional heat losses due thicker walls. The transmission power is 60 %, yet the provided strength is relatively high.
- A-sandwich wall - From [54]: '...two thin outer skins of a solid dielectric material separated by a lightweight, low-dielectric core material. This type of construction provides a high strength-to-weight ratio and good electrical qualities for X-band and lower frequencies'. The skins are usually electrically thin and placed integral amount of quarter wavelengths apart such that their reflections are cancelled. The transmission power ranges from 86 % to 92 %.
- B-sandwich wall - Is the reverse of the A-sandwich: low-dielectric skin material and a solid core. The B-sandwich has exceptional electric properties. However, low-dielectric skins are usually less durable when exposed to the environment.
- Multiple-layer - For high-frequency bands, the wavelength becomes lower, allowing layering of materials of specific thickness. The effectiveness of such walls varies.

The A-sandwich suits the requirements best. The core is taken 0.5λ in order to optimise the power transmission. The skin thickness is optimised to withstand the stress and be simple to produce.

The material considered for the design are hexcel Nylon Phenolic (NP) core with E-glass reinforced skins [56]. These materials provide sufficient strength while being light. Relevant material properties are given in table 6.4. Other materials considered are: ceramic foam core, heat resistant phenolic—discarded as it is designed with high temperatures in mind—S-glass, D-glass and quartz—discarded due to higher cost while not improving the design substantially.

Table 6.4: Relevant material properties [56].

Property	NP	E-glass
Density [kg/m^3]	64	2540
Youngs modulus [MPa]	83 (L-direction)	7200
Yield strength [MPa]	1.8 (L-direction)	1080 (compression)
		3445 (tension)

6.6 Mounting

This section discusses multiple installation options of the radar system on the nacelle. First the relevant design factors will be discussed, followed by a DOT and a final selected option.

6.6.1 Influencing Factors

Factors that influence the installation design are:

- Weight - Relatively unimportant factor. Some options come with larger total weight than other, however the difference is minor and will not be used as a driving factor.
- Aerodynamic loads and stability - An important factor as it influences the system operations and usability of obtained data. Aerodynamic loads are high at the top and side of the turbine and lower behind and under the nacelle due to the shadow of the wind turbine.
- Obstructions of view - Very important factor as it directly influences the usability of the system. Note that some wind turbines have some components mounted on top of the nacelle, see figure 6.2. If they come into the view of the radar the data will be corrupt.
- Installation complexity - An important factor as some options are too complex and would require unfeasible amount of resources in order to install the system.
- Amount of intrusion to wind turbine structure - Very important factor that stems from design weight, aerodynamic loads and position. Customers are highly against modifying the wind turbine structure due to Original Equipment Manufacturer (OEM) warranty regulations.

Figure 6.2: Vestas V80 [2], the radiator on top of the back of the nacelle obstructs the view of the radar.

6.6.2 Installation Design Options

Several installation options were considered, these are shown in the DOT in figure 6.3. Some design options can be directly eliminated: It is unfeasible to install the system on the side of the nacelle as it will result in asymmetric data and asymmetric loads on the wind turbine. Furthermore, it is unfeasible to design an installation behind the nacelle as the layout of the nacelle's rear wall differs substantially depending on the wind turbine. The design with extendable legs is questionable as it will require a height differential of approximately 1.5 m, which, in turn, results in larger loads in the connection points and larger intrusions on the wind turbine structures. Removing wind turbine elements that obstruct the view might be impossible as some of them are vital for wind turbine operations. Installing the system behind the tower is unfeasible as it does not rotate with the nacelle. Clamping the radar underneath the nacelle is neglected due to the complex installation process and high level of intrusion to the nacelle structure.

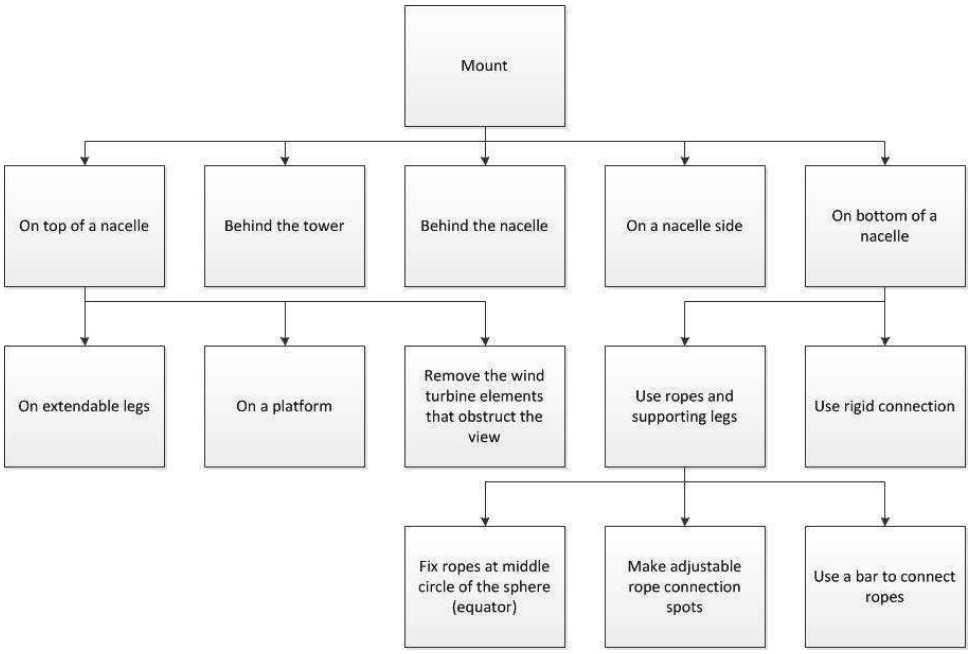

Figure 6.3: DOT of the radar mounting options.

All options discussed so far require clamping, which is highly discouraged due to structural intrusion limitations. There are, however, two options that do not require clamping: Some wind turbines have platforms on top of the nacelle that are suited for radome installation. It is assumed that clamping the radar to the platform is not considered as an intrusion to the stress bearing structures of the wind turbine. Furthermore, some wind turbines have safety rails that maintenance personnel attach to when on top of the nacelle. These rails are designed to support the weight of multiple humans. Therefore, it is assumed that rails can support the weight of the radome. Options with a hanging platform and bar are discarded due to added weight and more complex stability requirements.

Now, there are two design options left to trade off. The first one is to hang the radar underneath the nacelle on ropes and stabilise it with extendable legs. The ropes provide the upward force while the extendable legs will be used to stabilise the radar and if necessary provide an elevation angle. The second option is to fix the radar on top of the nacelle on the platform. This option also requires extendable legs that will be fixed to the platform and provide elevation if required.

Note that both options mentioned can be blended into a single design. This way the system will become universal. However, there will be two different load cases which must be satisfied.

6.7 Structures

This section discusses the design layout and corresponding dimensions of the mounting system. Furthermore, the stability of the system and installation design are discussed.

6.7.1 Structural Design and Dimensions

The layout of the radar components, including the shape of the radome, will be outlined in this section. After that, the dimensions and locations of the rope attaching the radome are given. The verification of these calculations is then discussed.

Radome Layout

The design is simplified to two spheres that are connected tangentially by a cone and an additional cone that connects the larger sphere to the disk base, see figure 6.4. The rotational system and electronics are placed on the disk base, this will be further referenced to as the base block. The inner radius of the larger sphere (transmitter) is set such that the focal point of the transmitter antenna is inside the radome:

$$r_{ti} = \sqrt{(\frac{D_t}{2})^2 + w^2} + d_{offset} \tag{6.13}$$

where D_t and w_t are the diameter and the width of the transmitter antenna and d_{offset} is the distance between the sphere of radius that antenna sweeps during rotation and inner radius of the radome given in equation 6.13. This distance is also used as an offset distance between transmitter and receiver dishes as well as between the transmitter antenna and the base block. The distance is deemed sufficient for possible additional components such as shrouds (see section 13.4.1), etc. Note that the antenna actually does not sweep a sphere but a cylinder with spheres on sides. For purposes of simplicity, it is assumed to be a sphere.

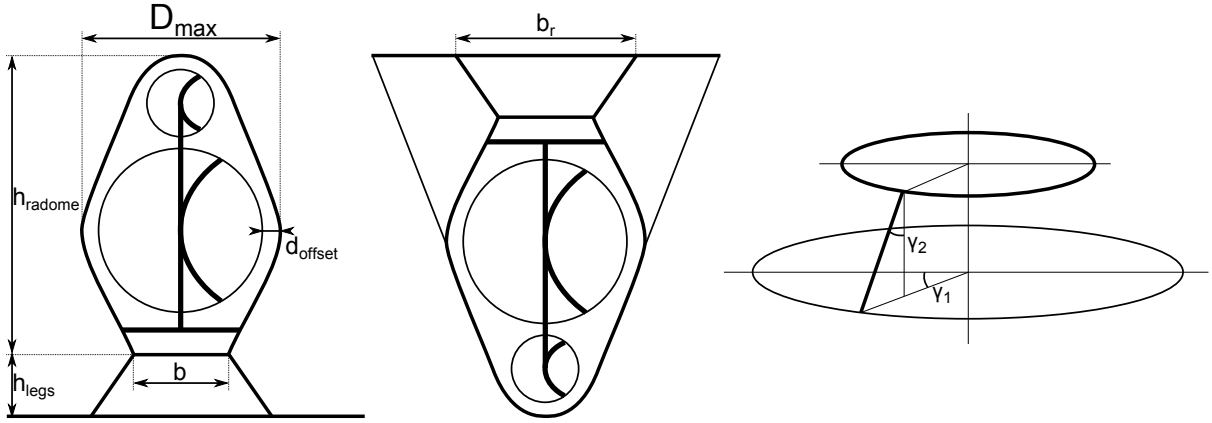

Figure 6.4: Radome layout schematics. Left: Side view of the radome installed on the platform. Middle: Rear view of the radome installed under the nacelle. Right: A leg layout.

Radome Dimensions

In order to obtain skin thickness, a simple Finite Element Model (FEM) analysis was performed to determine von Mises stresses in the radome. Calculations have been made for the hanging installation for the section of the radome loaded in compression. There, the loads are highest due to the weight of the payload and extendable legs. The rope connection is chosen at the widest point of the radome such that the angle between the rope and the horizontal is minimal—then the shear side force is minimal. Note that the shear stress in the skin is largest at the rope/radome connection location.

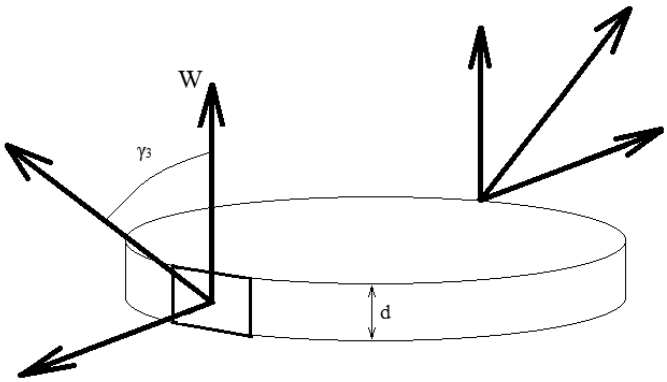

Figure 6.5: Forces at the rope/radome connection.

It is assumed that the radome is manufactured such that it is made by a finite amount of rings. In that case, the ring that is connected to the rope will experience highest stress, see figure 6.5. Using the safety factor of 1.5, the von Mises stress is satisfied at a ring width of 0.6 mm and skin thickness of 0.5 mm.

The ropes can either be designed in house or be taken off the shelf. The *8X19* wire rope with sisal fibre core provides an E-modulus of 110 GPa [57]. Using the *Vestas V80* as a reference, the length of the rope during the operations is 5.5 m. At the given radome mass, the elongation is negligible. The mass of a single rope is 1.2 kg. Note, however, that if the radome is hoisted to the nacelle from ground, the required rope length would be 80 m with a mass of 22 kg. The dimensions and masses of the radome are given in table 6.5, the technical drawing can be found in appendix B.

Table 6.5: Mechanical subsystem specifications.

Specifications	Value
h_{radome}	2.745 m
h_{legs}	0.2 m
d_{max}	1.83 m
d_{offset}	0.13 m
t_{core}	15 mm
t_{skin}	0.5 mm
γ_1	54.74°
γ_2	45°
γ_3	17°
b_r	1 m
b	1.4 m
m_{radome}	30 kg
$m_{rope(operations)}$	2.4 kg
m_{legs}	10 kg
$m_{payload}$	90 kg
m_{total}	132.4 kg

Radome Verification

The radome calculations used at the given stage are simplified and an additional in-depth FEM analysis is required to finalise and verify the design. Then, the prototype of the radome should be tested to check

if the subsystem requirements are met. These include the load bearing capabilities as well as electric properties. If the verification is successful, the subsystem can be integrated into the final design.

6.7.2 Stability

The stability is one of the design factors which influences the installation design. In this section, a basic estimation is done on the loads on the legs of the radar system in two configurations: one where it is positioned below and one on top of the nacelle.

Under the Nacelle

When the system is mounted under the nacelle, it will be pulled against the underside of the nacelle by ropes. The legs are supposed to support the system and stabilise it. To design the legs, first the loads on the legs must be calculated. In figure 6.6, a simplified side view overview of the forces can be seen. Point A and B are the positions where the legs touch the nacelle and point C is the location of the centre of gravity. For simplification, it is assumed that the centre of pressure due to drag and the connection point of the ropes are also located at point C.

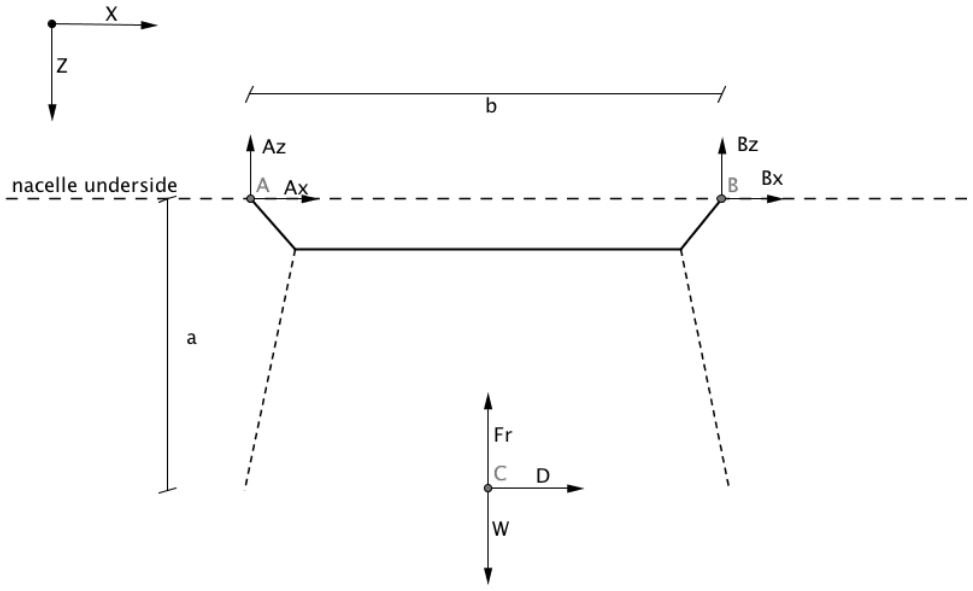

Figure 6.6: Side view of reaction forces on the legs of the system.

Taking the sum of forces and moments, we can obtain the reaction forces on the legs:

$$\begin{aligned}
&\sum F_x = A_x + B_x + D = 0 \\
&\sum F_z = A_z + B_z + F_{rope} - W = 0 \\
&\sum M_A = b \cdot B_z + \frac{b}{2}(F_{rope} - W) + a \cdot D = 0 \\
&\sum M_B = b \cdot -A_z + \frac{b}{2}(W - F_{rope}) + a \cdot D = 0
\end{aligned}
\qquad
\begin{cases}
A_x + B_x & = -D \\
A_z + B_z & = W - F_{rope} \\
B_z = -0.5F_{rope} + 0.5W - \frac{a}{b}D & < 0 \\
A_z = -0.5F_{rope} + 0.5W + \frac{a}{b}D & < 0
\end{cases} \tag{6.14}$$

The weight W of the system equals 1294 N. Length a equals 0.91 m and represents the distance between the nacelle and the centre of gravity. Length b equals 1.4 m and represents the distance between the leg points A and B. Drag is calculated between 0 and 290 N for wind velocities ranging from 0 to $0.6V_\infty$ (0 till 15 m/s). F_r is the vertical force of the ropes.

The reaction forces at A_z and B_z must have a negative value because the system is pressed against the nacelle and not clamped. To ensure that the system stays stably pressed, the vertical rope tension should be at least 1671 N in this configuration. The forces on the legs become

$$\text{for } D = 0 \text{ N: } \begin{cases} A_z = B_z = & -188.5 \text{ N} \\ A_x = B_x = & 0 \text{ N} \end{cases} \tag{6.15}$$

$$\text{for } D = 290 \text{ N: } \begin{cases} A_z = & 0 \text{ N} \\ B_z = & -377 \text{ N} \\ A_x = B_x = & -145 \text{ N} \end{cases} \tag{6.16}$$

On Top of the Nacelle

On top of the nacelle the radar will be positioned upward and clamped on a platform. There will be no rope attached in this configuration. Equation (6.14) can still be used, but F_{rope} equals 0 N and length a will be negative because the system is positioned upward. The vertical force on the legs in this configuration can be negative and positive because the legs are clamped. Figure 6.7 shows an overview of the configuration when the radar is mounted on top of the nacelles platform.

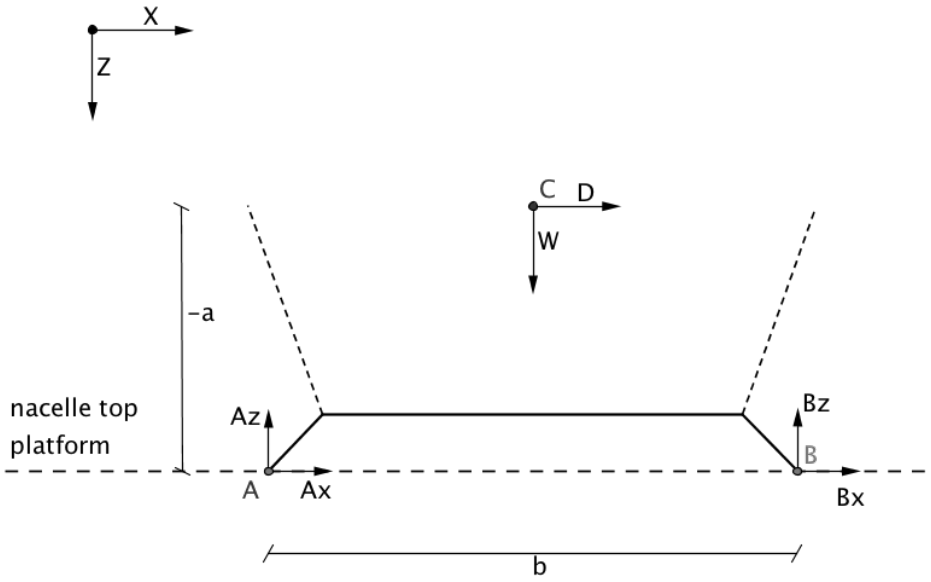

Figure 6.7: Side view of reaction forces on the legs of the radar mounted on top of the nacelle.

The force on the legs become:

$$\text{for } D = 0 \text{ N: } \begin{cases} A_z = B_z = & 647 \text{ N} \\ A_x = B_x = & 0 \text{ N} \end{cases} \tag{6.17}$$

$$\text{for } D = 814 \text{ N: } \begin{cases} A_z = & 118 \text{ N} \\ B_z = & 1176 \text{ N} \\ A_x = B_x = & -407 \text{ N} \end{cases} \tag{6.18}$$

In the case of max. drag, the legs at position B carries $\sqrt{B_x^2 + B_z^2} = 1244$ N of compression force and the legs at point A carries 424 N of tension force.

When a four leg configuration is used, two legs can be positioned at point B; this reduces the force on both legs to 622 N. The other two legs are positioned at point A, this reduces the max. force on both

legs to 212 N, this occurs when there is 814 N drag. For further design of the legs a max. force of 622 N will be considered.

Leg specifications

The length of the legs depends on the inclination of the underside of the nacelle. The max. inclination angle will be considered 10°. This means when the legs are positioned 1.4 m from each other the max. difference in height equals 24 cm.

To adjust for this size and horizontally align the system, a hydraulic jack can be used as a leg; the lifting capacity of this jack should be higher than the max. force of 622 N on one leg. A commercial hydraulic jack example for this requirements is *Enerpac RC-59* [58], it is capable of lifting 5000 N and its length ranges from 32.3 cm to 55.5 cm. The mass of this jack is 2.8 kg and the diameter is 3.8 cm. Note that although it does not fit the current dimensions perfectly it can be used as a benchmark for development.

Verification

The wind conditions on top and under the nacelle can be measured. Based on these conditions, the aerodynamic loads that are present on the radar system can be verified by means of a windtunnel test. The hydraulic legs are off-the-shelf products, so verification is not needed; however the connection of the legs should be verified for maximum loads.

7 | Electronics Subsystem Specifications

In this chapter, the design of the electronics subsystem is described. First, an overview of the system will be given in the form of a block diagram in section 7.1, then all components will be discussed in more detail in section 7.2. The subsystem verification is presented in section 7.3. Post-DSE finalisation of the subsystem is proposed in section 13.1. Finally the risk analysis, cost analysis and recommendations are given in sections 11.6, 12.1.3 and 13.4.1

7.1 System Overview

The block diagram of the radar system is given in figure 7.1. The core of the radar system is the control processor. This component drives the radar signal, it processes the received signal, it manages the rotation of the antennas and it uses the measured weather conditions to determine how to do this. The Voltage Controlled Oscillator (VCO) generates the high frequency radar signal as determined by the processor. The power divider splits the high frequency signal in two portions: one half continues to the power amplifier, the other half is sent to the demodulator. The power amplifier amplifies the radar signal to high power levels. The received radar signal is amplified by the Low Noise Amplifier (LNA). A LNA is capable of amplifying the weak received signals while adding only a small amount of noise to the signal. The high-frequency radar echo signal is then demodulated using the transmitter signal to a low frequency signal, the frequency difference between the two signals. This difference signal consists of a real I component and a complex Q component. The I and Q signal filtered by a low-pass filter to make sure that only the low frequency difference, or beat frequency signal is passed to the data acquisition. The data acquisition converts the analog beat frequencies to a digital data stream. This data stream is then partially processed by the control processor, after which it is sent to the data processing and storage system. The weather conditions determination component measures the current weather conditions to give the control processor the ability to determine whether the conditions are suitable for measurements. The rotation of the antennas is driven by the antenna rotation component as controlled by the control processor. The power management system finally provides and distributes power to all the system components.

7.2 System Components

In this section, the components of the radar system are discussed in further detail. For each component, a more detailed description of its functionality will be given, a specific device or design will be selected for that component and an estimation of the weight (if significant) will be made.

7.2.1 Control Processor

The control processor is the heart of the radar system. It controls the generation of the radar signal, it pre-processes the received signal and controls the rotation of the antennas. Especially the pre-processing of the received signal requires a strong processor. The selected processor board is the *EVMK2H* from Texas Instruments [59]. This is a powerful processor board that is flexible in usage due to its large variety of external connectors and extendable memory.

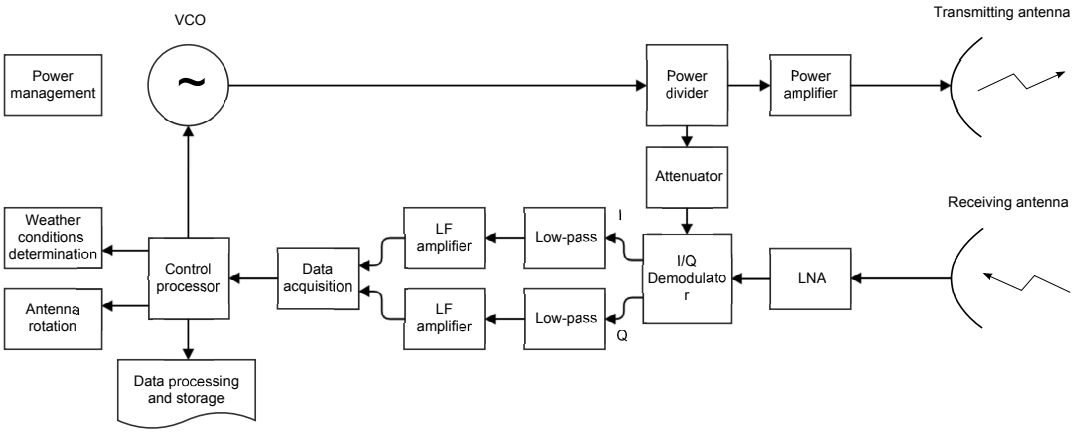

Figure 7.1: Block diagram of the T-WRAX electronic subsystem.

7.2.2 VCO

The VCO provides the radio signal at the desired frequency. Its oscillation frequency can be controlled by variation of a connected control voltage. Sweeping the control voltage in different fashions results in the corresponding FMCW signal. The VCO is typically integrated as part of a Phase-locked Loop (PLL) in order to ensure that the output signal's phase stays constant and induces as little phase noise as possible.

VCOs are common to provide frequencies in the range of 1–25 GHz with sweep bandwidths of 0.2–10 GHz. For lower or higher frequencies, frequency dividers or multipliers can be used, respectively. The advantage of using frequency multipliers or dividers is that the range of potential frequencies the circuit is able to generate becomes larger, which makes the radar system more flexible for different application cases. However, this comes at the cost of introducing noise for every additional unit in the circuit as well as the price of the units themselves. In the case of our system, we can settle with a single VCO that generates frequencies in the X-band since there is not expected to be a significant shift in operating frequencies in order to detect light precipitation.

A suitable VCO with an integrated PLL circuit is the *HMC778LP6CE* by Hittite [60]. This VCO is designed to output X-band frequencies and introduces a very low phase noise due to the PLL circuit. Its output power is 9 dBm, that is 7.9 mW (dBm is milliwatts expressed in the decibel scale), so for the power budget calculation, we take

$$P_{VCO} = 9 \text{ dBm} \tag{7.1}$$

7.2.3 Power Divider

The power divider essentially splits the signal into two parts with the same properties as the input signal except for the signal power. One of these output signals is then being transmitted via the radar antenna, the other one is being fed to the I/Q demodulator for mixing it with the signal the receiving antenna inputs to the demodulator.

A suitable power divider is the *1G0618-20* by Anaren [61]. It has an insertion loss of 0.6 dB, which means that the input signal to the primary output will be lowered by 0.6 dB. Its coupling factor is 20 dB, which means that the secondary output signal strength is lowered by 20 dB.

For the power budget calculation, we set

$$L_{split,1} = 0.6 \text{ dB} \tag{7.2}$$

and

$$L_{split,2} = 20 \text{ dB} \tag{7.3}$$

7.2.4 Amplifier

In order to achieve the desired output power at the transmitting antenna, the signal's power inside the circuit has to be amplified. Other components have certain requirements on minimum and maximum input power as well, which has to be taken into account when deciding at which locations to amplify the signal and by how much gain to amplify it.

After passing through the power divider, the signal is amplified before it is output by the antenna. A suitable power amplifier is the *AML618P4014* by Microsemi [62]. It can amplify signals in the X-band frequency range with a gain of 50 dB and has an output power of 49 dBm.

The two signals that are leaving the I/Q demodulator have to be amplified by 16.7 dB each. A suitable amplifier for this purpose is the *ZHL-6A+* by Mini-Circuits [63].

For the power budget calculation, we set the power amplifier's gain

$$G_{PA} = 38.6 \text{ dB} \tag{7.4}$$

and the low-frequency amplifier's gain

$$G_{LFA} = 21 \text{ dB} \tag{7.5}$$

7.2.5 Power Attenuator

In order to achieve the desired input power for the I/Q demodulator, the split signal from the secondary output of the power divider has to be attenuated by 52 dB. A suitable attenuater for this is the *BW-S50W2+* by Mini-Circuits [64].

For the power budget calculation, we set the power attenuator's loss

$$L_{att} = 50 \text{ dB} \tag{7.6}$$

7.2.6 LNA

The LNA is a special amplifier for very weak signals. It amplifies the signal received from the receiving antenna for further processing by the I/Q demodulator.

A suitable LNA is the *AMF-6F-09001100-09-10P* by Miteq [65] which provides a gain of 52 dB and has a noise figure of 0.9 dB. As the received signal strength is estimated to be -145 dBm, we may need two cascaded LNAs in order to amplify the signal enough for the I/Q demodulator.

For the power budget calculation, we set the LNA's gain

$$G_{LNA} = 52 \text{ dB} \tag{7.7}$$

7.2.7 I/Q Demodulator

The received echo signal is a too high frequency signal to directly process. Directly transforming this analog signal to a digital data stream and processing that data would require a very expensive data acquisition system and processing system. A significantly simpler method is first to demodulate the received signal.

During demodulation, the received signal is mixed with the transmitted signal. This generates an output signal that, besides the two original signals, also contains the sum of those two signals and the difference between them. The difference is interesting because it is a low frequency signal that can easily be processed. If, however, this signal is simply digitised, the frequency components of this signal can be determined, but phase information of the frequency components is lost in the process. To preserve this information, an I/Q demodulator can be used. Such a demodulator creates two low-frequency signals: one is the regular real signal, I, the other one is created using the 90° phase shifted received signal. This Q signal can be used to determine the phase of the measured frequencies.

A suitable demodulator is the *EVAL01-HMC1056LP4B* from Hittite [66]. This is a simple, integrated demodulator designed for X-band. The isolation between the transmitter input and the receiver input or the low-frequency output is 40 dB, which means that including a margin of 10 dB the transmitter signal that is put in to it should be no more than 30 dB higher than the receiver signal. The signal attenuation in the demodulator is 10 dB, which should be taken in to account in the amplifier sizing.

For the power budget calculation, we set the I/Q demodulator's loss

$$L_{IQ} = 10 \text{ dB} \tag{7.8}$$

7.2.8 Low-pass Filters

The maximum frequency present in the beat signal is, as given in chapter 5, 520 kHz. To prevent aliasing of the measured signal, frequencies above this value must be filtered out before data acquisition. Since an actual filter does not cut off at one frequency but more or less gradually starts weakening the signal around a certain frequency, a margin must be applied on the filter frequency. The selected filter frequency is 1 MHz. A suitable filter is a filter from Kiwa electronics [67]. The loss of this filter at passed frequencies is 0.5 dB.

For the power budget calculation, we set the low-pass filter's loss

$$L_{LPF} = 0.5 \text{ dB} \tag{7.9}$$

7.2.9 Data Acquisition

The data acquisition component converts the analog received signal to a digital representation. Since the maximum frequency present in the beat signal after the low-pass filter will be 1 MHz, the data acquisition component must measure at at least 2 MHz to prevent aliasing. A higher value is recommended to improve measurement accuracy and completely remove the risk of aliasing. If the sampling frequency turns out to be too high, superfluous measurements can simply be ignored. A suitable data acquisition component is the *AD9650-25EBZ* [68]. This analog to digital converter has a resolution of 16 bits and a sampling rate of 25 megasamples per second. The dynamic range of an Analog to Digital Converter (ADC) is calculated using the number of bits using $DR = 20 \log 2^n$ where DR is the dynamic range and n is the number of bits. The dynamic range for this ADC is thus 96.3 dB.

The maximum input power of an ADC is calculated using the equation from [69],

$$P_{max} = 10 \log \left(\frac{V_{RMS}^2}{R_{in}} \right) + 30 \tag{7.10}$$

where P_{max} is the maximum input power, V_{RMS} is the Root Mean Square (RMS) maximum input voltage which can be calculated from the peak-to-peak voltage with $V_{RMS} = V_{P-P}/(2\sqrt{2})$ and R_{in} is the input termination resistance. For this ADC the maximum input power is 10 dBm which using the dynamic range gives a minimum input power of -86.3 dBm.

7.2.10 Antenna Rotation

For the rotation of the antennas, a motor and motor driver is required. The angular pointing of the antennas must be accurate, since 0.1° of pointing error already gives an error of 1 m at 520 m. 0.1 m of pointing error is deemed acceptable, which means that an angular accuracy of 0.011° is required.

A cheap and accurate motor system is a closed loop stepper motor. A stepper motor is a motor with many stable positions. By powering the coils in the motor in a certain order, the motor can be turned to the next stable position. This is an accurate system, but it is open loop: if, for some reason, a step is missed, there is no way for the controller to know this. For that reason, a closed-loop stepper motor system is a suitable solution: a closed-loop stepper motor measures the rotation angle of the stepper motor, which makes the system closed-loop.

The angle in between steps is, however, quite large. For the selected controller and motor system, the *HBS57* and *HBSMd* from Leadshine [70] is suitable. Their step angle is 1.2°. To achieve the accuracy of 0.011°, a gearbox with a ratio of 1.2/0.011 = 109 to 1 is required. An additional advantage of this is that a less powerful motor is required. The torque from this motor, 2 Nm, is multiplied with 109 after the gearbox. The required torque is 7 Nm from the mechanical subsystem, this requirement will be easily met. The weight of this component is 1.6 kg.

7.2.11 Weather Conditions Determination

The purpose of the weather conditions determination module is to provide information to the control processor about when suitable weather conditions for radar measurements are present. Since the radar system might be left unattended for extended periods of time, it should be able to autonomously detect when and when not to take measurements in order to save energy. It is expected that the radar system has access to the atmospheric measurement unit data of the wind turbine it is mounted on. From this data, the system can at least determine when the wind turbine is active and what the operational wind speed is. However, wind turbines may not be equipped with sensory devices that can detect precipitation.

For this reason, the radar system will be equipped with a present weather sensor. Such a sensor measures the current visibility to detect the presence of fog and measures the type and rate of precipitation. A suitable present weather sensor is the *miniPWS* from Optical Sensors [71].

7.2.12 Power Management

The power management unit supplies power to the various components of the electronics subsystem. It is assumed that power can be drawn directly from the wind turbine's generator. The power management unit will contain a power converter to provide the necessary currents and voltages required by the subsystem's components. Since the wind turbine may also not provide power at times, it will be necessary to include a battery that can be charged during operation and/or using solar panels in order to power the control processor during those times.

The design of such a module is beyond the scope of this design project and is something to be considered during a later design phase. To facilitate this design, however, an estimation of the required power for the radar system can be made. The total required power of the system is mainly driven by the required power from the power amplifier, the rotation system, the control processor and the data processing and storage system. The power amplifier uses 322 W, the peak power for the rotation system is 800 W, the peak power for the control processor is 84 W and the maximum power for the data processing and storage system is 610 W. The other components require little power. A power consumption of 5 W per component is assumed, except for the divider, low-pass filters and attenuator, which are passive. This adds another 40 W, which makes the total required power of the radar system 1860 W.

7.2.13 Data Processing and Storage

The data processing and storage system has to process a large amount of data and the operations that have to be performed on the incoming data stream are computationally intensive. The data processing system therefore has to be a powerful computer system with large storage. A suitable computer is the *Lenovo Thinkstation S30* [72]. This computer combines large computational power with low power consumption and uses 65 % recycled plastics.

7.3 Subsystem Verification

From the gains and the losses of the discussed subsystem components, we can perform a power budget calculation to verify the design choices by checking that the chosen components fulfil the requirements on input and output power. At this point an estimation can also be given of the total noise figure of the receiver chain.

For the signal power transmitted by the antenna P_t, we have a requirement of 50 W, or 47 dBm. For this calculation, consider the upper path from the VCO to the antenna in figure 7.1. We can now write

$$P_t = P_{VCO} - L_{split,1} + G_{PA} = 9 - 0.6 + 38.6 = 47 \text{ dBm} \tag{7.11}$$

with P_{VCO} being the VCO's output power, $L_{split,1}$ being the power splitter's primary output loss and G_{PA} being the power amplifier's gain. The resultant matches the requirements. Note that the power amplifier's gain is variable and has been set to a lower value than its maximum gain.

The requirements of the I/Q demodulator are that the difference between the two inputs shall not be greater than 30 dB, with a safety margin of 10 dB. Consider the path from the VCO to the upper input

of the I/Q demodulator:

$$P_{in,IQ1} = P_{VCO} - L_{split,2} - L_{att} = 9 - 20 - 50 = -61 \text{ dBm} \tag{7.12}$$

where $P_{in,IQ1}$ is the power at the upper input of the I/Q demodulator and L_{att} the loss of the attenuator. Recall that the minimum received power of the receiving antenna P_r is -145 dBm. For the path from the receiving antenna to the lower input of the I/Q demodulator, we write

$$P_{in,IQ2} = P_r + G_{LNA} = -145 + 52 = -93 \text{ dBm} \tag{7.13}$$

where $P_{in,IQ2}$ is the power at the lower input of the I/Q demodulator and G_{LNA} is the LNA's gain. We see that the difference between $P_{in,IQ1}$ and $P_{in,IQ2}$ is 32 dB. This is not ideal but still acceptable.

Finally, from the I/Q demodulator to the data acquisition module, we write

$$P_{in,DA} = P_{in,IQ2} - L_{IQ} - L_{LPF} + G_{LFA} = -93 - 10 - 0.5 + 21 = -82.5 \text{ dBm} \tag{7.14}$$

where $P_{in,DA}$ is the input power at the data acquistion module, L_{IQ} the I/Q demodulator's attenuation, L_{LPF} the low-pass filter's attenuation and G_{LFA} the low-frequency amplifier's gain. The value is higher than the required -86.3 dBm.

To find the total noise figure of the receiver chain the individual noise figures of the LNA, the low-pass filter and the low frequency amplifier have to be combined. The noise figures for these components are 0.9 dB, 0 dB (the low-pass filter is passive) and 7.6 dB respectively. These noise figures can be combined using

$$NF_{total} = NF_1 + (NF_2 - 1)/G_1 \tag{7.15}$$

Where the NF are the noise figures in normal factors and G is the gain, again as a normal factor. The resultant noise figure is, rounded, still 0.9 dB. The large gain of the LNA combined with its low noise figure makes sure that the noise figure of subsequent components is largely irrelevant.

The characteristics of the actual electronic components and the combination of them should also be verified. The steps that have to be performed to do this are:

- *Amplifiers, splitter and filters*
  For the amplifiers, the splitter and the low-pass filters the manufacturer characteristics should be verified: the given gains, the noise figures and bandwidth.

- *Transmitter chain*
  The combination of the VCO, splitter and power amplifier should be constructed to measure the performance of this combination of components, such as frequency accuracy, phase noise, total gain and possibly other characteristics.

- *Receiver chain*
  The combination of LNA, demodulator, filters and low frequency amplifiers should be constructed to measure the total receiver gain, noise figure and possibly other characteristics.

- *Weather conditions determination*
  The measurements from the weather conditions sensor can be verified using a more advanced precipitation sensor or visibility sensor.

- *Rotation system*
  The performance and accuracy of the rotation motor and controller can be measured.

- *Full electronic system*
  After complete system integration, the total power consumption of the system can be measured and the cooperation of the individual components can be verified.

8 | Data Processing Subsystem Specifications

This chapter describes the way the radar system processes the received signals to obtain useful information. First section 8.1 elaborates on the radar signal characteristics. The following sections can be read as a step-by-step plan to perform the data processing. They contain every step from received signal to wake boundary determination, starting with the deramping of the received signal in section 8.2, followed by a low-pass filter in section 8.3 and windowing in section 8.4. To receive range and velocity information the signal is transformed by a double FFT in section 8.5. Afterwards it is shown how range and velocity information can be extracted in section 8.6. The resulting data is then cleared of radar clutter in section 8.7, smoothed in section 8.8 and noise-clipped in section 8.9. In section 8.10 the determination of the wake boundaries will be explained. The corresponding data processing algorithm is shown in figure 8.1. The verification of data processing is discussed in section 8.11. The computational cost is given in section 8.12. Post-DSE procedures are discussed in section 13.1. The risk analysis, cost analysis and recommendations can be found further in sections 11.6, 12.1.4 and 13.4.3 respectively.

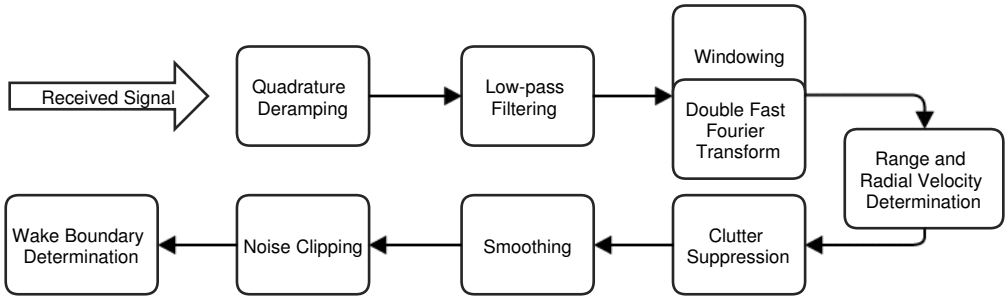

Figure 8.1: Data processing algorithm of the T-WRAX system.

8.1 Signal Characteristics

An important aspect of an FMCW radar system is the waveform generated by the frequency modulation. This waveform has a large influence on the data processing subsystem, because it determines how the system extracts information out of the signal. This section presents the waveform that is chosen for T-WRAX and explains in general the way the system will determine range and velocity.

The transmitted signal will have the shape of a sawtooth wave as shown in figure 8.2 as this is a common choice for weather radars, including reference radars such as IDRA [39]. The frequency difference, the so called beat frequency f_b, between transmitted and received signal can be related to range as the time delay of the received echo increases with range and with it the beat frequency. If the target has a radial velocity the echo signal will have a Doppler frequency f_D caused by the well known Doppler effect. This Doppler frequency will then shift the frequency of the whole echo signal either up or down depending on the radial direction of the movement. The Doppler frequency is a measure of the radial velocity. It will be added to the beat frequency and will occur as an error in the range calculation. In order to determine range and velocity the beat frequency and Doppler frequency need to be determined which will be described within this chapter.

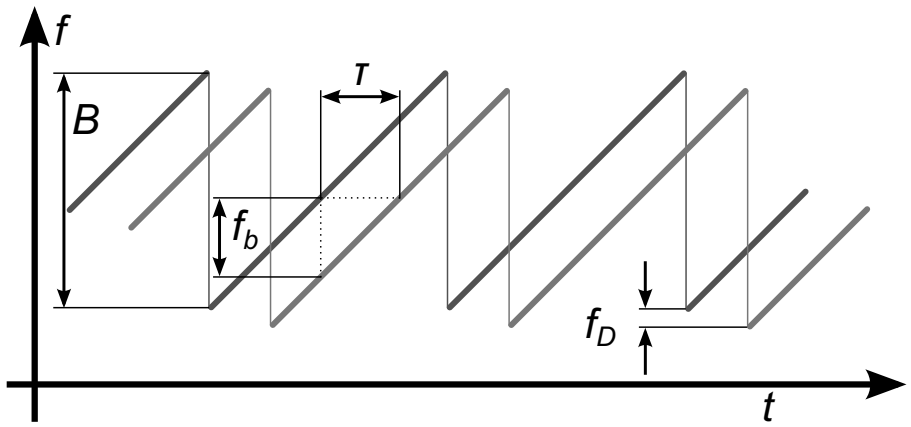

Figure 8.2: A sawtooth wave modulation as used for this FMCW radar. The red (darker) curve is the transmitted signal, the green (brighter) curve is the delayed received echo.

According to [39], the transmitted signal can be written as

$$s_T(t) = \sum_{n=0}^{\infty} A_T cos\left(2\pi\left[f_o(t-t_n) + \frac{B}{2T_c}(t-t_n)^2\right]\right)\Pi\left[\frac{t-\frac{T_c}{2}-t_n}{T_c}\right] \tag{8.1}$$

where A_T is the signal amplitude depending on the transmitted power, f_o equals the initial chirp frequency also known as carrier frequency, and slow time variable $t_n = nT_c$, with n equal to the chirp number and T_c the chirp duration.

Π is the rectangular function:

$$\Pi(x) = \begin{cases} 0 & \text{for } |x| > \frac{1}{2} \\ 1 & \text{for } |x| \leq \frac{1}{2} \end{cases} \tag{8.2}$$

As can be seen in equation (8.1), the signal is composed of an infinite amount of chirps all having the same shape of a linear frequency increase in time with rate B/T_c followed by a sudden drop to the carrier frequency, leading to a sawtooth shaped signal.

As the transmitted signal hits a point scatterer, it will be reflected. Then the received signal has a lower amplitude delayed form of the transmitted signal and it will include receiver noise η. Assuming the point scatterer is moving at a constant velocity V at a certain range R, the raw received signal can according to [39] be written as

$$s_R(t) = \sum_{n=0}^{\infty} A_R \cos\left(2\pi\left[f_o(t-t_n-\tau) + \frac{B}{2T_c}(t-t_n-\tau)^2\right]\right)\Pi\left[\frac{t-\frac{T_c}{2}-t_n}{T_c}\right] + \eta(t) \tag{8.3}$$

The time delay equals

$$\tau = \frac{2(R + V_D t_n)}{c} \tag{8.4}$$

with Doppler derived radial velocity V_D which is the actual velocity that will be measured by the radar equal to

$$V_D = V\cos(\theta) \tag{8.5}$$

where θ equals the antenna pointing angle.

8.2 Quadrature Deramping

As outlined in section 8.1, the beat frequency (f_b) of the transmitted and received signals is needed to obtain range and velocity information of scatterers. The way this beat frequency is extracted starts by creating the beat signal. This is done in a process called quadrature deramping or quadrature demodulation. This section explains the process of quadrature deramping.

Quadrature deramping is performed by an I/Q demodulator, where the I and Q stand for real and complex signal, respectively. The process works by multiplying the received signal with a sine and cosine version of the transmitted signal. This results in the following signals:

$$\begin{aligned} 2\sin\alpha\cos\beta &= \sin(\alpha+\beta)+\sin(\alpha-\beta) \\ 2\cos\alpha\cos\beta &= \cos(\alpha+\beta)+\cos(\alpha-\beta) \end{aligned} \tag{8.6}$$

where α and β contain the frequencies of the transmitted and received signals respectively. The signals with the sum term $(\alpha+\beta)$ have a higher frequency and will be filtered out after the I/Q demodulator by an analog low-pass filter. This leaves the signals with difference term $(\alpha-\beta)$, which are converted to the digital domain by an analog-to-digital converter and complexly added:

$$\cos(\alpha-\beta)+i\sin(\alpha-\beta)=\cos\xi+i\sin\xi=e^{i\xi} \tag{8.7}$$

In this equation, $\xi=\alpha-\beta=2\pi f_b t$—it is the phase difference between the transmitted and received signals, and contains the beat frequency f_b.

The quadrature deramping results in a complex signal which has two important implications. The first one being the fact that the frequency spectrum obtained through a Fourier transform will be asymmetric, concentrating signal power in the positive (or negative) frequencies. Because the noise power is spread over both positive and negative frequencies, this results in an increase in signal to noise ratio of 3 dB. Secondly, quadrature demodulation allows you to surpass the Nyquist criterion, allowing the use of the full sampling bandwidth in the sampling of the outgoing signal while doubling the amount of bits per sample.

8.3 Low-pass Filter

After the I/Q demodulation, analog low-pass filter and analog-to-digital converter only a digital beat signal is left. This signal contains the beat frequencies from every echo signal received during the entire chirp—or range. However, for the purpose of this project, only the first 520 m are of interest. Additionally, 560 m behind the radar (x-direction) the rest of the wind farm is located, which causes significant clutter that has to be suppressed. As outlined in section 8.1, higher beat frequencies correspond to a longer range. To suppress the signals of scatterers located outside our measurement range a low-pass filter is applied.

A certain beat frequency corresponds to a certain range. This relation is shown by

$$f_b=\Delta t\frac{\mathrm{d}f}{\mathrm{d}t}=\frac{2R}{c}\frac{B}{T_c} \tag{8.8}$$

From this formula, we can determine the passband of the low-pass filter. With $B=45$ MHz, $T_c=3$ ms and $R=520$ m, the passband becomes 520.36 kHz. Because the first row of turbines is located at 560 m behind the turbine, frequencies higher than 560.39 kHz have to be suppressed. The passband and the stopband provide the information needed to design a digital low-pass filter.

The filter is designed using MATLAB, with help from the filter builder application. The application uses a Kaiser window to design a low-pass filter. The pass- and stopband have been defined as calculated before. The amplitude at the passband is 1 dB, the signal is suppressed to -60 dB at the stopband. The filter's magnitude response is shown in figure 8.3.

8.4 Windowing

The radar system obtains range information by sampling the beat signal over one chirp and performing a frequency analysis by means of a FFT. The most basic way of sampling the signal over just one chirp is by taking a certain number of samples (256 in the case of T-WRAX) starting at the same time the transmitted chirp starts. This process is called windowing as it can be seen as multiplying the signal with a windowing function, 'windowing' the signal in time. The basic windowing function just described is called the rectangular window, since every sample simply has the same weight. As it happens, the rectangular window leads to strong sidelobes when the windowed signal is transformed to the frequency domain. This process is called spectral leakage and is undesirable. To reduce this effect a large amount of

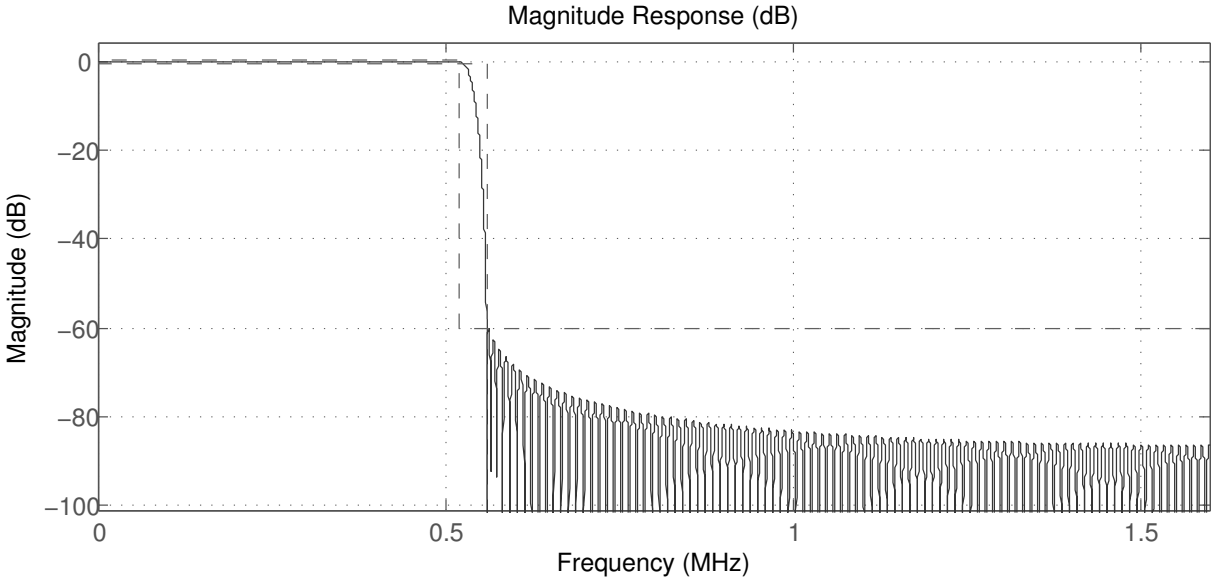

Figure 8.3: Magnitude response of the low-pass filter.

different windowing functions have been designed over the years, with a variety of frequency responses. This section describes the chosen windowing function.

For the received signal sidelobes, meaning unwanted frequencies with a certain signal power, are most of the time below noise level and therefore removed. However, for the application in a wind farm strong reflections from neighbouring wind turbines could occur and thus signal power of sidelobes would be above noise level and therefore disturb the measurements of interest. Therefore windowing is applied in order to decrease the signal power of the sidelobes.

Sidelobes in the frequency spectrum occur especially due to the reason that the observation period is not infinite in time, as it is sampled at discrete time periods. This causes spectral leakage, or generation of sidelobes, due to non periodic signals. This non-periodicity is caused by 'chopping' the signal up in chirps, which creates irregularities at begin and end of each chirp.

This spectral leakage will be reduced by using a window function. A window function can be seen as giving certain parts of each observation period of the signal different weights, thus giving signal of low interest (the sidelobes) a low weight so that it will have low influence on the measured data while keeping the part of the signal which one is interested in occurring at the dominant frequencies. Therefore applying double FFT as explained in section 8.5 is related to windowing. In the time domain the signal y is multiplied by a window function w as shown in (8.9). Equivalently in the frequency domain this means a convolution of the signal Y with the window function W:

$$Y = \mathcal{F}\{y \cdot w\} = Y * W = W(f - f_b) \tag{8.9}$$

Many different windows have been used during the last years all with certain advantages and disadvantages. An overview of the most common ones is shown in table 8.1. The first and second column are representing the bin width at different main lobe power, this width can be related to range resolution, as explained in section 8.5. A lower bin width means a better frequency resolution and therefore a higher range resolution as range is related to beat frequencies. However as can be seen in the table a lower bin width is connected to a higher maximum sidelobe level. The maximum sidelobe level should be as small as possible in order to be able to distinguish the part of interest in the signal from the sidelobes. Due to the reason that wind turbine reflections could occur it is decided to use a Blackman-Harris window as this has a low maximum sidelobe level of -71 dB and therefore reduces leakage a lot and makes it possible to distinguish atmospheric reflections from wind turbine reflections for instance. The range resolution will suffer slightly but it will still be sufficient and leave a margin because the required x-direction resolution

Table 8.1: Characteristics of different window functions taken from [39].

Window	**−3 dB main lobe width (bins)**	**−6 dB main lobe width (bins)**	**Maximum sidelobe level (dB)**	**Sidelobe roll-off rate (dB/decade)**
Rectangular	0.88	1.21	−13	20
Hann	1.44	2.00	−32	60
Hamming	1.30	1.81	−43	20
Blackman-Harris	1.61	2.25	−71	20
Exact Blackman	1.61	2.25	−71	20
Blackman	1.64	2.30	−58	60
Flat top	2.94	3.56	−44	20

is 10 m. The chosen Blackman-Harris window will be of the following form:

$$W[k,n] = \frac{K_{atd}}{\sqrt{P_{wink}P_{winn}}} \left(a_0 - a_1\cos\left(\frac{2\pi k}{N-1}\right) + a_2\cos\left(\frac{6\pi k}{N-1}\right) - a_3\cos\left(\frac{4\pi k}{N-1}\right)\right) \cdot \left(a_0 - a_1\cos\left(\frac{2\pi n}{N-1}\right) + a_2\cos\left(\frac{4\pi n}{N-1}\right) - a_3\cos\left(\frac{6\pi n}{N-1}\right)\right) \tag{8.10}$$

with constants $a_0 = 0.35875$, $a_1 = 0.48829$, $a_2 = 0.14128$ and $a_3 = 0.01168$ and conversion constant K_{atd}, converting the numerical output of the analog-to-digital converter. K_{atd} is a function of the number of chirps and samples and the output range of the analog-to-digital converter.

The power of the window is defined as

$$P_{win} = \frac{1}{N}\sum_{j=0}^{N-1}\left(a_0 - a_1\cos\left(\frac{2\pi j}{N-1}\right) + a_2\cos\left(\frac{4\pi j}{N-1}\right) - a_3\cos\left(\frac{6\pi j}{N-1}\right)\right)^2 \tag{8.11}$$

which will be evaluated for the number of samples and chirps yielding P_{wink} and P_{winn}.

Finally, each sample will be multiplied by the window W to reduce the leakage related to the double FFT. The reduction of leakage for a Blackmann-Harris window compared to a rectangular one are shown in figure 8.4. As can be seen, the Blackmann-Harris window results in less sidelobes with a lower power and therefore seems to be a good choice.

8.5 Double Fast Fourier Transform

This section describes the way range and velocity information is obtained through a double FFT of the beat signal. First, the range information is extracted using the first FFT, followed by an explanation of the second FFT, used to obtain velocity information. An overview of the process and how the obtained matrices look like is given in figure 8.5.

8.5.1 First Fourier Transform

As explained in section 8.1, the frequency of the beat signal contains information about the range of the scatterer. To obtain the range, the signal is sampled over one chirp using a windowing function, as described in section 8.4. The signal contains a spectrum of frequencies corresponding to different scatterers along the range. This spectrum is extracted using a FFT algorithm.

The FFT divides the frequency spectrum into a number of frequency bins, this number is called the FFT size and is equal to the amount of samples during one chirp K. FFT size K and sampling frequency f_s determine the frequency resolution as shown in equation and the frequency resolution, in turn, determines range resolution. This is shown by the following relation:

$$\Delta f = \frac{f_s}{K} \tag{8.12}$$

The sampling frequency is dependent on the highest frequency expected to be present in the signal. After the low-pass filter, the signal only contains frequencies of the passband plus a small margin—approximately up to 540 kHz. Normally, the Nyquist criterion mandates the use of a sampling frequency

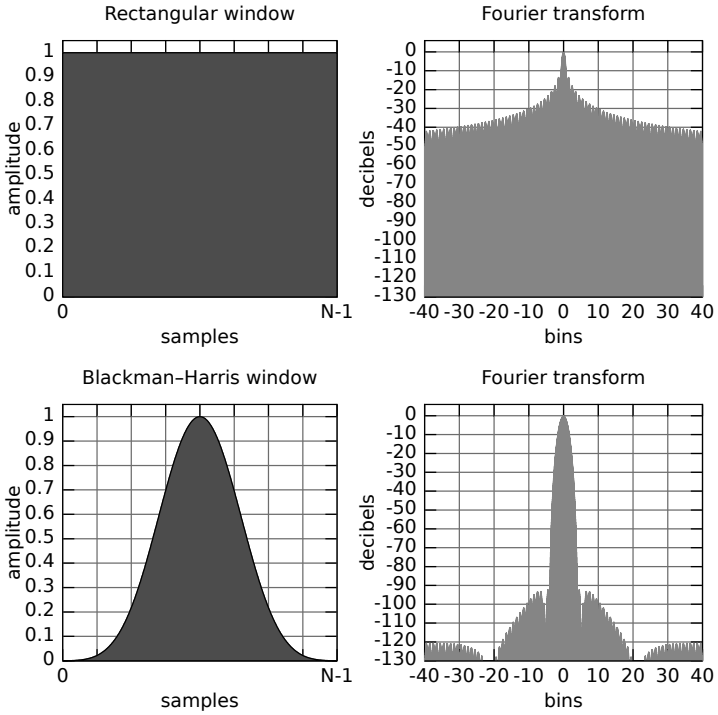

Figure 8.4: Rectangular and Blackmann-Harris window and their corresponding Fourier transform for a windowed sinusoid [73].

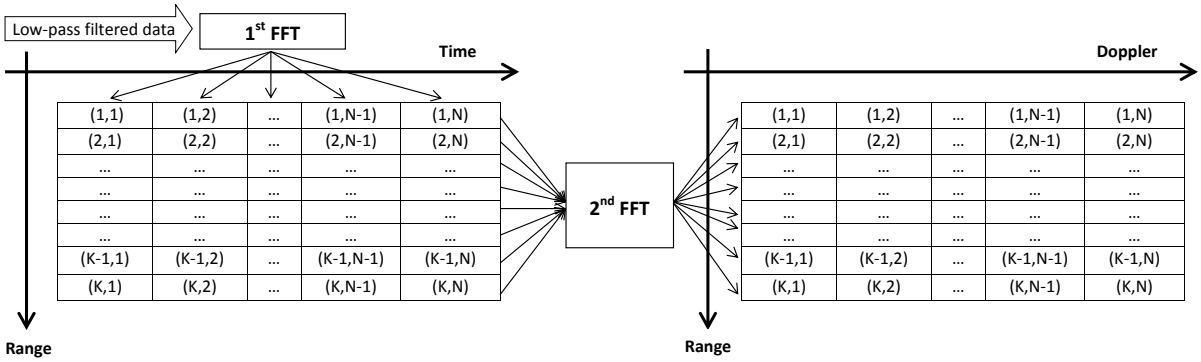

Figure 8.5: Range-Doppler double FFT processing.

of twice the highest frequency in the signal. However, since the quadrature deramping allows surpassing the Nyquist criterion (see section 8.2), the sampling frequency can be decreased to 540 kHz. This is the minimum sampling frequency needed to measure the whole spectrum without aliasing and therefore presents the lower bound of the sampling frequency.

The FFT size is determined by

$$K = T_c \cdot f_s \tag{8.13}$$

where T_c stands for chirp length. Assuming the lower bound for sampling frequency (540 kHz) and taking the chirp length of 0.3 ms, the FFT size is 162. However, since the FFT algorithm works fastest using sizes of base 2, the nearest power of 2 is used; 256 or 2^8. This increase in sample size is facilitated by increasing $T_c \cdot f_s$. Since the chirp length cannot change because of the Nyquist criterion on the highest Doppler frequency (see section 5.3.5), the sampling frequency is increased to 853.3 kHz. This combination of chirp length and sampling frequency leads to a frequency resolution for the range columns of 3.33 kHz or an ideal range resolution of 3.3 m (see section 5.3.7).

8.5.2 Second Fourier Transform

The first FFT creates column-vectors consisting of frequency bins, where each bin stands for a certain range resolution cell. Using several consecutive chirps a matrix is formed in which the row vectors contain the amplitude information per range resolution cell over a number of chirps, this is called the range-time matrix and is shown in figure 8.5. The amount of chirps N used per matrix is determined by the chosen integration time. The integration time is calculated by $N \cdot T_c$ and is determined by the time on target (see section 5.3.6). It should be low enough to justify the assumption that the scatters have not left the range resolution cell. Considering 64 chirps and a chirp length of 0.3 ms the integration time is 0.0192 s, during this time even a particle travelling at the maximum expected wind speed (25 m/s) only travels 0.48 m, which is only 14.4 % of a range resolution cell and therefore justifies the assumption.

The scatterers in a certain range resolution cell all move at different velocities. The movement during a chirp causes them to change the phase of the reflected signal per chirp, this phase-change shows as a periodic change in amplitude of the frequency bin. The periodic change in amplitude creates a signal per row vector that contains the Doppler spectrum at the corresponding range. To obtain this spectrum a second FFT is performed over the columns of the range-time matrix to create a range-Doppler matrix. The frequency resolution for the Doppler rows can be determined using equation (8.12). Considering 64 chirps (instead of samples) and a sampling frequency of $1/T_c$, the frequency resolution is 52.1 Hz.

Every 64 chirps, a range-Doppler matrix is created. To determine the actual location of the scatterers the range information is combined with the angle of the antenna. In reality, each chirp has its own unique angle, but since the 64 chirps only take 0.0192 s to complete, the angle is assumed to be constant. The mean angle of the 64 chirps is taken as the angle of the corresponding range-Doppler matrix.

8.6 Range and Radial Velocity Determination

This section describes how the double FFT frequency bins are related to range and radial velocity. This information allows for the range-Doppler matrix to become a range-velocity matrix.

The rows of the range-Doppler matrix represent different frequency bins and correspond to range-resolution cells. The corresponding range frequency resolution is determined by equation (8.12) and is equal to 3.33 KHz. From the frequency, a range R is obtained in the following way:

$$R = \frac{f_b \cdot c \cdot T_c}{2B} \tag{8.14}$$

where c is the speed of light and B is bandwidth. With a bandwidth of 45 MHz and f_b equal to the frequency resolution of the first FFT, the range resolution can be determined to be 3.3 m. This means the first row of the range-velocity matrix contains the radial velocity spectrum at 0 to 3.3 metres, the second at 3.3 to 6.6 metres etc.

The second FFT is performed over the rows of the range-matrix to create the range-Doppler matrix. The radial velocity resolution is related to its frequency resolution in the following way:

$$\Delta v = \frac{\lambda}{2NT_c} = \frac{c}{2(NT_c)f_o} \tag{8.15}$$

Taking the frequency resolution from equation (8.12) with a sampling frequency of $1/T_c$ and 64 chirps, the radial velocity resolution becomes 0.781 m/s. Since both positive and negative radial velocities are measured, the row vectors contain 64 elements that span a total radial velocity range of -25 to $+25$ m/s in steps of 0.781 m/s.

8.7 Clutter Suppression

Clutter suppression is the removal of echoes from nearly static targets, such as trees or other wind turbines, as these are captured within sidelobes and main beam. After applying the double FFT the range-Doppler matrix is obtained with range information in f_b given by each rows and radial velocity information in f_D described by the column. As static targets do not move their radial velocity will be zero. However, the antenna introduces an error as it is rotating and thus a small radial velocity could

follow. Another aspect is that wind could introduce movements of trees, waves or even of the turbine tower the radar is mounted on or from other turbines. These echoes are generally mainly captured due to the sidelobes, but for this application other wind turbines in particular could reflect the main beam and lead to unwanted frequencies. Most of these echoes will be filtered out by the low-pass filter, see 8.3, but an additional way to remove these reflections from nearly static targets increases the reliability of the system.

Note that clutter suppression will also remove targets which are moving perpendicular to the beam as these have zero radial velocity. This could especially occur at the edges where the pointing angle θ is $\pm 45°$. Therefore the atmospheric targets will only require an offset angle in the direction of movement of $45°$ to the x-direction, the main wind direction, to move perpendicular to the beam. However it can be assumed that the velocity component in y-direction is very small according to [13] such that the targets will mainly move in x-direction, thus the case where they will move perpendicular to the beam is unlikely to happen.

Clutter suppression is very useful as it removes the whole signal content of nearly static targets, which can be seen as noise. The minimum radial velocity V_D that has to be measured is 2.8 m/s according to equation (8.5), using the maximum pointing angle of $45°$ and minimum velocity requirement of 4 m/s. It is assumed that every scatter with a velocity below this level does not correspond to the wake and can be removed. The radial velocity resolution is 0.78 m/s as stated in section 8.6. Therefore at least 3 positive and also negative neighbouring columns of the 0 radial Doppler velocity column, which is the column of the range-Doppler matrix containing information of 0 radial velocity, can be suppressed as well as the 0 radial Doppler velocity column itself. This is due to the reason that these columns will only contain nearly static targets with a radial velocity of less than 2.34 m/s. Therefore those columns will be set to zero in order to suppress their signal content.

Additionally, rows from the range-Doppler matrix containing range information that corresponds to a range larger than 520 m could be suppressed as well by removing them from the the range-Doppler matrix. This could be of high value as reflections from targets outside the measurement area will be discarded.

In conclusion it can be said that clutter suppression is a useful tool in order to remove unwanted parts of the signal stemming from non-atmospheric scatterers as these will not add any value to determine the wake boundaries.

8.8 Smoothing

Stored in the range-Doppler matrices are Doppler-spectra for every range resolution bin along the radar beam. Obviously this spectrum contains significant noise stemming from a plethora of phenomena. To increase the quality of the spectrum it is smoothed by a smoothing-algorithm. This process is explained in the following section.

Data sets can be further improved by applying a moving average in the time domain. This is known as smoothing, and can also be performed in the Fourier transformed domain but with a low-pass filter. Smoothing in the time domain is done with the purpose of making a sequence $s[n]$ semi-continuous and to reduce the number of outliers. The moving average achieves this by applying a weighted average to the samples around a point, and replacing that point's value with the new point to ultimately create a new sequence $s_m[n]$. Taken from Figueras i Ventura [39], the moving average is

$$s_m[n] = \frac{1}{P_w} \sum_{j=n-\frac{N_m}{2}}^{n+\frac{N_m}{2}} s[j] w_f[j-n] \tag{8.16}$$

where w_f is the weighting function, P_{wf} the weighting function's total power and N_m is the number of elements averaged (half of the samples are previous and half are consecutive). Weighting of the elements can be done using different weighting functions. They will weight the neighbouring elements differently and therefore filter noise differently. A Gaussian weighting function will be used because it is effective in removing noise-induced high frequencies [39]. The Gaussian moving average $w_f[n]$ is defined as

$$w_f[n] = e^{-\frac{n^2}{2}}; n \in [-\frac{N_m}{2}, \frac{N_m}{2}] \tag{8.17}$$

The total power of the weight function can accordingly be expressed as:

$$P_{wf} = \frac{1}{P_w} \sum_{n=-\frac{N_m}{2}}^{N_m 2} e^{-\frac{n^2}{2}} \tag{8.18}$$

Due to the properties of the digital Doppler spectrum, namely that it is periodical, the latest and initial samples can be averaged together. The period of the digital Doppler spectrum is $2f_{Dmax}$, the maximum Doppler frequency. An example of a moving average using smoothing can be seen in figure 8.6 taken from Figueras i Ventura [39], where seven samples are used in a Gaussian moving average.

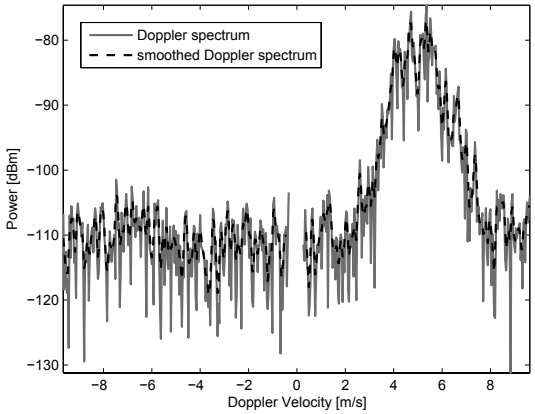

Figure 8.6: Example of a Doppler spectrum that has been smoothed. The grey line is the original Doppler spectrum, and the black dashed line is the smoothed spectrum [39].

Another consideration when applying this smoothing technique, is that increasing the number of points included in the moving average improves the smoothness of the averaged signal, but diminishes Doppler velocity resolution [39]. Averaging a large amount of elements can also can also cause a significant increase in computational time, which may be constrained.

8.9 Noise Clipping

Noise can interfere with returned atmospheric signals or be mistaken for a return. Noise clipping is a technique that can minimise the effect of noise by suppressing range cells with a signal power below a certain threshold, so that they are not used in further computations. This section explains how this is done

One source of noise is thermal noise due to the receiver, which is added to the return signal. Thermal noise behaves as white Gaussian noise. White Gaussian noise is identically distributed and uncorrelated, whereas atmospheric signals are narrowband and approximately Gaussian [39]. From this an atmospheric signal with a total power lower than the total noise power can be detected. For example the peak from 4–6 m/s seen in figure 8.6 is visibly higher than the average noise power.

The receiver generally has a response that varies with different frequencies, which affects both the atmospheric signal and signal noise. The receiver noise power can be estimated by sampling the received signal without actually transmitting one, to approximate the noise power per range cell. This may be done several times and averaged again to minimise variance. This average noise power is used to determine the clipping threshold, but a margin is added due to the nature of noise power, which can peak far above the average noise power [39]. This margin depends on the noise signature and will have to be configured and calibrated depending on the case at hand.

Weak atmospheric signals may also be unintentionally clipped when the signal power is below the threshold. The Doppler spectrum will then be reduced in width, and the signal reduced in power [39]. As mentioned earlier, the Doppler spectrum can be approximated as a Gaussian curve, and the clipped portions of the spectrum can therefore be extrapolated from the unsuppressed portion.

8.10 Wake Boundary Determination

In this section, the final step of the data processing will be explained, which is how the actual wake boundaries are determined. First the way the range and radial velocity measurements are converted to a location and streamwise velocity is presented, followed by the determination of the wake boundaries.

After obtaining the radial velocities V_D and the corresponding radial range R as explained in section 8.6 the first step will be to convert the radial velocity to the streamwise velocity V. The velocity V in x-direction, which is of highest value for the wake boundary determination follows from equation (8.5) knowing the antenna pointing angle at every time, which will be stored. To achieve a time varying wake, thus to actually visualise the meandering every range and velocity measurement will receive a certain time stamp. In order to plot the velocity field in a two dimensional plane the coordinates of each measurement must be known as well as the velocity. The coordinates are in a polar representation (R,θ) and could be converted to Cartesian (x,y) if desired. Then, knowing the velocity V in x-direction, the relevant flow field can be visualised.

An algorithm to deduce the wake boundaries at a certain x-coordinate, called x_{ref} at a certain time stamp, could be to first detect the freestream velocity V_∞ occurring at (x_{ref}, y_{max}) and (x_{ref}, y_{min}) thus at the most outward locations. Then the wake boundary locations could be derived by setting the wake boundary definition as $V_b = 0.95V_\infty$ according to section 2.6 with 0.95 as an initial value which of course could be changed. Then the corresponding (x_{ref}, y) coordinates of the boundaries can be found by reducing y_{max} for the right boundary or equivalently increasing y_{min} for the left boundary until the corresponding velocity V equals the predefined boundary velocity V_b. It has to be noticed that Gaussian regression will be applied to the velocities as they are only discrete measurement values and an exact measurement of $0.95V_\infty$ is most likely not obtained. Therefore, the Gaussian regression will be used within velocity measurements in order to achieve a continuous velocity field containing values of $0.95V_\infty$. A Gaussian regression was chosen as the velocity deficits as function of y-coordinate (the velocity profiles) have a Gaussian shape according to Sanderse, [20].

The algorithm needs to be applied for the whole measurement period at all x-coordinates in order to determine the wake boundaries and their meandering in time. Of course this algorithm could be varied for instance the threshold of 0.95 could be changed. Finally, a visualisation of the wake boundaries and how they vary in time will be obtained from the (x, y) boundary coordinates as well as their corresponding time stamp.

8.11 Subsystem Verification

This section describes how the data processing subsystem will be verified. Verification will ensure that the data processing sub-system will work as intended and also expose any flaws in the code of each process and interactions between processes. First a set of unit-tests will be treated, followed by the system test to complete the verification.

The verification of the data processing will consist of several unit tests followed by a system test. The unit tests will verify that each separate process (I/Q-deramping, low-pass filter, FFT, etc.) will work as intended. This is done by feeding a simulated signal into each separate process and analysing the output. From the analysis it can be determined if the process works as it is supposed to.

For the quadrature deramping process a single chirp will be generated, along with several echos from simulated targets at different ranges. This signal is generated digitally and converted to analog, allowing the feeding of the signal into the I/Q demodulator. The demodulator will create a beat signal which can be analysed to verify the workings of the process.

To verify the low-pass filter the magnitude response of the filter has to be investigated. This is done by applying the filter to an artificial white noise signal. Since the signal will contain each frequency with equal power the output of the filter shows the exact magnitude response. Comparing this measured response with the designed filter response can be used to verify the filter.

The FFT algorithm that will be used will be a very well documented and tested algorithm, verifying this algorithm is not strictly necessary. However, for the sake of completeness and the fact that there could be mistakes in the implementation of the algorithms the verification is still conducted. To verify the FFT algorithm a signal can be generated containing a range of frequencies. The output of the FFT can be matched with the known frequency content to check the correctness of the algorithm.

Next comes the range and radial velocity determination. Checking the correctness of the calculation is relatively easy and consists only of checking that the range vector ranges from zero to 520 metres in steps of 3.3 metres and the velocity vector from -25 to $+25$ m/s in steps of 0.781 m/s.

The clutter suppression algorithm is verified by checking if the correct columns are set to zero in the range-velocity matrix. A matrix of 256 rows and 64 columns is created and filled with ones. This matrix is then fed into the clutter suppression algorithm and the output is checked for columns containing zeros. If the zero-columns correspond to the intended clutter columns the process is working correctly.

Verification of the smoothing process is done by generating a noisy signal and analysing the output of the smoothing algorithm. The amount of smoothing necessary for the radar is a trade-off between noise-suppression and velocity resolution and it is up to the engineer to determine the right amount.

The noise clipping process is easily verified by feeding a noisy signal into the algorithm and analysing the output. It should be checked whether the algorithm indeed sets the velocity bins with a power below the threshold to zero, if this is the case the noise clipping process is verified.

The wake boundary determination can be verified by feeding the algorithm a flow field that has been transformed to a radial velocity similar to the way the radar will measure the flow. It then has to be checked to what extent the algorithm can reconstruct the original flow field, verifying the process.

After every unit test is completed and passed, the total data processing system has to be tested in a system test. This test verifies the system as a whole, ensuring the system does what is intended and meanwhile exposing flaws in the interaction between processes.

The system test is conducted by feeding the system an artificial chirp, similar to the signal used in the I/Q deramping unit test, but instead of just one signal the amount of chirps is increased to a multiple of 64 (N). This signal should correspond with an actual flow field and could be generated by a simulation (see chapter 10. This signal will be used by the system to create an entire plot of the velocity field. To verify the system the generated velocity field is compared with the original one, the comparison is analysed to determine if the system works as intended.

8.12 Computational Cost and Data Storage Estimation

This section gives an estimation of the costs which are related to data processing: computational power and data storage. Cost of electronic components is omitted as it is already treated in section 7. Every process that involves digital computations and data storage is covered to ultimately determine the total computational and data storage requirements.

To determine the data storage requirement the upper bound on the number of bytes that need to be stored will be derived from the amount of range-Doppler matrices which will be processed as these are mainly the data which will be stored. The amount of matrices M can be deduced from

$$M = \frac{t_{meas}}{T_c N} \tag{8.19}$$

where t_{meas} is the measurement time (in s) and T_c times N equals the time at which one range-Doppler matrix will be generated.

Assuming one cell of a range-Doppler matrix stores one byte the required number of bytes N_{bytes} which needs to be stored is equal to

$$N_{bytes} = 2MKN \tag{8.20}$$

where the multiplication of two accounts for real and imaginary data.

Taking into account the requirement of 12 hours of measurement (corresponding to 2 250 000 matrices), the required bytes which need to be stored are 73.73 GB with a write speed of 1.71 MB/s. This seems to be quite achievable as modern HDD or SSD have a capacity up to several TB and a write speed of hundreds of MB/s. The chosen capacity should be at least 1 TB to account for longer measurement periods and extra data which could be stored, for instance antenna pointing angle θ and the time stamp, which will be a few bytes for one range-Doppler matrix.

To obtain the computational power the number of operations which is required for performing one double FFT is calculated. It is according to Barrick [74] equal to:

$$N_{op} = KN \log_2(KN) \tag{8.21}$$

This yields 229 376 operations for one range-Doppler matrix. For 12 hours of operations this has to be multiplied by M resulting in a total number of operations of approximately $516 \cdot 10^9$. Within one second this corresponds to $11.95 \cdot 10^6$ operations. Thus the required processor should have at least 11.95 MFLOPS. However this will only be the required MFLOPS due to the double FFT, other aspects such as low-pass filtering and windowing will require several operations as well. Especially the low-pass filter requires a lot of operations. For the low-pass filter the filter builder application in MATLAB requires 585 floating point operations per sample, multiplying this by the sampling frequency of 45 MHz, which equals the bandwith, and by 2 to account for a complex signal this will result in 52.65 additional GFLOPS. Thus 52.66 GFLOPS at least for the double FFT and low-pass filter are needed. Additionally clutter suppression, smoothing and noise clipping further increases the number of operations per second, but by an negligible amount in comparison with the FFT and low-pass filter. The actual number of required operations per second is difficult to predict. It can be assumed that it will be lower than 100 GFLOPS which is easily within the capabilities of the control processor chosen in section 7.2, since the FFT and the low-pass filter are normally the largest percentage. For safety a certain margin is left, which ensures that it will not be a problem to process the data in real-time if an up to date processor will be chosen.

9 | Operations and Logistics

This chapter will discuss the operations and logistics involved in operating the radar system. First the section 9.1 will give a short overview of all the procedures and the section 9.2 will describe each step in further detail.

9.1 Operations and Logistics Overview

The radar system is designed to function both on- and offshore. The steps in the operations and logistics procedures are the same for both scenarios—merely the means of transportation is different and less complex for onshore application. The operations and logistics procedures can be broken down in the following way:

1. Transportation (to turbine)
2. Installation
3. Operation
4. Deinstallation
5. Transportation (from turbine)
6. Storage
7. End of Life

Steps 1 through 6 can be repeated until the system reaches the end of its lifetime, which is denoted by step 7. The items of this list are elaborated on in section 9.2.

9.2 Operations and Logistics Procedures

This section explains in more detail the individual steps of the radar system's operations and logistics procedures.

Transportation

With its estimated mass of 130 kg and maximum volume of about 10 m^3, the radar device is easy to transport using a car with a small trailer for transporting it to a harbour or an onshore wind turbine, and a medium-sized offshore turbine workboat access vessel like the Windcat series [75] for offshore applications. The transportation of the radar system can be combined with regular maintenance of the wind turbine and should require no extra vehicles in most cases.

There is no expected difference between transporting the system to or from a wind turbine site. When disassembled, the system is not sensitive to vibrations, so rough roads or sea pose no problem to the device's integrity.

Installation

As explained in chapter 6, depending on the nacelle configurations of different turbines, two different installation methods can be used: When possible, the system will be mounted on top of the nacelle. If this becomes difficult, the option exists to hold the system up underneath the nacelle. This of course requires different installation steps which will each be explained in this section. In order to install the system, several steps need to be followed:

- **Shut down turbine**—In both cases, since some work needs to be done on, in or around the wind turbine nacelle, the turbine needs to be shut down, blades pitched, and braked.
- **Transport radar system from ground level to nacelle (Installation on top)**—In the case where the system is mounted on top of the wind turbine, the most convenient way would be to bring the system up in different parts. If present, the service crane can be used to lift up the radar system.
- **Transport radar system from ground level to nacelle (Installation below)**—When the system is mounted below the nacelle, assembly at hub height becomes a more difficult task. Therefore the decision was made to use the cable system present at the nacelle for the mounting to hoist up the radar system as a whole, as to avoid assembly on the nacelle.
- **Mechanical fix**—After transport (and assembly) of the system, one or more persons will be required at the nacelle to mechanically fasten the system to the nacelle.
- **Test mechanical system**—After properly positioning the radar system, all mechanical subsystems should be initially tested. An example of this is the test of the rotational system.
- **Connect electronics and initiate data processing**—After mechanically positioning the system into place and testing mechanical links, the electronics can be connected and calibrated.
- **Initiate Internet interface with radar control**—In order to be able to remotely control the radar, a link with a ground station is made through an Internet connection using the wind turbine control link (most often using GPRS). Using this link, information about the system itself can be read from the ground and if necessary, some data can also be transferred.
- **Calibration and full system test**—After the installation of the system, it is calibrated and a full system test is performed in order to eliminate any issues.
- **Start up turbine and radar system**—When calibration and full system tests are performed, the turbine can go into operation and the radar system measurements can initiate.

Operation

Once the system has been installed, it should be powered on and perform tasks as specified in a program containing a set of instructions. These depend on whether the wind turbine is currently running, as determined by the data the system obtains from the wind turbine's sensory system, and what kind of weather conditions are currently present, as determined by the radar system's weather sensor.

If the wind turbine is running at the desired operational speed and if the desired weather conditions are present, the radar system starts taking measurements. These requirements may be set individually but are usually 4–25 m/s for wind speed and fog for weather conditions.

The system can operate autonomously for an indefinite amount of time as long as it gets provided with power and ir has free storage space. Using sensory data, it can determine when to start and stop taking measurements.

It is assumed that the radar system can get an Internet connection—or some other kind of remote connection—facilitated by the wind turbine itself. With this, status updates about the radar system can be requested. This is useful to obtain information about the current health of the components as well as free disk space. Should it not be possible to fix possible issues the system has remotely, it must be repaired on-site.

Deinstallation

Considering deinstallation of the radar system, the steps to be followed are similar to the installation. Again, differences exist between mounting the radar system on top of the turbine nacelle and mounting it below.

- **Shut down turbine and radar system**—In both cases, again the turbine needs to be shut down, blades pitched and braked. Operation of the radar system is also shut down.

- **Disconnect radar system from turbine**—Depending on the turbine type, all possible links with the wind turbine should be broken (for example Internet (GPRS) connection, power,...).
- **Disconnect system electronics and data processing**— The electronics and data-processing block is disconnected from the radar system.
- **Mechanical disassembly (installation on top)**—The system is disassembled on top of the turbine and transported to ground level part by part using the same device used for installation.
- **Mechanical disassembly (installation below)**—The system is mechanically disconnected from the wind turbine and again the radar system as a whole is transported using the cable system, to be disassembled on ground level.

Storage

The radar system can be divided into multiple components, the mounting base, the electronics subsystem, the radar dishes and the radome, and stored separately. The electronics subsystem should be stored in an environment appropriate for sensitive electronics and the radar dishes should not receive any loads that may cause deformation. The remaining components do not require particular storage environments.

End of Life

At the end of its lifetime, the system should be disassembled and as many of its components as possible recycled. It should be noted that this is assuming complete failure of every component of the system. Individual components, particularly within the electronic subsystem, may be replaced during the lifetime of the system.

Components made of metals, such as the radar dish which is made of aluminium and various other parts of the mounting can be easily recycled. The electronics components should be disposed of appropriately: rare earth elements and metals can be extracted from them.

The radome wall materials can be recycled as well. The e-glass reinforced sandwich skin panels can be detached and broken down such that the fibres are extracted and reused for other purposes [76]. The nylon phenolic core can also be recycled using the technique described in [77].

10 | Simulation

The main purpose of the simulation is to get more insight in the workings of a radar system and the integration of the various subsystems. Furthermore, the simulation will be used to determine the feasibility of measuring the wake with a radar-based system. Finally, it will provide useful data about the accuracy of the system. The chapter layout is as follows: Section 10.1 presents the simulations operations. Then the simulation is verified in section 10.2. The results of the simulation are given in section 10.3 and discussed in section 10.4.

10.1 Simulation Operations

The simulation consists of a large number of functions working together. In order to clarify the operations performed by the simulation and the underlying relations between functions, a flow chart was created. This flow chart can be seen in figure 10.1.

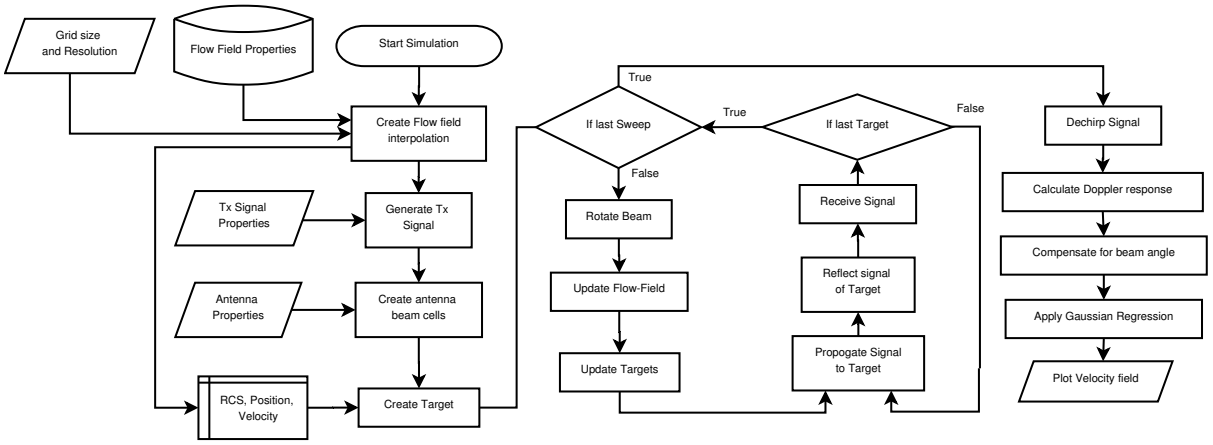

Figure 10.1: Flow chart of the simulation program.

When the simulation is initialised, the first step is to create the flow-field around the wind turbine. The flow-field around the wind turbine is based on the Larsen model [78]. The wake model is dependent on the Rotor diameter (D), the thrust coefficient (C_t), the turbulence intensity (Ia), the undisturbed wind speed U_∞ and the hub height (H).

After determining the flow-field data, an interpolation of this flow-field is created using a spline. This will allow the simulation to evaluate the flow field properties on each point, even if it is not exactly on a grid node.

The next step is to generate the signal that is transmitted by the radar. The shape of this signal is based on the calculations performed in section 5.4.2. A spectrogram of the signal can be seen in figure 10.2.

After the signal has been generated, the antenna beam is created. The antenna beam is a cone with the same width as the half-power beamwidth. The cone is then divided into individual cells. For each cell in the beam, the volume and the radar cross-section is determined, and a radar target is then created in the centre of each cell. The environment grid and beam grid are shown in figure 10.3, the blue dots represent the radar targets.

The signal propagation from the transmitter to the target and the reflection from the target to the receiver is handled by the MATLAB Phased Array System Toolbox [79]. This toolbox includes verified

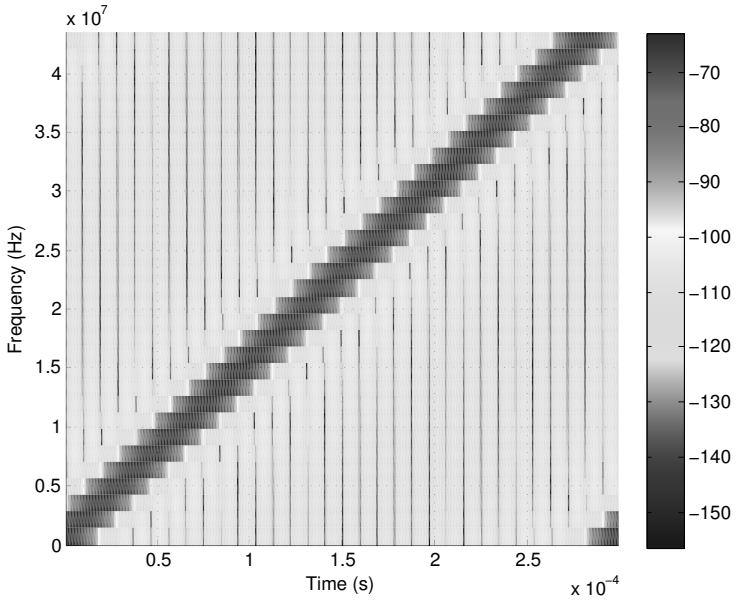

Figure 10.2: Spectrogram of the transmitted signal.

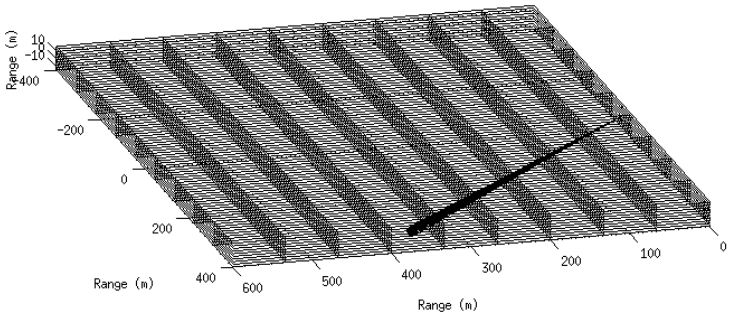

Figure 10.3: Simulation grid used in the simulation.

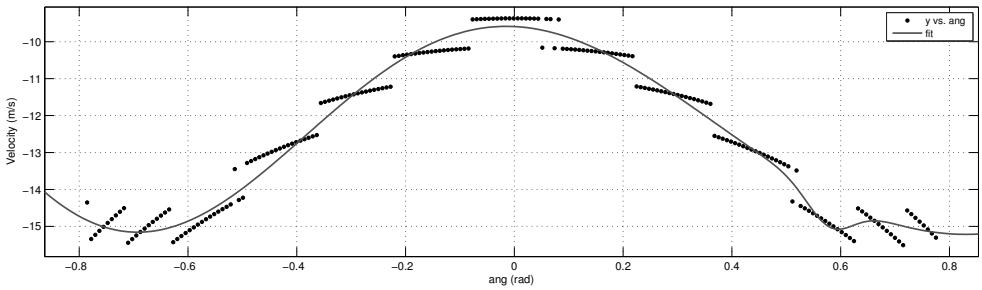

Figure 10.4: Example of a Gaussian regression.

functions for radar wave propagation and allows interaction of the signal with targets that are present inside the scanned volume.

The simulation treats each radar target individually. The signal, as generated before, is amplified and one chirp is transmitted towards a target, reflected off the target and received by the antenna. This process is repeated for each target in the beam. After the response is calculated for each target, the received signals are summed up and are post processed.

After one chirp, the transmitter beam is rotated, the flow-field is updated and the target properties are updated. This process is repeated until the beam has scanned the entire flow-field.

When the complete flow-field has been scanned, the post-processing is performed. The received signal is mixed with the reference signal (dechirped) and a range-speed response is calculated for each bin. An example of a range-speed response can be seen in figure 10.5a.

For each bin, per range, the velocity belonging to the highest signal strength is selected. This results in a colour-map showing the flow field velocity. After this step, the radial velocity is converted to the velocity in x-direction using equation (8.5). However, since the velocity resolution is 0.75 m/s, the change in velocity is not smooth but shows jumps. In order to filter out this effect, a Gaussian regression is performed as explained in section 8.10. This regression is applied to all the points at the same radial distance. An example of such a regression can be seen in figure 10.4.

10.2 Verification

To ensure that the simulation will produce valid and reliable results, some verification tests will be preformed on the simulation. The verification of the radar simulation will consist of a number of checks, to see if the results from the simulation hold up to basic calculations on radar systems and some simple test cases.

Velocity resolution

One of the factors that determine the the shape of the transmitted signal is the velocity resolution that can be acquired, as determined in section 5.3.5. This velocity resolution is dependent on the signal wave-length, chirp time and the FFT size. From the initial calculation, a velocity resolution of 0.75 m/s has been determined. In order to verify this, it will be compared with the Range-Speed response pattern generated by the simulation (Figure 10.5a). Each of the cells in the response pattern is a point on which the Range-Speed is evaluated. The number of cells in the horizontal direction is directly related to the velocity resolution. The range of -25 to $+25$ m/s is divided into 64 cells which lead to an velocity resolution of 0.78 m/s. This matches very well with the initial calculation. The difference in caused by the measurement integration period. In section 5.4.2 an measurement integration period of 19.2 ms was assumed, which corresponds to a FFT size of ≈ 67. However in section 5.3.6 it was shown that the amount of chirps over which an FFT can be preformed, needs to be a base of 2. The closest base of 2 is 64. When taking 64 sweeps, the measurement integrating time becomes 19.2 ms. This will result in the same velocity resolution as the simulation.

Range Resolution

In a similar way as the velocity resolution, the range resolution can also be determined. In section 5.4.3, the range resolution was determined to be 3.33 m. Looking at the Speed-Range response pattern, a total of 157 cells are evaluated over an range of 0 to 520 m. This, in turn, leads to a range resolution of 3.31 m, which matches the initial design.

Maximum Velocity

In section 5.3.5, the maximum velocity range is set at -25 to 25 m/s. To check whether the simulation also obeys this limit, the free stream velocity was set at a speed that exceeds this limit. Due to the nature of the FFT analysis, the response is expected to show up at the other side of the velocity spectrum. From the Speed-Range response pattern in figure 10.5b, it can be seen that the targets crosses the maximum velocity and shows up again at the other side of the spectrum.

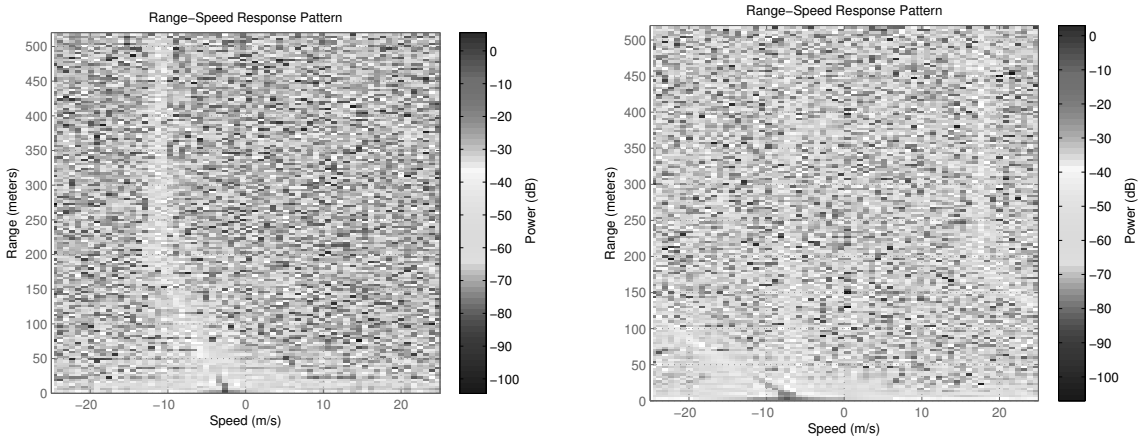

(a) Regular response pattern.

(b) Too high velocity resulting in aliasing.

Figure 10.5: Range-speed response pattern.

Radar Sweep

During one sweep, the radar rotates from left to right. After each chirp, the position and the velocity of each target is updated. To show that this process is performed correctly, a test case is ran. The test case consist of a constant flow field with a velocity of 7 m/s in the x-direction. Since the radar only measures the radial velocity, it is expected that the velocity will be $\cos(45) \cdot 7 = 4.94$ m/s at $-45°$, 7 m/s at $0°$ and 4.94 m/s at $45°$ again. From figure 10.6, the full flow-field from one sweep can be seen. This flow-field matches very well with the Previously mentioned expectations.

When looking at the radar sweep response, it can be seen that the change in velocity is not gradual as one would expect. However, it is divided into three sections with more or less constant velocity. This is due to the velocity resolution of the radar system. Since the free-stream velocity was only 7 m/s, the velocity at $45°$ is equal to 4.94 m/s. This leads to a maximum change in velocity of 2.06 m/s.

Future Verification

In order to verify the complete simulation, it should be compared with other radar simulation tools and/or with existing measurements from radar system. This will be outside the scope of this report but can be implemented in the future.

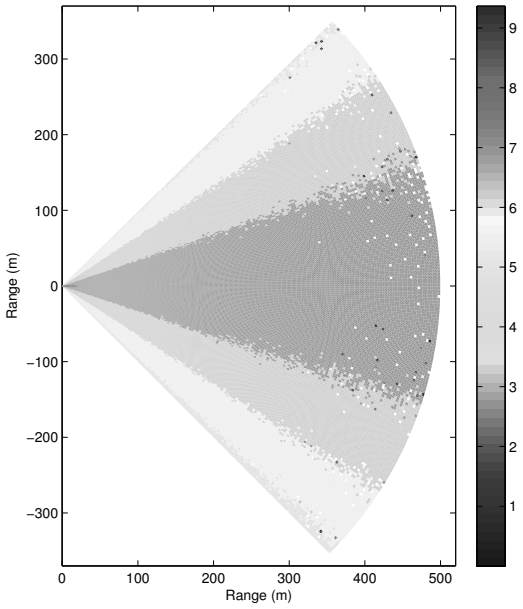

Figure 10.6: Radar sweep velocity response.

Limitations

The simulation of the radar system can be very computational intensive, due to the high sample rate of the system and the high number of chirps. In order to keep the computational time of the simulation to an acceptable level, a number of concessions had to be made. These concessions will lead to limitations in the use of the simulation which will be discussed here.

- Antenna Radiation Pattern
  The antenna radiation pattern is not included in the simulation, this means that the signal has an equal gain over the entire beam angle. In real life the returned signal will have a Gaussian distribution, where the strongest signal that is returned originates from the centre of the beam. This will mean that the image returned by the simulation will be slightly more blurred.

- Constant radar target velocity
  The velocity of the radar targets is kept constant during the FFT bin. For a FFT size of 64 chirps, this would amount to 19.2 ms. This leads to a slightly sharper image than if the target velocity would be changing.

- Constant beam angle
  The angle of the beam is kept constant during the length of the FFT size. Therefore the beam will rotate each 19.2 ms.

- Target reflectivity estimation
  The target reflectivity is estimated by taking the reflectivity per unit volume times the volume of the target cell. This discretisation has an effect on the accuracy and the computational time.

10.3 Results

The simulation tool was ran with a number of different flow-fields to see the effect of the quality of the recovered data on the shape of the wake. For the simulation results presented in this section, the flow-field remained constant over time. The simulation is however suitable to simulate time dependent flow-fields. This could be incorporated in further research.

Case 1

During the first case, a flow field was generated using the Larsen model [78] with the following input parameters: $U_\infty = 15$ m/s, $C_t = 0.5$, $Ia = 0.05$, $D = 80$ m and $H = 70$ m. The input flow-field can be seen in figure 10.7a. The black line in the figure represents the wake boundary based on the 95 % free-stream velocity definition as presented in section 8.10. Figure 10.7b shows the output of the radar sweep before the Gaussian regression. Again, the black line represents the position of the wake boundary. Figure 10.7c shows the reconstructed flow-field after the Gaussian regression. The results can be improved further by filtering out the outliers outside a specific range. The results can be seen in figure 10.7d.

In order to get a good idea of the difference between the real wake boundary and the wake boundary estimated from the radar sweep (both before and after outlier removal), the location of both wakes are shown in figure 10.9.

Case 2

The wake for this case is less wide than the one shown in the previous case. As an input to the Larsen model, the following parameters were used: $U_\infty = 15$ m/s, $C_t = 0.7$, $Ia = 0.06$, $D = 40$ m and $H = 70$ m. Figure 10.8a shows the wake generated by the Larsen model. Figure 10.8b shows the raw response from the radar system. Figure 10.8c shows the wake after the Gaussian regression. Finally, figure 10.8d shows the wake after outlier removal and Gaussian regression.

Figure 10.10 shows the location of the wake from the Larsen model, and the wake location derived from the radar sweep (both before and after outlier removal).

10.4 Discussion

From case 1 presented in section 10.3, it can very clearly be seen that the flow-field without post processing does not follow the wake very well. This is caused by the relatively large steps in the velocity resolution. However, applying a Gaussian regression to the simulation result significantly improves the quality of the determined flow-field. The wake boundary location is matched very well, especially for small ranges. When looking at the results for larger ranges, more noise will become present. This is caused by the expanding beam emitted by the transmitter and will cause the resolution to decrease with increasing range. It is expected that better outlier filtering can improve the result for large ranges.

The wake generated in case 2 is smaller, but the same pattern can be seen as for case 1. The location of the wake is measured accurately for the first 350 m. However, after this range, more artifacts start to show up. The artifacts are mainly caused by errors in the Gaussian distribution. The removal of the outliers does improve the result, but it is not yet optimal. Next to the lower resolution at a higher range, the lower velocity deficit in the wake makes makes it more difficult to determine the position of the boundary. The results could be further improved by removing the data on the outside of the measurement area, where the wake could not exist, which would improve the Gaussian fit. Furthermore, a higher order fit and better outlier detection will also improve the wake location determination.

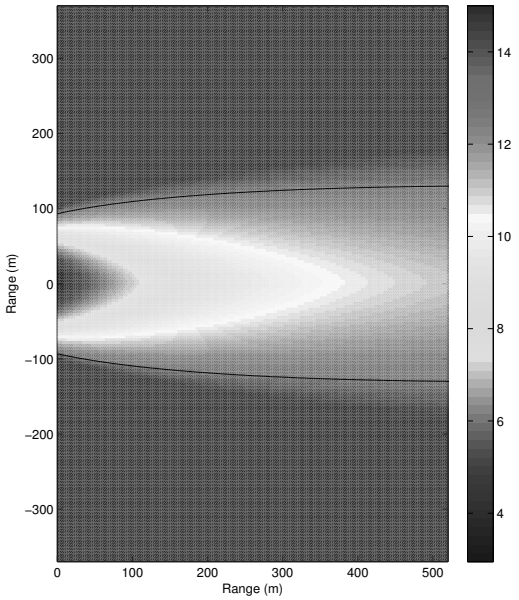

(a) Larsen model reference wake.

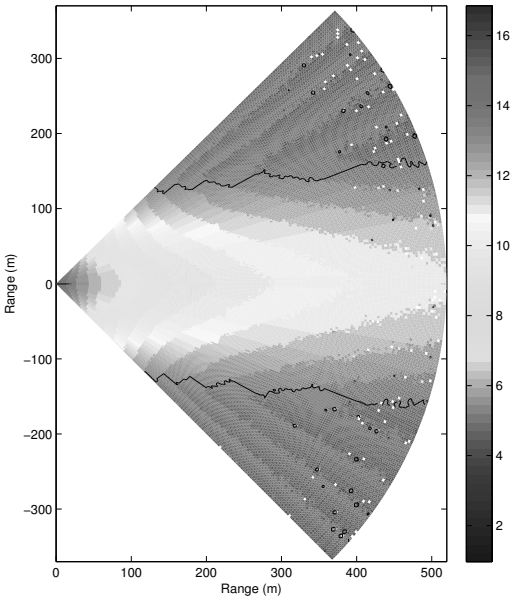

(b) Raw radar simulation response.

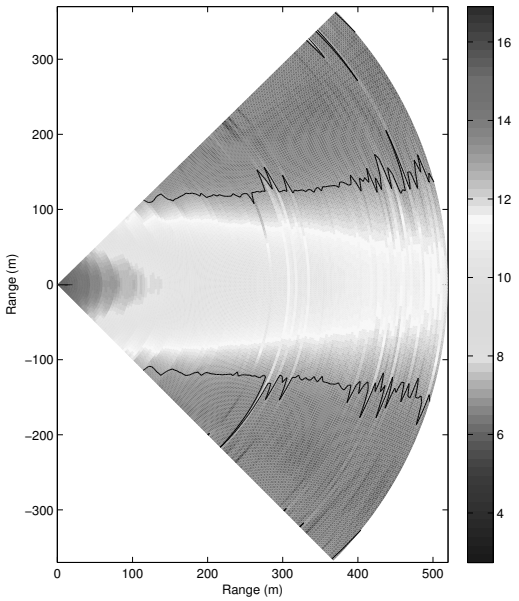

(c) Simulation wake response after post-processing.

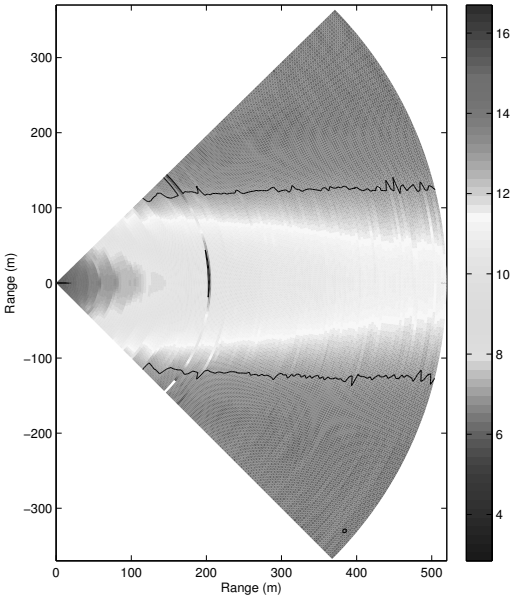

(d) Simulation wake response after post-processing and outlier removal.

Figure 10.7: Results for case 1: $U_\infty = 15$ m/s, $Ct = 0.5$, $Ia = 0.05$, $D = 80$ m, $H = 70$ m.

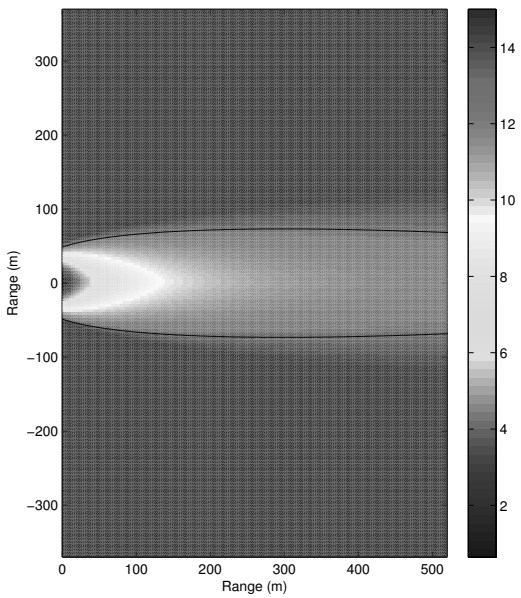

(a) Larsen model reference wake.

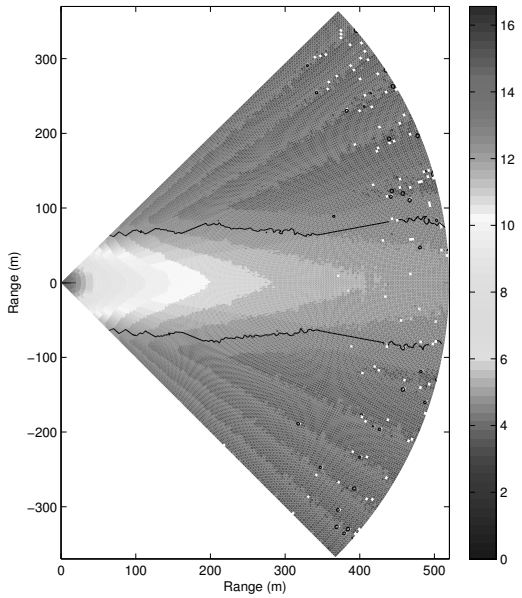

(b) Raw radar simulation response.

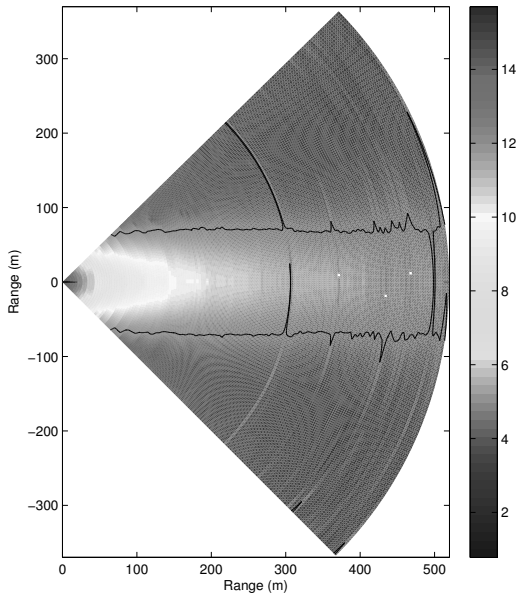

(c) Simulation wake response after post-processing.

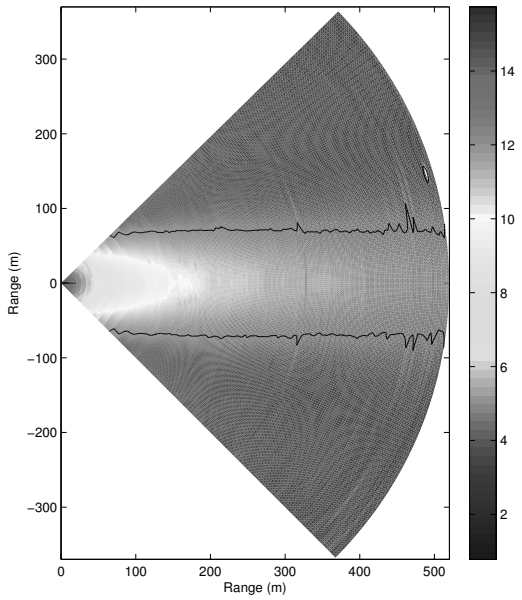

(d) Simulation wake response after post-processing and outlier removal.

Figure 10.8: Results for case 2: $U_\infty = 15$ m/s, $C_t = 0.7$, $Ia = 0.06$, $D = 40$ m, $H = 70$ m.

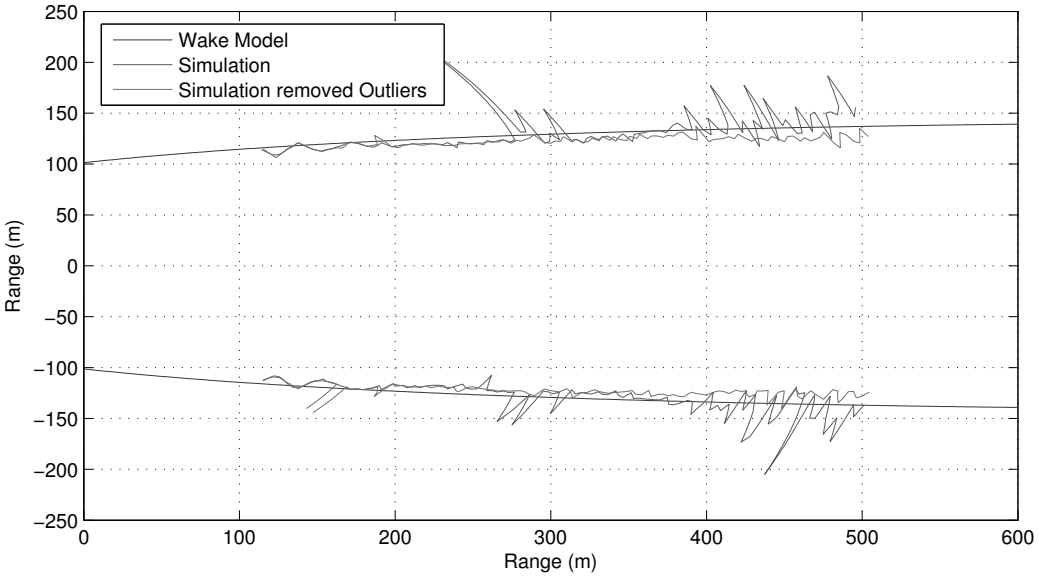

Figure 10.9: Wake boundary position case 1.

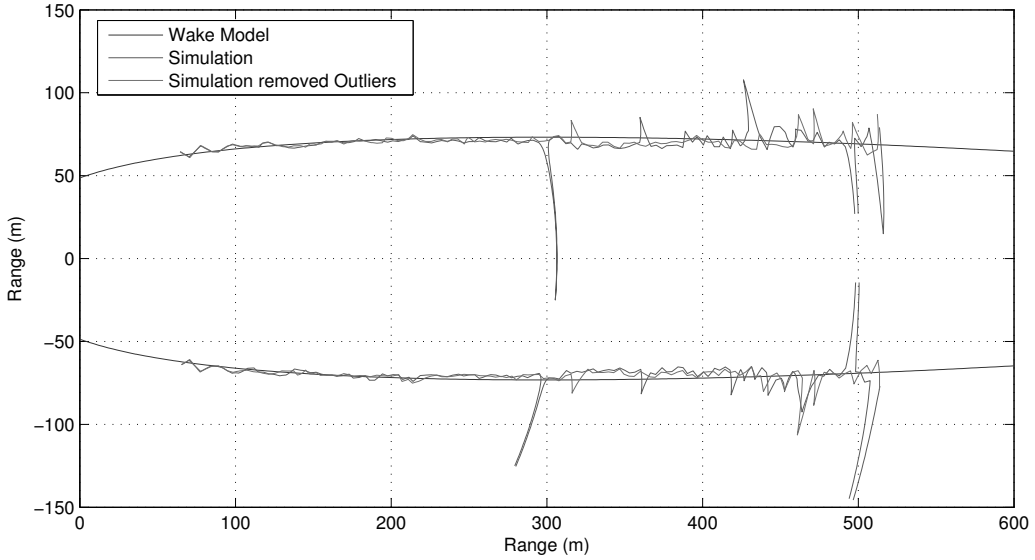

Figure 10.10: Wake boundary position case 2.

11 | System Evaluation

In this chapter the T-WRAX system is evaluated from several different perspectives. The full system should be verified and validated if the design were to be developed further. An overview of system verification is given in section 11.1. Section 11.2 will discuss the validation of T-WRAX. Following verification and validation, a requirements compliance matrix is presented in section 11.3. T-WRAX is then analysed for its sensitivity to requirement changes and environmental conditions in sections 11.4 and 11.5 respectively. Finally, the technical risk analysis studies the probability and consequence of undesired events are presented in section 11.6.

11.1 System Verification

This section describes the way the radar system is verified, by testing if the system requirements are met. Verification will be done by first conducting unit tests, which test the individual subsystems, followed by a full system test to make sure the entire system meets the requirements and to find potential flaws in the interactions between subsystems. In each subsystem chapter (chapters 6, 7 and 8) the verification of the corresponding subsystem is treated, which checks if the subsystem meets the set requirements.

The purpose of the full system test is to test whether T-WRAX meets the system requirements. Each subsystem has different requirements that stem from the mission requirements, which are tested by the system test. Most of the system requirements are already tested during the unit tests, however the interaction between different subsystems has not been tested yet. The main purpose of the system test will be to verify the subsystems interact properly and ensure there are now flaws in the communication between subsystems, also the velocity and position accuracy of the system will be tested.

11.2 System Validation

The system validation will not be possible during the scope of the DSE project. However the following section will discuss the steps that are necessary to validate the radar system.

After the verification of each subsystem and the full system, the radar system is validated to make sure it meets the requirements set at the beginning of the project (presented in section 2.2). The validation is used to test whether the system can reconstruct the flow field and determine wake boundaries of a wind turbine within the requirements. This is done by placing the radar on a wind turbine, conducting measurements and process the data to generate a flow field and the wake boundaries. The flow field and boundaries generated by the radar will have to be compared to the flow field as generated by a different measurement system to check the validity of the results.

The challenge lies in finding a measurement system that can generate comparable data, at the same moment in time as the radar system. The main candidate would be a LIDAR system, since both techniques are comparable and provide similar results. However, the fact that the radar system is designed to work only during (light) precipitation and LIDAR measurements are distorted by rain, it may be hard to get radar and LIDAR measurements simultaneously. Because of this, the radar system should be validated during the lightest amount of precipitation that still provides sufficient signal to noise ratio to accurately detect the scattered signals. These conditions should be such that LIDAR systems can still provide accurate flow data to be used in the validation.

11.3 Compliance Matrix

Table 11.1 shows the compliance matrix for the designed FMCW radar system. The compliance matrix provides an overview of the mission requirements that the designed system should have met and which

requirements it did actually meet.

Table 11.1: Compliance matrix of the requirements for the T-WRAX system.

Requirement	**Required Value**	**Achieved Value**	**Requirement Achieved?**
Measurement Height	Hub-level	Hub-level	Yes
Measurement Range	500 m	520 m	Yes
Spatial Resolution	10 m	3.3 m	Yes
Sampling rate	0.25 Hz	0.25 Hz	Yes
Continuous Operation Time	12 hours	Depending on precipitation conditions	No
Accuracy	1 m	up to 4 m depending on range	No
Allowable Data Loss	5 %	n.a.	Yes
Cost	less than €100,000	€25,000	Yes
Operation location	Onshore & Offshore	Onshore & Offshore	Yes
Operational range	4–25 m/s	4–25 m/s	Yes
System lifetime	10 years	20 years	Yes
Constraints	No modifications/constructions on the wind turbines	Nacelle mounted system (No intrusion to the load bearing structures of the nacelle)	Partially
Sustainable	Recyclable	Partially	No

As shown in the compliance matrix most of the mission requirements are met or even exceeded. The achieved value on the data loss requirement will be a lot lower than 5 percent although an exact number can not be provided. In theory no data will be lost at all. Practically, data could be lost due to certain design risks as will be discussed in section 11.6. However a few mission requirements are not met entirely. Therefore an explanation will be provided regarding why it is not possible to achieve a radar system that fulfils all mission requirements.

First of all, the mission requirement on the continuous operation time was not met entirely. In theory the radar system can operate continuously for a much longer time than just twelve hours. However, the main drawback of using radar technology for wake field flow visualisation is that light precipitation is needed in order to have detectable targets inside the flow field. Of course, the required conditions in order to measure continuously over a time span of twelve hours do only occur a few times per year in the Netherlands and not even once in some other regions. Therefore, it is suggested to install the radar system for a couple of days to operate until twelve hours of data is acquired.

Further, the requirement on wind turbine modifications and constructions is only met partially. Careful evaluation determined that nacelle mounting is by far the best location to mount the radar system. Multiple reasons for this can be provided. The most important advantages of nacelle mounting are automatic yawing with the wind turbine, hub height measuring without the need of masts placed inside the wake field and the option to power the radar system directly from the wind turbine itself. Meeting the requirement would not outweigh the advantages gained by nacelle mounting. From a meeting with Mr. Schepers[1], it was concluded that neglecting this mission requirement is possible as long as nacelle mounting would not require the wind turbine to be shut down for a substantial time and as long as mounting is at all possible regarding the system's weight and dimensions. The chosen installation design makes use of elements of the nacelle that already exist. These elements - safety rails and a platform are designed to carry loads corresponding to multiple body weights and can support the design. Utilising them requires little to no modifications to the wind turbine structure. Therefore it is considered that the requirement is partially achieved.

Also, the requirement regarding recyclability is not fully met. As for most electrical devices, materials are required that are difficult to recycle. The radar system requires many complex components made from specific materials, including rare earth metals. The biggest component, the radar dish, is usually made from aluminium. This material is easily recyclable. The materials used in the electronic components of the radar system will not all be recyclable, but only small amounts of these materials are required. For the housing of the radar system, it is important that the radar signals are blocked as little as possible, which might limit the possibility of using a recyclable material. A commonly used radome material is fibreglass. Fibreglass is hard to recycle, but recycling methods are being researched. Nevertheless, the electronics will meet the Restriction of Hazardous Substances Directive (RoHS) environmental requirements.

[1] G. Schepers is a research scientist and project coordinator at Energieonderzoek Centrum Nederland (ECN) and a professor in Wind Energy at NHL Hogeschool.

Finally and most importantly, the mission requirement on accuracy has not been met. This is an important requirement since it determines how accurate the wake boundaries can be located in tangential direction and therefore how accurate the wake meandering can be tracked. The achievable accuracy depends on both the beam width and the rotation angle over the length of one chirp. As mentioned in chapter 5, the maximum theoretical accuracy is up to 4 metres. Since the wake is assumed to meander within a range of 3 rotor diameters an accuracy of up to 4 metres would still produce valuable data on the wake meandering effects. However, it is trivial that a more accurate measurement would have been preferable but that is simply not possible using radar technology without decreasing the system performance on other equally important parameters. When designing a radar system trade-offs simply cannot be avoided.

11.4 Sensitivity Analysis

This section presents the results of a sensitivity analysis of the radar system. The analysis is performed in order to get an overview of how the design and operational parameters change if the mission requirements are changed. The requirements considered are range, spatial resolution, accuracy, sampling rate, wind speed, continuous operation time, system life time and measurement height.

Range

This design concept is required to locate the wake boundary over a 520 m distance. If this parameter's value would be changed to 1040 m (for example) the design itself would need to be adapted. Which design specifications need to be changed in order to increase the range of the radar system can be derived from the radar equation. Recall equation equation (5.1) which is re-written as

$$R = \sqrt{\frac{P_t G_t G_r \lambda^2 \theta_t^2 \Delta R}{P_r 512 \ln(2) \pi^2} \eta} \tag{11.1}$$

where R is the measurement range, P_t the transmitted power, G_t and G_r the transmitting and receiving antenna gain, respectively, λ the signal's wavelength, θ_t the beamwidth, ΔR the range resolution, P_r the received power and η the target reflectivity per unit volume. There are several ways to increase the range but not all of them are feasible.

Increasing the power is feasible in small ranges, but quadrupling it would not be possible without completely re-designing the electronics subsystem. Introducing stronger amplifiers may also cause more noise which negatively affects the quality of the received data. The amplifier used in the current design can provide powers of up to 80 W, as opposed to the design's 50 W, which would result in a range increase by a factor of 1.27.

Increasing the antenna gains is a more feasible solution, but requires larger antennas. The antenna gain is related to its diameter D and the signal wavelength as follows:

$$G = \frac{\pi^2 D^2 e_A}{\lambda^2} \tag{11.2}$$

where e_A is the antenna's efficiency factor. Due to the antenna gain's quadratic dependence on its diameter, doubling the diameter of an antenna can result in a doubled range. This, of course, increases the weight and size of the mounting construction required and it should be kept in mind that a bigger antenna means a lower beamwidth. This also negatively affects the maximum range but its effect should be smaller than the increase in range due to the bigger antenna. More importantly, a lower beamwidth increases angular accuracy, but may require a slower rotational rate of the radar dish in order to guarantee the same time on target. A higher time on target is necessary for a sufficient velocity resolution. Therefore, at some point, a trade-off would have to be made between settling with a lower velocity resolution or a worse temporal resolution, that is getting less data points in time of the complete wake. Overall, increasing the antenna size is a more feasible way of increasing the radar's range but it requires several trade-offs and possible hardware changes.

From equation (11.2), we also see that we actually have to decrease the signal wavelength (and increase the frequency) in order to obtain more range, not increase it like equation (11.1) suggests. Decreasing

the wavelength, however, means that, at some point, the scattering behaviour of the signal changes due the relative size to the reflecting precipitation. As the TTUKa shows, it is possible to track precipitation at Ka band frequencies, but it comes with requiring much more expensive hardware.

Increasing the range resolution, that is making it more coarse, can also increase the range. The range resolution is dependent on the reciprocal of the bandwidth, so that would have to be decreased by a factor of 4. The range resolution is currently 3.3 m and it could be increased by a factor of 3 to still meet the spatial resolution requirement. This could make for an increase in range by a factor of 1.73.

In total, the maximum range could be increased by a factor of 2.19 to 1140 m at the cost of a higher power consumption and a lower spatial resolution.

Spatial Resolution

One of the major mission requirements for the radar system is a spatial resolution of 10 m. The range resolution corresponding to this is 3.3 m for our design. If the required resolution became much finer than that, the bandwidth would have to be increased. The currently considered VCO circuit can generate larger frequency sweeps but a larger bandwidth also means a larger noise power and a lower signal to noise ratio. Recalling equation (11.1), this would also decrease the maximum range.

Overall, a more strict requirement on spatial resolution is accounted for as the current range resolution already exceeds the requirement. If an even finer resolution is required, changes could be made at the expense of a lower range and more noisy data.

Accuracy

For this design concept, an accuracy of 1 m is required. A higher accuracy can be achieved by either lowering the beamwidth or by decreasing the speed of the radar dish rotation. This accuracy is depending on the angular accuracy of the radar system. Changing the required accuracy would require a change in the design. Since the angular accuracy is mainly depending on the antenna beamwidth of the FMCW radar system, this beamwidth must be adapted. The beamwidth can easily be adjusted by changing the diameter of the antenna dish. However, changing the dish diameter has a direct effect on the size of the radar device itself. Therefore a better option to increase the angular accuracy of the radar system is to decrease the rotational rate of the system to ensure that more data can be obtained for a more accurate interpolation.

Sampling Rate

The sampling rate for capturing the whole wake is dependent on the rotational speed of the radar dish. Increasing this speed would increase the sampling rate but, at the same time, decrease angular accuracy and the velocity resolution. The designed radar just meets the requirement of a 0.25 Hz sampling rate, so increasing the sampling rate would come at the cost of getting less accurate data.

Wind Speed

The radar system is designed to be able to measure wind speeds in the range of 0–25 m/s in positive and negative radial direction. Higher wind speeds can be measured as well, but it is questionable whether this measurement data is valuable for wind park optimisation. The wind turbine with the highest cut-out speed was found to be *E-126* by Enercon with a cut-out speed of 34 m/s [80].

Continuous Operation Time

Technically, the radar system is capable of achieving a continuous operation time of the required 12 hours. However, the actual continuous operation time is limited by the times during which the system receives power from a wind turbine and during which precipitation is present.

System Life Time

Generally, a system life time of 20 years is assumed for FMCW radar systems. This is twice the time that is initially required. Therefore, minor changes in the required system life time will not affect this

design concept at all. If a system life time of even more than 20 years would be required, chances are that worn-out system components need to be replaced at some point. However, the cost of such a replacement is low compared to the overall system cost.

Measurement Height

The radar system itself can only measure in horizontal direction at hub height. If the hub height changes due to the radar system being mounted on a wind turbine smaller or larger than the considered reference wind turbine, minor considerations have to be made.

Clutter due to the ground or sea is a general problem. If the radar is situated closer to the ground, those clutter echoes become stronger and may influence the maximum range and precipitation the radar is able to detect. That is, weaker signal reflections become more difficult to detect if the clutter becomes too strong, so precipitation further away or otherwise not reflective enough will not be detectable. It is difficult to say at which point this happens exactly, so it is something that should be further investigated.

Conversely, the effect of ground clutter diminishes if the radar is mounted on a wind turbine with a higher hub location.

11.5 Environmental Sensitivity

Since the radar system requires fog or precipitation to be able to perform measurements it is dependent on the environment and weather for its operation. For fog, a thick fog layer is required with a minimum reflectivity of -28 dBZ. Precipitation will always have a higher reflectivity than this, but the reflectivity should not be too extreme, to prevent receiver saturation. The sensitivity of the system will be treated for three conditions: onshore in the Netherlands, offshore near the Netherlands and in other geographical locations. An estimation of the validity of precipitation measurements will also be given.

11.5.1 Onshore

In onshore conditions in the Netherlands, thick fog with a visibility of less than 100 m occurs for about 12 days per year, or 3.3 % of the time [81]. Precipitation occurs in the Netherlands for 7.5 % of the time [82], which makes the average available measurement time for the radar system 10.8 % for onshore wind turbines.

11.5.2 Offshore

For offshore locations very little climate information is available. Exact numbers of the available measurement time can therefore not be given. However, since offshore wind farms are usually relatively close to land, it can be assumed that the available measurement time offshore will be the same as the available measurement time onshore.

11.5.3 Other Geographical Locations

Since fog and rain have a large effect on the ability of the system to acquire measurements the local climate has a large effect on the usability of the system. Countries with a wet sea climate are the best location for the radar system. These climates have a large percentage of rain time, but usually without extreme cases of rainfall. Fog is also common in these climates. Tropical climates will likely suffice, since rain is also common in these climates. Fog however does not occur often here. In dry land climates, found for example in the middle-south of the US, the middle east and many other inland locations, rain is so rare that it might be unfeasible to perform measurements in these locations.

11.5.4 Precipitation Measurements Validity

For measurements during precipitation the measured velocities by the radar system are not the actual velocities of the flow, but the velocities of the precipitation. Especially larger raindrops will not follow the flow perfectly. It can however be assumed that the velocity component of the raindrops in the horizontal

plane follows the flow to a large extent. In personal communication Dr. L. Schroeder[2] mentioned that '...we've done significant validation work w.r.t. a 200 m tower onsite and have found things line up exceedingly well.' Dr. O. A. Krasnov[3] confirmed these foundings during a personal meeting, the PARSAX radar team from the TU Delft has the same experience. However, if the precipitation velocity does not match the actual flow velocity this should not be a problem. The radar system finds the wake boundaries by finding the velocity difference between the freestream flow and the wake flow. If the precipitation has for example a 10 % lower horizontal velocity component the velocity difference will still be at the same location, which gives the same wake boundary location results.

11.6 Risk Analysis

In order to keep track of the risk associated with the operation of the FMCW radar system, the following section will provide a technical risk analysis. The corresponding risk map can be found in table 11.2. This risk map classifies specific undesired events in terms of probability of occurrence (vertical axis) and consequence severity (horizontal axis).

General Performance Issues

- **GP1** - *Due to Turbine Tower Vibrations.* One scenario that has to be analysed is if the tower's vibrations due to wind loads is strong enough to disturb the Doppler effect measurements. This would make flow velocity measurements highly unreliable. Additional literature study on this subject revealed that for a reference turbine with a hub height of 60 m the maximum hub displacement is 11.1 cm and the maximum hub acceleration is $0.063g$ [51]. Therefore, the measurement errors for wind speeds between 4 m/s and 25 m/s are negligible.
- **GP2** - *Due to low tangential resolution at long range.* Another risk that must be evaluated is the possibility of not being able to detect meandering at long range due to a low tangential resolution. As discussed in section 11.3 the tangential resolution can go up to 4 meters which means that low amplitude meandering might not be noticable at long range. However, due to continuous measuring the probability of this scenario is very small.

Electronics Subsystem Issues

- **E1** - *Due to lightning strike.* The possibility of lightning strikes must be accounted for since the removal time of the system is too long to protect it from certain incoming weather conditions. It is possible that the lightning conducting capabilities of a wind turbine are not good enough to prevent the radar system from getting damaged.
- **E2** - *Due to radio Interference.* If another radio transmitter, for communications or radar purposes, transmits in the vicinity of the radar system, it might cause interference. However, this risk is limited since the dish antenna has a small beamwidth in which it can receive signals. If the interfering signal comes from a different direction than the direction in which the dish is pointing, it will not be received by the radar system. Since it is safe to assume that there will be no other radio transmitters at hub height, let alone transmitting in the direction of the radar system, this risk can be regarded as low.
- **E3** - *Due to receiver saturation.* If the reflectivity of the observed wake is much higher than usual, for example during heavy precipitation or when a large reflecting device is placed somewhere in the wake, the receiver can saturate. This means that the power put in the receiver is higher than the receiver amplifiers can handle, which could result in damage to the receiver chain. A simple way of reducing this risk is by using components in the electronic system with a selectable gain, to reduce the system sensitivity when that is required.

[2]Dr. John L. Schroeder is a research scientist at the Texas Technical University. He is the Director of the National Wind Institute and a Professor of Atmospheric Science. On Monday, the 9th of June, Daniël Bakker had e-mail contact with him regarding experiences with the TTUKa radar system.

[3]Dr. Oleg Krasnov is a research scientist from the TU Delft institute IRCTR and an expert on radar systems.

- **E4** - *Due to insufficient protection from the atmosphere.* The radar system is expected to operate in humid conditions which poses the risk that the electronics corrode or short circuit due to moisture. The housing of the electronics subsystem should prevent this from happening but the risk remains because the system is assumed to be left unattended for extended periods of time.

Mechanical Subsystem Issues

- **M1** - *Due to the radome vibrations* The wind loading on the radome will cause vibration of the radome. These vibrations might introduce some noise to the measurements. Furthermore, if vibration become extreme, radome structures might be damaged putting the radar in danger.
- **M2** - *Due to storm conditions* If the windspeed exceeds the maximum windspeed the radome might be damaged. In the upward position if the radome/nacelle connection is broken the radar will tip over and likely fall. In case of the radar mounted underneath the nacelle the radome will have lower drag coefficient. Thus the maximum allowed windspeed is higher. Yet if it is reached the radome will fail and the radar will fall.
- **M3** - *Due to the OEM warranty agreements* If the manufacturer withdraws its warranty due to the radar installation the customer might be unwilling to use it. Note however that the radar installation was made such that intrusion to the wind turbine is minimal.
- **M4** - *Due to the rotation system malfunctioning* If the rotation system malfunctions the radar will not be able to complete sweeps as intended. Then the data will be corrupted and would require some additional post-processing to obtain some useful data.

Data Processing Risk

- **DP1** - *Due to residual noise signal content* If the chosen low-pass filter, the window function, clutter suppression or noise clipping fails there will be unremoved noise signal content within the range-Doppler matrices. In the worst case this could lead to noise which is higher than the actual target reflection, thus making an accurate wake boundary determination impossible. Since the algorithms are quite simple the risk of an algorithm failure is small, the risk mainly stems from calibration errors and therefore is reduced by more carefully calibrating the data processing subsystems.
- **DP2** - *Due to inappropriate smoothing* When smoothing will be performed in a wrong way, for instance averaging over too many or too less cells, the spectrum could not be as desired. For instance too much smoothing can significantly reduce the velocity resolution, making accurate detection of the wake boundary impossible. Not enough smoothing leads to an increased noise content of the velocity which might lead to erroneous velocity determination and gaussian fitting. This risk stems from errors in the calibration which are resolved by calibrating more carefully.
- **DP3** - *Due to hardware requirements* If the requirements on hardware such as data storage capacity and computational power will actually be higher than expected the data processing could not be performed as it should. In the case of a too low storage capacity data will have to be discarded, which reduces the potential of the system. Since the data storage capacity is quite cheap a large safety factor can be used, reducing this risk. If the computational power requirement is not met the system can not keep up with the data that comes in, which results in either discarded data or a system failure. However, the workstation that is used provides a large enough margin to reduce this risk to a minimum (see section 8.12).
- **DP4** - *Due to low received signal power* If the reflectivity of the atmosphere is too low the received signal power could be too low to distinguish noise from peaks corresponding to targets in the range-Doppler matrices, resulting in insufficient data for wake boundary determination. To reduce this effect the processing of the data has to be adapted to reduce the noise even more, which will result in a lower resolution. If this does not provide usable data the data should be discarded and the radar should wait for a more intense precipitation event to measure. This risk is inherent to the nature of the radar system since it is dependent on sufficient precipitation to operate.

Table 11.2: Risk Map for the radar system design concept.

Consequence probability					
	Very high				
	High				
	Moderate			DP4,M3	
	Low	GP1	M1	E1	M2
	Very low		E2,DP2,M4	GP2,E3,E4 DP1,DP3	
		Negligible	Marginal	Critical	Catastrophic
		Consequence severity			

12 | Economic analysis

The economic analysis chapter first presents a cost analysis of production, operation, and logistics of T-WRAX in section 12.1. The analysis is made using off-the-shelf component prices, and estimates that are explained in the text. With section 12.2, the chapter continues and ends with a discussion of the existing market for wake visualisation devices and the role that radar has in this market.

12.1 Cost Analysis

The total cost of producing the system is estimated to be €24,324. This is split into an estimated component cost of €17,924, an estimated software cost of €4,000 and an estimated assembly cost of €2,400. The breakdown of those costs for the subsystems are given in this section. A cost estimate for operation of the system is not given yet.

12.1.1 Radar Dishes

The reference radar dishes, as selected in chapter 5, cost €67 and €309 respectively. This is however for a normal offset antenna type, not a gregorian offset antenna. The additional reflector in the gregorian setup will add some cost, so the actual antennas are assumed to cost €90 and €400.

12.1.2 Mechanical Subsystem

The mechanical subsystem consist of a rotatable positioner for the antennas, a radome which surrounds the antennas, hydraulic legs and a base block for the electronics housing which also connects all the parts.

The price of four *Enerpac RC-59* hydraulic legs is €1,535 [83]. The price of the *ORBIT FR AL-260-1* antenna rotation positioner is estimated at €1,000. To mount the system ropes are used, the price of an 80 m 8X19S rope is €65 [84].

The radome production is relatively complicated process. Although the material costs are low, the manufacturing costs are rather high. However, using historical data it can be stated that the price depends on the area of the dish [85]. At the reference radius of 3 m—the height of the radome—the radome cost is estimated in 20–25 % of the total radar price. The cost of the remaining system, including assembly, is €18,243. Using the estimate of 25 %, the radome cost is estimated to be €6,081. This makes for a total component cost of €8,681.

For assembly, we assume that four mechanics working for 3 days and 8 hours per day at an hourly wage of €20 are required, resulting in an assembly cost of €1,920. This includes mounting the dishes and fitting the module housing the electronics and data processing subsystem. The total cost of materials for the mechanical subsystem as well as assembly of those and components of the other subsystems is then €10,601.

12.1.3 Electronics Subsystem

The electronics subsystem has been designed to consist if off-the-shelf components. Table 12.1 shows the individual cost of each component of the subsystem and the total, which amounts to €7,953.

For most of the components, price data has been gathered from the electronics distributor Digi-Key's website [86]. Some components have price data listed directly from the manufacturer and for some components, a price has been estimated based on similar components available. It should also be noted that the prices listed of all components, if applicable, are for prototyping boards that provide the circuitry ready to be connected with each other using coaxial cables. The chips themselves are usually at least 10 times cheaper which should be considered in case of potential bulk production of this system.

Table 12.1: Cost-breakdown of the electronics subsystem components.

Unit type	**Unit name**	**Amount**	**Price per unit [€]**
VCO	HMC778LP6CE [60]	1	750
Power divider	1G0618-20 [61]	1	329
Power amplifier	AML618P4014 [62]	1	(estimate) 500
Attenuator	BW-S50W2+ [64]	1	67
LNA	AMF-6F-09001100-09-10P [65]	1	(estimate) 446
I/Q demodulator	EVAL01-HMC1056LP4B [66]	1	500
Low-pass filter	N/A [67]	2	105
LF amplifier	ZHL-6A+ [63]	2	147
Data acquisition	AD9650-25EBZ [68]	1	150
Control processor	EVMK2H [59]	1	740
Weather determination	miniPWS [71]	1	1,167
Rotation motor system	HBS57, HBSMd [70]	1	250
Power management	N/A	1	(estimate) 1,000
Data processing	Lenovo Thinkstation S30 [72]	1	1,550
Total			7,953

The housing of the subsystem is assumed to cost another €300 and cables and other materials €200. Furthermore, for the assembly and testing of the system, we assume that the work of three electricians and mechanics is required for 8 hours, receiving an hourly wage of €20, resulting in another €480. The subsystems total cost for components, assembly and testing is therefore assumed to be €8,933.

12.1.4 Data Processing Subsystem

The software performing the real-time processing as well as post-processing must be written or bought from a third party software company. The cost of such software is estimated to be €4,000. The hard drives required are estimated to be another €300, making for a total of €4,300.

12.1.5 System Operation

It is difficult to estimate the cost of the system operation (as well as the logistics of getting it mounted on a wind turbine). Since the system is assumed to obtain power from a wind turbine, it is up to the user to negotiate this with the operator of the wind turbine. This also includes the cost of having to shut down the wind turbine for mounting the radar system.

12.2 Existing Market

The existing market for velocity field visualisation for wind farm optimisation has largely headed one direction, namely LIDAR. The current main competitor is SODAR, an acoustic remote sensing technology. Interesting however is the fact that using radar for optimising wind farms was first considered in 2009 by the National Wind Institute of the Texas Technical University. This different perspective lead to a radar system called TTUKa which successfully tracked a wind turbine wake over 30 rotor diameters in October 2011.

LIDAR is a remote sensing technology that works very similar to that of radar. Instead of radio waves LIDAR measures distance and velocity by illuminating the target object with a laser and analysing the reflected light. This leads to highly accurate measurements that can be obtained even in clear air conditions. The downside of this technology however is the rather low range of up to 2500 m and the high cost in the order of €100,000 for the simplest version with an even lower range in the order of 300 m.

SODAR, the main competitor of LIDAR in the current market is an acoustic remote sensing technology. While SODAR is a less expensive technology that is capable of visualising a velocity flow field from distance it does have some major drawbacks. First of all, acoustic energy decreases quadratically with distance

which limits the range of measurement with a decent signal to noise ratio. Increasing the transmitted power is limited since the transmitted tones are in theaudible range. Therefore a measurement range of only 300 metres can be achieved. SODAR is also relatively inaccurate due to the large measurement volumes.

Interestingly, radar is never seriously considered for the purpose of visualising the wake field behind a wind turbine. However, recent experiments using the TTUKa radar system showed that when correctly optimised radar can accurately visualise a flow field over a range of more than 5 kilometres. Therefore the wake field of an entire wind plant could be visualised at once. The only drawback of using this technology is that light precipitation is required in order to receive a signal strong enough to be detected.

To determine the reason radar technology has been neglected for wake field flow visualisation, Dr. L. Schroeder[1] was addressed regarding his point of view on this subject. In his opinion the industry is headed in LIDAR's direction without fair consideration of the alternative. He thinks there is tremendous opportunity to alter the industry and promote wind plant optimisation through radar technology, measurements and associated techniques. Further, Dr. L. Schroeder fears the industry is 'sensitive' when it comes to radar given the interference issues faced in some areas. In this sense, radar gets a 'bad' reputation in the industry. With that said, radar artifacts are a real issue and have to be dealt with when compiling the complex flow measurements, but the work performed by the National Wind Institute of Texas has shown this can be done in almost all cases.

To conclude, it is our expectation that in the near future radar and associated techniques will be used more and more for the purpose of wake field flow visualisation for wind farm optimisation. Already, numerous successful field tests have been performed showing accurate measurement results over an impressive range.

[1]Dr. John L. Schroeder is a research scientist at the Texas Technical University. He is the Director of the National Wind Institute and a Professor of Atmospheric Science. On Monday, the 2nd of June, Daniël Bakker had e-mail contact with him regarding the reason why radar technology is still never seriously considered for the purpose of wake field flow visualisation, even after the success of the TTUKa radar.

13 | Future Design Development and Integration

Finalising the radar device and implementing it in a field test in the future will require several intermediate steps. In this chapter an overview is given of how to proceed after this report to complete the design and construction of the radar system. First, section 13.1 presents the diagram of the Project Design & Development (PD&D) logic in figures 13.1 and 13.2 to show the order of activities to be done. Afterwards the activities are elaborated on, in the following order: the finalisation of the design, production & assembly, configuration of the system, customisation of the logistics and operation. These theoretical future activities will be chronologically ordered in the Gantt chart in section 13.2 and appendix A. The sustainable strategy for the final radar system is then described in section 13.3 and lastly recommendations for further research are given in section 13.4.

13.1 Post-DSE Design and Development Logic

The additional steps to finalise the radar design and implement it can be logically illustrated using a PD&D logic diagram, which has been split in two, in figure 13.1 and figure 13.2. The blocks represent different activities that will need to be performed and the arrows indicate the order in which this is done. Note that some activities are performed in parallel, some are inter-dependent and others still are done iteratively.

13.1.1 Finalise Detailed Design

Finalisation of the system's design involves finalising all subsystem designs, as well as designing the operations and logistics. The final subsystems design and total system design are made through an iterative process. It is important to note that while performing these iterations, it will be necessary to produce prototypes and test to check design choices and assumptions. They may also need to be modified to pass verification and validation tests. Some of the subsystems will also be dependent on each other, such as the signal power loss of the radome design (mechanical subsystem) being dependent on the required transmitted power (electronic subsystem). Therefore entire design will also have to be prototyped, tested and iterated if required, as can be seen by the red arrow in the PD&D logic diagram 13.1. Finally, the output should be a final design that is ready for production.

Electronic Subsystem

All components for the electronic subsystem have been selected, except for the power supply. It is likely that this part needs to be designed specifically for the radar system to interface with the power from the wind turbine. This design is outside the scope of this research, which means that it must be performed after the DSE. The exact power and voltage requirements of all radar components must be used to size the power supply. The selected electronic subsystems should be a good choice for the function that they need to perform, but the functionality of the combination of the components must first be verified. For this tests are required. Specific parts of the electronic design, such as the amplifier chain, can be assembled and its performance can be measured, such as the actual gain and the total noise figure. The calculations from the power budget should be verified by measurements. The performance characteristics of the complete system can be partially tested by verification, but some characteristics, such as the accuracy, must be validated using the completed system. The proposed development steps for all components are:

- Power supply: the design of the power supply must be made and its functionality verified by measurements.

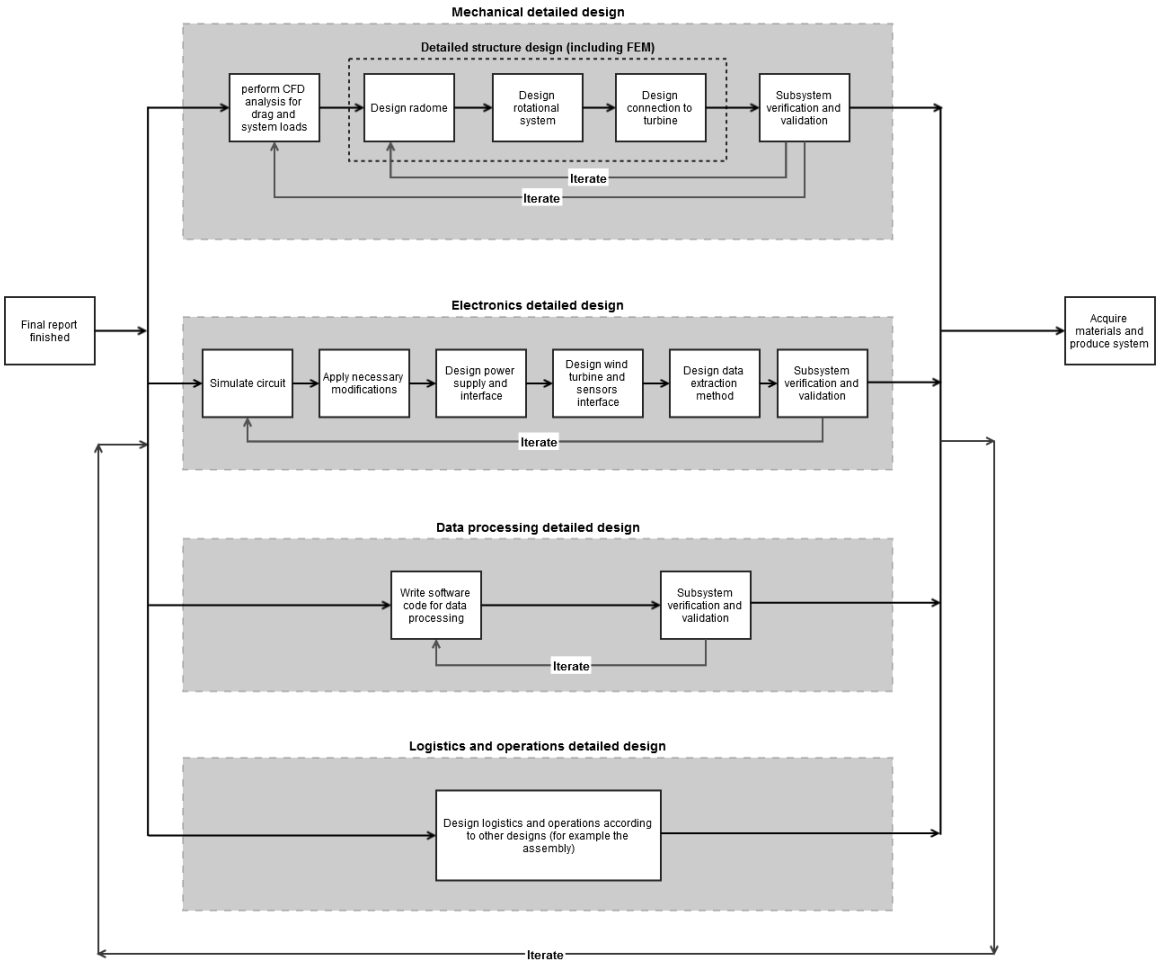

Figure 13.1: Project design and development logic (detailed design).

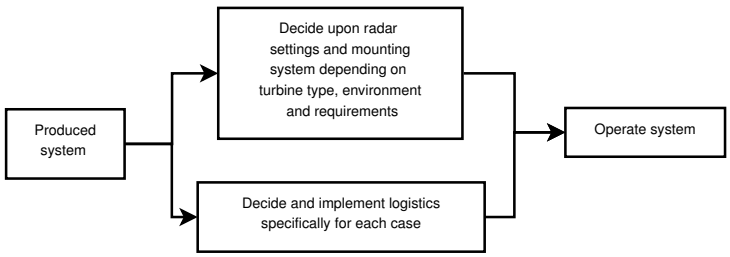

Figure 13.2: Project design and development logic (case specific configuration).

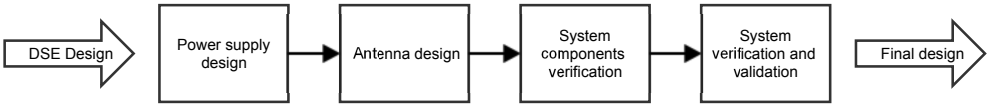

Figure 13.3: Post-DSE design logic for the electronic system.

- Amplifiers: their performance must be verified by measurements and especially the characteristics of the combinations of amplifiers and filters or other components must be measured.
- I/Q demodulator: its performance characteristics should be measured, especially in combination with the other components.
- VCO: the performance of the VCO should be verified, especially for the modulation waveforms used in the radar system.
- Weather conditions measurement: the accuracy of the weather measurement system should be verified.
- Antenna rotation: the accuracy of the antenna rotation system is important for the performance of the radar system. This accuracy must therefore be verified.
- Antennas: the antennas are not designed yet. For the best system performance a customised antenna design is required. To design an antenna system, the initial design will be sized using analytical equations. Using a finite element simulation this design can then be improved. As a last step, this simulation result can be validated with actual measurements.

After the verification of the functionality of the individual electronic components or combinations of components it is likely that small design changes will be necessary. After these changes have been implemented the complete electronic system can be assembled and the functionality of the complete system can be verified by measurements. Once the electronic system works properly the complete radar system can be assembled, to perform the full system verification and validation. This will most likely again result in modifications to the electronic system, so after it has been improved the development of the electronic subsystem is finished. An overview of the post-DSE steps in the electronic design is given in figure 13.3.

Data Processing Subsystem

The general layout of the data processing has been discussed in chapter 8. Post-DSE procedures start with choosing and obtaining software to use for the data processing. This includes picking an FFT algorithm

The second step is verifying the data processing subsystem as outlined in section 8.11. This will ensure that the system performs as intended and system requirements are met.

The final step is calibrating the data processing processes (chapter 8), which is necessary before the system can be validated. This includes calibrating the amount of filtering of the low-pass filter, the amount of smoothing done by the moving average and the noise-clipping threshold. Calibration has to be performed while the radar is on-site, placed on top of the turbine. To optimise performance the radar can be calibrated each time it is placed on a new location or wind turbine. Following the calibration is the validation of the entire radar system.

Mechanical Subsystem

The general post-DSE guideline of the mechanical subsystem is drawn in figure 13.4. The requirements on the electromagnetic properties of the radome must be refined with respect to aimed power loss, sidelobe sizes and boresight shift. Then the layout of the radome can be optimised to meet those requirements. The new layout then should be processed in CFD in order to obtain precise stresses on the radome. On

basis of those stresses a detailed FEM analysis should be made in order to determine the required skin dimensions. Then these dimensions are fed back to the electromagnetic calculations and the whole process is repeated until the optimum design is achieved. Then the design can be verified and validated.

There are some additional substeps that are not shown in the general guideline. It is important to catalogue the various wind turbine dimensions, allowable stresses and wind regimes for correct CFD calculations as well as for connection interfaces sizing. Note that the antenna used in current design has a general parabolic shape but it should be adjusted to represent an offset antenna. The same holds for the radome layout. The radome wall material should be analysed in more detail to ensure that the chosen materials fit the design requirements best. Further one needs to incorporate the bonding material properties to the FEM analysis. It is likely that the stochastic wind regimes will result in differential loading on the radome. Therefore the vibration of the subsystem will also need to be analysed for the final design. Additionally a hydrophobic coating needs to chosen to ensure that there is no reflection due to a water film on the radome outer skin.

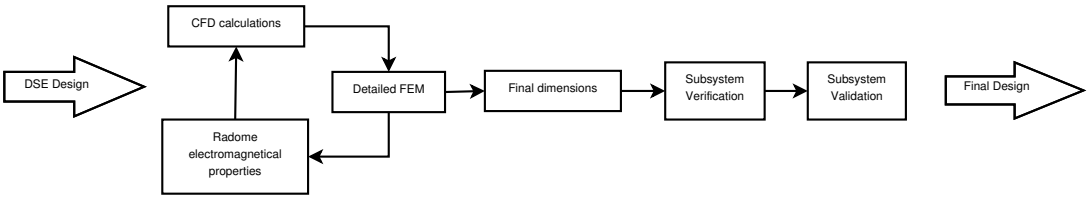

Figure 13.4: Post-DSE work guideline for mechanical subsystem.

13.1.2 Acquire Materials & Produce System

If the design is finalised and tested, a full working prototype may be produced for a field test. Firstly, the materials will need to be acquired and inventoried. The production will then have to be planned, if it is not outsourced to a third party, and a suitable workshop must be found. The steps to be taken in the future for production are divided into two sections, the electronic subsystem production and the mechanical subsystem production.

Acquire Materials

The materials required for production include off-the-shelf components, tools and raw materials. They will also have to be delivered to the workshop on time and will have to be inventoried to ensure everything required for production is available.

Electronic production

The electronic system consists almost entirely of off-the-shelf components, where production therefore is not relevant. An exception however is the power supply. Since it must, at least partially, be custom designed it must also be custom produced. Assuming that the radar system will only be made in quantities of a few units at most, prototype production techniques will be used. This means that the Printed Circuit Board (PCB) can be factory produced, but the soldering of the electronic components will be done manually. The assembly of the electronic system is also a manual process. All modules must be fixed in the electronics housing and connected to each other. Power must be supplied to all components. This is all in all not a complicated process.

Mechanical production

After the final specifications are established the production plan and assembly methods can be set. The potential production methods for the A-sandwich are [87]:

- Wet lay-up
- Prepreg lay-up

- Adhesive bonding
- Liquid moulding
  - Resin transfer moulding
  - Structural reaction injection moulding
  - Vacuum Injection moulding

At the current stage it is expected that the radome wall layout might be optimised towards inhouse manufacturing capabilities. The antenna positioner and hydraulic legs are off-the-shelf components. The base block will be optimised for the radome, positioner and legs connections outside the block and the electronic housing inside the block. The assembly of the mechanical system is a manual process. The electronic housing shall be mounted inside the base block. The antenna, positioner, radome and legs shall be bolted to each other. The connection between the electronics and the antenna feeder will be made. For the attachment of the radar under the nacelle, ropes are used; they can be easily obtained off-the-shelf [84].

13.1.3 Case-specific Configuration

If a wind turbine has been designated for the device's usage, the subsystems need to be configured to perform optimally for that specific turbine. The system's configuration can vary with the wind turbine's location, the weather conditions and the size and shape of the nacelle.

Mechanical Subsystem Configuration

Of the subsystems, the mechanical subsystem's configuration will vary the most between cases. The wind turbine used in the given case will have to be analysed to determine which of the two installations explained in section 6.7, on top or under the nacelle, is appropriate. Depending on the installation, it will also need to be outfitted and configured for being attached with ropes, and the leg lengths will have to be configured for the appropriate elevation angle. The effect of inclining the radar on the swath has not been fully explored, and therefore the optimal elevation angle will have to be found experimentally in the future. Depending if the wind turbine is off- or onshore, and its height, the system will also have to be outfitted appropriately for being hoisted up onto the nacelle depending on the chosen method for lifting it in logistics. Any other necessary structural and mechanical aspects will need to be configured at this stage, keeping in mind that safety regulations will need to be met.

Electronic Subsystem Configuration

If the velocity, temporal, and spatial resolution requirements change, the variable radar characteristics of the electronics subsystem can be modified to meet them and optimise the system's performance. How these variable characteristics are selected is mostly understood and has been explained in section 5.4.2, but the optimal configuration for the electronic subsystems has not been tested as it does not fall under the scope of this project. However the radar has been designed such that it should be able to take measurements for any free-stream velocity in the range of 4–25 m/s up to a range of 520 m. Optimising the configuration and studying how it can vary based on, for example, weather conditions should be done at this activity block after production.

Data Processing Subsystem Configuration

For data processing, only the noise level and signature are relevant case-specific variables. Depending on the environment of the wind turbine, the undesired reflected signals will have different levels and be at different frequencies. At this stage, testing and calibration will have to be done to select appropriate filters and noise clipping levels, so that noise is minimised without compromising the returned atmospheric signal.

13.1.4 Customise Logistics

With the exception of the installation type (under or on top of nacelle), the logistics of implementing the radar system may be performed parallel to deciding the system's configuration. Depending on the location of the wind turbine, several logistical issues will need to be considered and designed for, The transportation from storage to the wind turbine site will need to be considered. Accessibility issues include the existence of roads and their quality for onshore transport, and chartering and navigation of boats for offshore transport. The same applies for removal of the system and bringing it back to a storage location. The nacelle will also have to be analysed to determine the most appropriate mounting technique. Hiring and transport of the corresponding installation mechanics will also have to be considered. Ensuring a power source for the system's approximately 1800 W, as determined in section 7.2.12, will also require some logistic planning and will depend on the case-specific turbine. Under these considerations, and other problems that may arise in the future, the logistics of implementing bringing the produced radar system from storage to the wind turbine will have to be designed and implemented.

13.1.5 Operate System

Once the system is installed, the system will be operated. It will operate autonomously once it is initialised, and will transmit and receive signals when it detects a sufficient amount of precipitation. It will potentially have the capability of being remotely controlled, to manually control its operation times and configurations, should they need to change.

13.2 Gantt Chart

Should T-WRAX's design be taken to a final design, production, and operation stage, an estimated schedule can be created for the post-DSE activities. The non-case-specific activities of the PD&D logic have been chronologically presented in a Gantt chart which can be found in appendix A. If T-WRAX has been designated for a specific turbine, the measurement start and end dates can not be estimated because they are completely dependent on the research preferences. Therefore the schedule ends after T-WRAX is produced.

As mentioned, the start and end dates of the activities are estimated, and may vary greatly, for reasons including but not limited to faulty components, logistical challenges and clients wishes. Post final report activities that will be done before the end of the DSE are also included in the Gantt chart.

13.3 Sustainable Strategy

The following section will present the sustainable development strategy. Both the sustainability in the design and the way the system contributes to sustainability will be taken into account. The sustainability of the design is split up in two parts, regarding the sustainability of the production and operation respectively.

13.3.1 Sustainability in Production

The production of the designed radar system is probably the least sustainable part of the radars lifecycle. As mentioned in section 11.3 for most electrical devices, materials are required that are difficult to recycle. Not all the materials used in the electronic components of the radar system will be recylable, but only small amounts of these materials are required. Nevertheless, it will be ensured that the electronics will meet the RoHS environmental requirements. The amount of mechanical components is limited to the rotating antenna dish on which only small loads act. It is therefore simple to design this component such that its lifetime meets or exceeds the ten years product life requirements. Because of the simplicity of the mechanical part of the radar system, designing the rotating system such that broken components are quickly and easily replaceable should be possible. For the housing of the radar system, it is important that the radar signals are blocked as little as possible, which might limit the possibility of using a recyclable material. A commonly used radome material is fibreglass. Fibreglass is hard to recycle, but recycling methods are currently being researched. To conclude, using unsustainable materials when producing an

FMCW radar system is unavoidable. However, the extent of this matter can be brought to a minimum by only using these materials if more sustainable options are not available.

13.3.2 Sustainability in Operation

The operation part of the systems lifecycle is much more sustainable. Radar is a remote sensing technology which means that a radar system can visualise the turbine wake flow field from a distance without inserting any material into the environment. Further the designed radar system is a FMCW radar which has much lower power requirements than regular pulsed radar systems. The most power consuming part of the system will likely be the computer system used for post-processing which, using modern computer technology, can also be limited. Furthermore, in case of failure, the radar system poses no environmental hazards. Also, the required power is directly provided by the wind turbine itself in the form of electrical energy. Radar is a durable and easily maintainable system. Since the power requirements for the electronics are relatively low, a lifetime of ten years is certainly feasible. The electronic system consists of many individual modules; in case one of the modules becomes defective, it can be replaced without having to replace the complete system. Therefore it can be concluded that the operation of the designed radar system is very sustainable.

13.3.3 Contribution to Sustainability

In terms of contribution to sustainability the designed radar system would do an important job. Of course, contributing to sustainability is one of the main tasks that the system fulfils. The radar system can be used to optimise wind farms by visualising the wake boundary location and movement. Ultimately this could lead to a more efficient wind farm in terms of both energy production and wind turbine design. Due to a better understanding of the wind turbine wake field boundaries and the meandering effects the fatigue loads on downstream wind turbines can be decreased. Improving the efficiency of a wind farm by just one percent would be a huge improvement in terms of sustainability.

13.4 Recommendations

In this section recommendations will be given for further research. These recommendations will be split up in recommendations relevant for electronic design, mechanical design and data processing.

13.4.1 Electronic Design Recommendations

During the design of the electronic system a few assumptions were made that should be investigated in further detail. The required antenna isolation between the transmitter and receiver antennas is high. Without designing the antennas in detail it is nearly impossible to know how hard it is to achieve this isolation. It might be necessary to place shrouds around the antennas to improve the isolation, this should be investigated in further detail. It might also happen in real life that the received signal strength is stronger than what the receiver chain can handle. This will lead to receiver saturation which in extreme cases can lead to damage to the receiver chain. To prevent this from happening it might be wise to use one or multiple components in the radar system with a switchable gain. If for example the power amplifier can be set at different gain levels the transmitted power can simply be lowered during times where the echo strength is high, for example during heavy precipitation.

13.4.2 Mechanical Design Recommendations

To improve the mechanical design, additional analysis of the aerodynamics around the nacelle should be done. If the maximum stream-wise and crosswind velocities on top and under the nacelle are known, the structural design can be adjusted to the maximum loads.

Additional analysis on the height differences on the underside of the nacelle can be used to improve the design of the legs. The rotation positioner and radome size are based on a parabolic antenna, possible corrections should be made for an offset antenna. The wind turbine vibrations should be investigated, based on this the mechanical design should be checked for structural strength. Another issue that should

be addressed is the centre of gravity of the system. Currently the centre of the gravity of the design is above the rope connection. This makes the installation potentially unstable. This problem however is easy to solve by moving the centre of gravity under the rope connection. In order to do so a small weight should be suspended on a rope of considerable length. For instance a point weight of 3 kg at a distance of 6 m is sufficient.

Further it is recommended to discuss clamping possibilities with potential customers and OEMs. A better understanding of warranty restrictions is necessary to make correct design choices. Additionally the power supply cable requires a hatch in the base block. Positioning of such hatch depends on layout of the electronics in the base block and can be made in the final stage of the design.

13.4.3 Data Processing Recommendations

This radar system relies on precipitation in the turbine wake to obtain flow velocity information. Also, it is assumed for locating the wake boundary that precipitation in the air follows the air flow. This assumption has been confirmed as a valid assumption by external experts in section 11.5, but the influence of this assumption on the measured wake boundary locations should be investigated using actual measurements. Because operating in a wind farm has the potential to be very clutter intensive (reflections of other wind turbines) clutter suppression is very important. Another very reliable way of clutter and artifacts suppression is using polarimetric filtering techniques [39]. These advanced techniques use differently polarised signals which can be used to differentiate between reflections from precipitation, other objects and even artifacts coming from the radar system itself. Future research should focus on the cost associated with making the radar system capable of performing this kind of filtering. This would include the increase in hardware costs and computational/storage requirements. The increase in cost and data quality could then be put in a trade-off to determine if such a system would be feasible.

14 | Conclusion

In this report the design of the wake boundary measurement system is discussed. Resulting from previous work, the selected measurement technique is radar. Using basic radar equations the preliminary sizing of this radar system is done. It is found that, amongst others, the radar system will at least require thick fog or drizzle to operate, heavier precipitation types will also work. Using these preliminary sizing results, the detailed designs of the mechanical and electrical subsystems are made. It is found that these designs will meet the performance estimations established in the preliminary design. The algorithms used in the data processing of the radar measurements are also described in detail. Some results are that the radar system will have a mass of 130 kg, it will be mounted on top or below the wind turbine nacelle, it can measure during fog or precipitation and it will be able to locate the wake boundaries over 500 m with an estimated accuracy of 4 m. The total power usage is 1.9 kW.

In the simulation and the system evaluation, a further analysis of the usability of the system is made. The simulation suggests that the radar measurements are suitable for determining the wake boundary locations. The radar system meets the requirements well, the only requirements that are not met are the continuous operating time and the accuracy requirements. This does, however, not affect the usability of the radar system. A change in requirements will only have small effects on the system design and usability. A limit on this research is that practical measurements and tests are not possible. The verification and validation must therefore be performed at a later time. A description of the required verification and validation steps is however given.

In the analysis of the existing market, it is found that radar is not commonly used for wake measurements. From the cost analysis of the wake measuring radar system it is clear that radar is a financially very interesting alternative to existing measurement techniques such as Laser Imaging Detection And Ranging (LIDAR) or Sonic Detection And Ranging (SODAR). The estimated cost for a prototype radar system is €25,000. Radar can also complement these techniques since those techniques can not function during precipitation, while radar requires it. The radar system is slightly polluting during production and disposal due to the usage of some specific materials that are hard to recycle, but the usage of the system is energy efficient and does not require consumables.

During this design study, some aspects of the design were deemed out of scope for the current project and simplified with assumptions. In further research, the effect of these simplifications should be investigated, practical measurements on the performance of individual system components and the full system should be made and some additional features might have to be added. In general, before the radar system can be built and put on a wind turbine, it should first be designed in greater detail. The current design, however, already is of sufficient detail to draw important conclusions. Radar is a technology that can measure the wake of a wind turbine and can track the meandering of this wake with sufficient detail, but for a significantly lower price than for existing technologies. This study gives a detailed analysis on the feasibility of radar for this purpose and it is expected that this study can be used as a solid basis for further work in this field.

Bibliography

[1] J. Melkert. *Design / synthesis exercise*. Presentation Slides.

[2] Vestas. *2 MW Platform*. Vestas Wind Systems A/S. 2013. URL: http://nozebra.ipapercms.dk/Vestas/Communication/Productbrochure/2MWbrochure/2MWProductBrochure/.

[3] L. E. M. Lignarolo et al. "Experimental analysis of the wake of a horizontal-axis wind-turbine model". in press, to be available online on 24 February 2014 in "Renewable Energy".

[4] G. S. Settles. *Schlieren and Shadowgraph Techniques*. Second Edition. Springer, 2006.

[5] A. Mazumdar. *Principles and Techniques of Schlieren Imaging Systems*. 2013-06-18.

[6] H. Breyer et al. *The measurement of velocity gradients in fluid flow by laser light scattering*. 1993.

[7] J. Derksen and W. van de Water. *Light scattering off Brownian particles in shear flow*. 1989-04-14.

[8] H. Tezuka et al. *Field Application Development of Super-Long-Range PIV System by using Cassegrain Telescope*. 2004.

[9] H. Johari and W. W. Durgin. "Direct measurement of circulation using ultrasound". In: *Experiments in Fluids* 25.5-6 (1998), pp. 445–454.

[10] K. Rogers and A. Finn. "Three-Dimensional UAV-Based Atmospheric Tomography." In: *Journal of Atmospheric & Oceanic Technology* 30.2 (2013).

[11] B. D. Hirth et al. "Measuring a Utility-Scale Turbine Wake Using the TTUKa Mobile Research Radars". In: *Journal of Atmospheric and Oceanic Technology* 29 (2012), pp. 765–771.

[12] D. Bakker et al. "Wind Turbine Wake Visualisation - Mid-Term Report. Design of a system to measure the wake boundaries of a wind turbine and keep track of wake meandering". 2014-05-22.

[13] D. Medici and P. H. Alfredsson. "Measurements on a Wind Turbine Wake: 3D Effects and Bluff Body Vortex Shedding". In: *Wind Energy* 9 (2005-05), pp. 219–236.

[14] *Clear air Radar Scatterers*. Website. URL: http://www.atmos.washington.edu/~justin/radar_project/clearair.htm (visited on 2014-06-16).

[15] ISIS. *ISIS Small Ground Station Datasheet*. 2013. URL: http://www.isispace.nl/brochures/ISIS.GS.DS.v13.7%20Data%20Sheet%20Gound%20Station-1.pdf.

[16] N. Timmer, M. Zaaijer, and J. de Bakker. *AE3W02TU - Introduction to Wind Energy*. University Lecture. 2013.

[17] L. J. Vermeer. *A Review of Wind Turbine Wake Research at TU Delft*. A01-16944. 2001.

[18] J. F. Manwell, J. G. McGowan, and A. L. Rogers. *Wind Energy Explained: Theory, Design and Appl*. John Wiley & Sons Ltd., 2009.

[19] S. Lynum. "Wind Turbine Wake Meandering". MA thesis. Norwegian University of Science and Technology Trondheim, 2013-06.

[20] B. Sanderse. *Aerodynamics of wind turbine wakes. Literature Review*. ECN-E–09-016. 2009.

[21] F. Bingöl, G. C. Larsen, and J. Mann. "Wake Meandering - An Analysis of Instantaneous 2D Laser Measurements". In: *Journal of Physics: Conference Series 75* (2007).

[22] Z. Yang, P. Sarkar, and H. Hu. *An Experimental Investigation on the Wake Characteristics of a Wind Turbine in an Atmospheric Boundary Layer Wind*. 2011.

[23] D. Medici and P. H. Alfredsson. "Measurements on a Wind Turbine Wake: Further Evidence of Wake Meandering". In: *Wind Energy* 10 (2007-10), pp. 211–217.

[24] G. España, S. Aubrun-Sanches, and P. Devinant. "The Meandering phenomenon of a Wind Turbine Wake". In: *European Wind Energy Conference and Exhibition, Marseille* (2009).

[25] W. Bierbooms. *Project Guide Design Synthesis Exercise - Wind Turbine Wake Visualisation*. Tech. rep. Delft University of Technology, 2014.

[26] M. I. Skolnik. *Introduction to Radar Systems*. Third Edition. McGraw-Hill Companies, Inc., 2001.

[27] C. Wolff. *radartutorial*. website. URL: http://www.radartutorial.eu/ (visited on 2014-05-08).

[28] R. Rauber. *ATMS410 course slides—Weather Radar Equation*. Department of Atmospheric Sciences, University of Illinois, 2014.

[29] J. R. Probert-Jones. *The radar equation in meteorology*. 1962.

[30] Desktop Doppler. *NWS NEXRAD*. Website. URL: http://www.desktopdoppler.com/help/nws-nexrad.htm#rainfall%20rates (visited on 2014-06-11).

[31] Hyper Physics. *Blue Sky and Rayleigh Scattering*. URL: http://hyperphysics.phy-astr.gsu.edu/hbase/atmos/blusky.html (visited on 2014-06-11).

[32] H. Ottersten. "Atmospheric structure and radar backscattering in air". In: *Radio Science* 4.12 (1969-08-06), pp. 1179–1193.

[33] Texas Tech University. *Ka-band Mobile Doppler Radar Trucks*. Website. 2014-03-10. URL: http://www.depts.ttu.edu/nwi/facilities/ka-band-radar.php (visited on 2014-06-11).

[34] Texas Tech University. *Measuring the Complex Flows Found in Wind Plants*. Website. 2014-05-19. URL: http://www.depts.ttu.edu/nwi/research/radar-research/index.php (visited on 2014-06-11).

[35] M. A. Harral, Z. Long, and N. Marathe. "The Wake Effect: Impacting turbine siting agreements". In: *North American Clean Energy* (2013).

[36] *PARSAX radar examines development and lifespan of water droplets in clouds*. Website. URL: http://www.stw.nl/en/content/parsax-radar-examines-development-and-lifespan-water-droplets-clouds (visited on 2014-06-15).

[37] O. Krasnov et al. *PARSAX: Polarimetric Agile Radar in S- and X-band — new generation of polarimetric radar*. Presentation Slides. Delft University of Technology, 2009-10-29.

[38] *Parsax*. Website. URL: http://www.tudelft.nl/en/research/irctr/research/radar/research-projects/parsax/ (visited on 2014-06-15).

[39] J. Figueras i Ventura. "Design of a High Resolution X-band Doppler Polarimetric Weather Radar". Dissertation. Delft University of Technology, 2009-10-08.

[40] Delft University of Technology. *Near-Realtime Reflectivity Measurements of IDRA*. Website. URL: http://ftp.tudelft.nl/TUDelft/irctr-rse/idra/index.html (visited on 2014-06-11).

[41] I. S. Kostadinova. "An UHF Frequency-Modulated Continuous Wave Wind Profiler - Development and Initial Results". Thesis. University of Massachusetts - Amherst, 2014-02.

[42] H. R. Anderson. *Fixed Broadband WirelessSystem Design*. Wiley, 2003. ISBN: 9780470861288. URL: http://books.google.nl/books?id=r-o3SmNsvD8C.

[43] *Parabolic reflector antennas*. Website. 2012-10-31. URL: http://www.microwaves101.com/encyclopedia/antennadish.cfm (visited on 2014-06-10).

[44] *Frequency-Modulated Continuous-Wave Radar (FM-CW Radar)*. Website. 2014. URL: http://www.radartutorial.eu/02.basics/Frequency%20Modulated%20Continuous%20Wave%20Radar.en.html (visited on 2014-06-12).

[45] R. Boers et al. *Ground-based Radar Observations of Visibility in a Radiation Fog Layer*. 2012.

[46] D. I. L. de Villiers. *Analytical Prediction of Feed Efficiency in Offset Gregorian Reflector Antennas with Non Planar Log-periodic Type Feeds*. 2011.

[47] *Offset gregorian dish antenna*. Website. 2014. URL: http://www.smtconsultancies.co.uk/workdone/dogreg/g2o.GIF (visited on 2014-06-15).

[48] *Satellite Dish - ANTENNA*. Website. 2014. URL: http://satellitedish.com/cata0052.htm (visited on 2014-06-14).

[49] *True Focus V-Sat Antennas*. Website. 2014. URL: http://www.anderseninc.com/satellite/kuoffset.pdf (visited on 2014-06-14).

[50] Global Navigation Systems. *Standard Parabolic Antennas*. Global Navigation Systems. 2014.

[51] C. van der Woude. *A Study on Vibration Isolation in a Wind Turbine Subjected to Wind and Seismic Loading*. 2011.

[52] M. Jelavic, N. Peric, and I. Petrovic. "Damping of wind turbine tower oscillations through rotor speed control". In: (2007).

[53] S. F. Hoerner. *Fluid-dynamic drag*. Sighard F. Hoerner, 1965.

[54] Aero-electronic technology department. *Ka-band Radome Design*. 1969-05-20.

[55] *Fundamental and Technical Review of Radomes*. Website. 2008-05-01. URL: http://www.mpdigest.com/issue/articles/2008/may/mfg/default.asp (visited on 2014-06-06).

[56] R. H. Cary. *Avionoc Radome Materials*. 1974.

[57] *Elevator ropes from BRUGG LIFTING*. Website. URL: http://www.brugglifting.com/elevator-ropes/index.php/en/ropes/traction-ropes (visited on 2014-06-06).

[58] Enerpac. *Enerpac Hydraulic Cylinders*. Website. URL: http://www.enerpac.com/en/industrial-tools/hydraulic-cylinders-jacks-lifting-products-and-systems/general-purpose-hydraulic-cylinders/rc-series-single-acting-hydraulic-cylinders (visited on 2014-06-13).

[59] *66AK2Hx Evaluation Modules*. Website. 2014. URL: http://www.ti.com/tool/evmk2h (visited on 2014-05-14).

[60] Hittite Microwave Corporation. *HMC778LP6CE*. 2014. URL: https://www.hittite.com/content/documents/data_sheet/hmc778lp6c.pdf.

[61] Anaren. *Model 1G0618-20*. 2014. URL: http://www.anaren.com/sites/default/files/1G0618-20.pdf.

[62] Microsemi Corporation. *AML618P4014*. URL: http://www.microsemi.com/existing-parts/parts/127614?catid=1509#overview (visited on 2014-06-13).

[63] Mini-Circuits. *ZHL-6A+*. 2014. URL: http://217.34.103.131/pdfs/ZHL-6A+.pdf.

[64] Mini-Circuits. *BW-S50W2+*. 2014. URL: http://217.34.103.131/pdfs/BW-S50W2+.pdf.

[65] Miteq. *AMF Amplifier Products*. 2014. URL: http://miteq.com/docs/C23C.PDF.

[66] *EVAL01-HMC1056LP4B*. Website. 2014. URL: http://www.digikey.com/product-search/en?FV=fff40036,fff802bc,fffc0467&k=HMC1056LP4BE (visited on 2014-06-12).

[67] *1 MHz Low Pass Filter*. Website. 2014. URL: http://www.kiwa.com/LPF3.html (visited on 2014-06-12).

[68] *AD9650 Evaluation Board*. Website. 2014. URL: http://www.analog.com/en/analog-to-digital-converters/ad-converters/ad9650/products/EVAL-AD9650/eb.html (visited on 2014-06-13).

[69] *Noise Figure of ADC*. Website. 2011-11-23. URL: http://a2d2ic.wordpress.com/2011/11/23/noise-figure-of-adc/ (visited on 2014-06-13).

[70] Damen CNC. *NEMA 23 Closed Loop Stepper Systems*. Website. 2014. URL: http://damencnc.com/nl/componenten/motoren-en-aansturingen/closed-loop-stepper-systems/544 (visited on 2014-06-13).

[71] *Mini PWS*. Website. 2013. URL: http://www.opticalsensors.se/MiniPWS.html (visited on 2014-06-14).

[72] *ThinkStation S30*. Website. 2014. URL: https://www.bluelink.nl/product/RFCB6MH (visited on 2014-05-15).

[73] *Window function*. Website. 2014-06-09. URL: http://en.wikipedia.org/wiki/Window_function (visited on 2014-06-18).

[74] *FM/CW RADAR SIGNALS AND DIGITAL PROCESSING*. National Oceanic and Atmospheric Administration, 1973-07.

[75] Windcat. *Windcat Workboats*. Website. URL: http://www.windcatworkboats.com/#/fleet/ (visited on 2014-06-16).

[76] J. Chu and J. L. Sullivan. "Recyclability of a Continuous E-Glass Fibre Reinforced Polycarbonate Composite". In: *Polymer Composites* 17.4 (1996).

[77] M. Suzuki et al. "Method for recycling a cured phenolic resin into a molded article and a vacuum thermal insulator of the molded article". Pat. US6013684 A. 2000-01-12.

[78] S. Lynum. "Validation of wind turbine wake models". MA thesis. Delft University of Technology, 2007.

[79] *Phased Array System Toolbox - MATLAB - MathWorks Benelux*. Website. 2014. URL: http://www.mathworks.nl/products/phased-array/ (visited on 2014-06-18).

[80] Enercon. *E-126 / 7,580 kW*. Website. URL: http://www.enercon.de/en-en/66.htm (visited on 2014-06-17).

[81] *Mist en nevel zijn de afgelopen 30 jaar sterk afgenomen*. Website. 2009. URL: http://www.knmi.nl/cms/content/69838/mist_en_nevel_zijn_de_afgelopen_30_jaar_sterk_afgenomen (visited on 2014-06-17).

[82] *Neerslagduur*. Website. 2013. URL: http://www.knmi.nl/cms/content/24936/neerslagduur (visited on 2014-06-17).

[83] Hyjacks. *Hydraulic jacks*. Website. URL: http://www.hyjacks.com/espring.htm (visited on 2014-06-17).

[84] *Elevator ropes price for 8X19S*. Website. URL: http://www.alibaba.com/product-detail/Elevator-steel-ropes-8X19S_220353898.html?s=p (visited on 2014-06-16).

[85] *Radome Capabilities*. Website. URL: http://www.radome.net/rad_cap.html#initial (visited on 2014-06-16).

[86] Digi-Key. *DigiKey Electronics*. Website. URL: http://www.digikey.com/ (visited on 2014-06-15).

[87] K. F. Karlsson and B. T. Astrom. "Manufacturing and applications of structural sandwich components". In: *Composites* 28A (1997), pp. 97–111.

Appendices

A | Post DSE Gantt Chart

	Name	Duration	% Complete	Start	Finish	Predecessors
1	Final report	2d	100%	19/06/2014	20/06/2014	
2	Jury summary	1d?	100%	20/06/2014	23/06/2014	
3	Poster design	3d	0%	25/06/2014	27/06/2014	1,2
4	**Final review**	**4d?**	**0%**	**23/06/2014**	**27/06/2014**	**1,2**
5	Prepare for presentation	3d	0%	23/06/2014	26/06/2014	
6	Practice run	1d?	0%	25/06/2014	25/06/2014	
7	Presentation	1d?	0%	26/06/2014	27/06/2014	5,6
8	**Symposium**	**5d?**	**0%**	**27/06/2014**	**04/07/2014**	**4**
9	Prepare symposium	3d?	0%	27/06/2014	02/07/2014	
10	Practice run	1d?	0%	02/07/2014	03/07/2014	9
11	Presentation	1d?	0%	03/07/2014	04/07/2014	10
12	Executive summary	2d?	0%	01/07/2014	02/07/2014	1,2,4
13	**Detailed design (including prototyping and testing)**	**150d?**	**0%**	**04/07/2014**	**30/01/2015**	**8**
14	Mechanical detailed design	150d?	0%	04/07/2014	30/01/2015	
15	Electronics detailed design	150d?	0%	04/07/2014	30/01/2015	
16	Data processing detailed design	150d?	0%	04/07/2014	30/01/2015	
17	Logistics and operations detailed design	144d?	0%	14/07/2014	30/01/2015	
18	**Acquire materials and produce system**	**22d?**	**0%**	**30/01/2015**	**03/03/2015**	**13**
19	Acquire materials and off the shelf components	7d?	0%	30/01/2015	10/02/2015	
20	Build Electronic subsystem and power supply	2d?	0%	10/02/2015	12/02/2015	19
21	Build mechanical components	5d?	0%	10/02/2015	17/02/2015	19
22	Assemble and test	10d?	0%	17/02/2015	03/03/2015	20,21

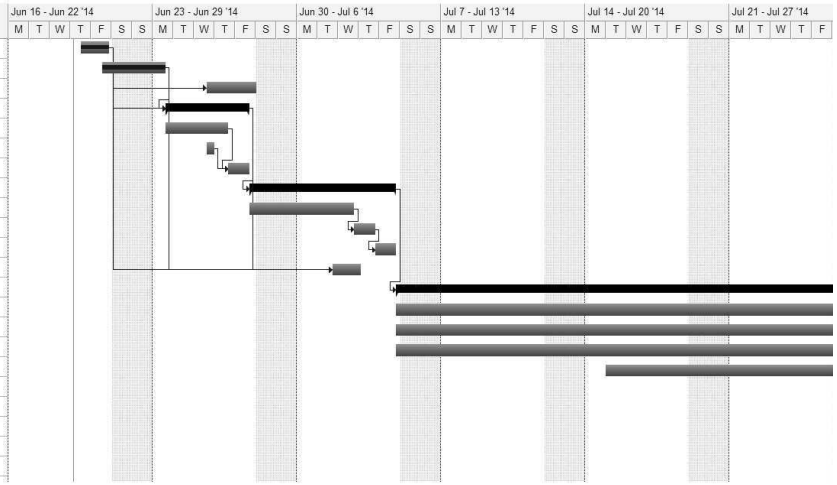

Figure A.1: Post DSE Gantt chart part 1.

	Name	Duration	% Complete	Start	Finish	Predecessors
1	Final report	2d	100%	19/06/2014	20/06/2014	
2	Jury summary	1d?	100%	20/06/2014	23/06/2014	
3	Poster design	3d	0%	25/06/2014	27/06/2014	1,2
4	**Final review**	**4d?**	**0%**	**23/06/2014**	**27/06/2014**	**1,2**
5	Prepare for presentation	3d	0%	23/06/2014	26/06/2014	
6	Practice run	1d?	0%	25/06/2014	25/06/2014	
7	Presentation	1d?	0%	26/06/2014	27/06/2014	5,6
8	**Symposium**	**5d?**	**0%**	**27/06/2014**	**04/07/2014**	**4**
9	Prepare symposium	3d?	0%	27/06/2014	02/07/2014	
10	Practice run	1d?	0%	02/07/2014	03/07/2014	9
11	Presentation	1d?	0%	03/07/2014	04/07/2014	10
12	Executive summary	2d?	0%	01/07/2014	02/07/2014	1,2,4
13	**Detailed design (including prototyping and testing)**	**150d?**	**0%**	**04/07/2014**	**30/01/2015**	**8**
14	Mechanical detailed design	150d?	0%	04/07/2014	30/01/2015	
15	Electronics detailed design	150d?	0%	04/07/2014	30/01/2015	
16	Data processing detailed design	150d?	0%	04/07/2014	30/01/2015	
17	Logistics and operations detailed design	144d?	0%	14/07/2014	30/01/2015	
18	**Acquire materials and produce system**	**22d?**	**0%**	**30/01/2015**	**03/03/2015**	**13**
19	Acquire materials and off the shelf components	7d?	0%	30/01/2015	10/02/2015	
20	Build Electronic subsystem and power supply	2d?	0%	10/02/2015	12/02/2015	19
21	Build mechanical components	5d?	0%	10/02/2015	17/02/2015	19
22	Assemble and test	10d?	0%	17/02/2015	03/03/2015	20,21

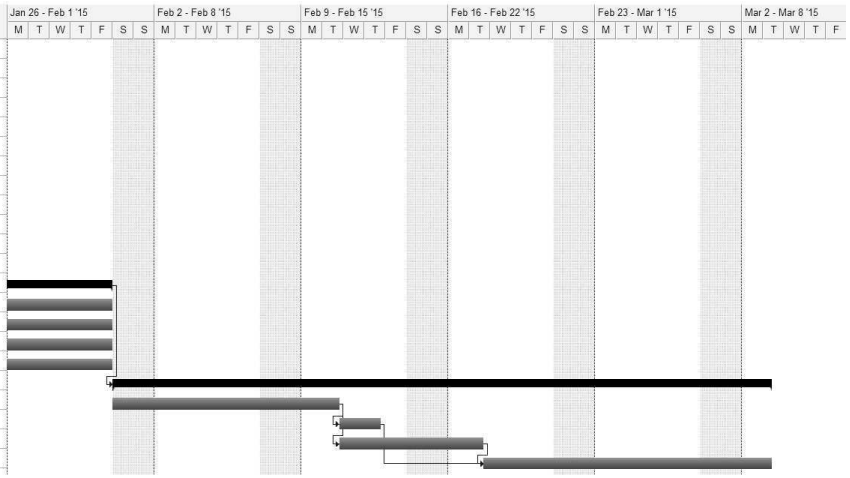

Figure A.2: Post DSE Gantt chart part 2.

B | Design Specifications Summary

This appendix contains the table summarising the specifications of Turbine Wake RAdar in X-band (T-WRAX). It also contains a technical drawing of T-WRAX on the next page.

Antenna characteristics	
Antenna efficiency	0.75
Receiver noise figure	0.9
Transmitter power	50 W / 47 dBm
Receiver power	−145 dBm
Transmitter/Receiver power ratio	−192 dB
SNR — all gains	9.8 dB
Sweep range	90°
Rotational rate	22.5 °/s
Half-power beamwidth	1.4°
Maximum beamwidth	12.2 m
Minimum target reflectivity factor	−28 dBZ
Signal specifications	
Waveform	Sawtooth
Carrier frequency	10 GHz
Bandwidth	45 MHz
Range and resolution	
Maximum range	520 m
Blind range	50 m
Range resolution	3.3 m
Velocity resolution	0.781 m/s
Tangential resolution	4 m
Data processing	
Measurement integration period	19.2 ms
Computational power (FFT+filter)	52.66 GFLOPS
Data storage required capacity	1 TB
Number of samples per chirp	256
Number of chirps per integration period	64
Physical specifications	
Mass — radome	30 kg
Mass — rope (operations)	2.4 kg
Mass — legs	10 kg
Mass — payload	90 kg
Number of dishes	2
Transmitting dish diameter	1.5 m
Receiving dish diameter	0.6 m
Radome height	2.745 m
Leg length	32.3–55.5 cm
General specifications	
Total production cost estimate	€24,324
Total power usage	1860 W
Mass — total	132.4 kg

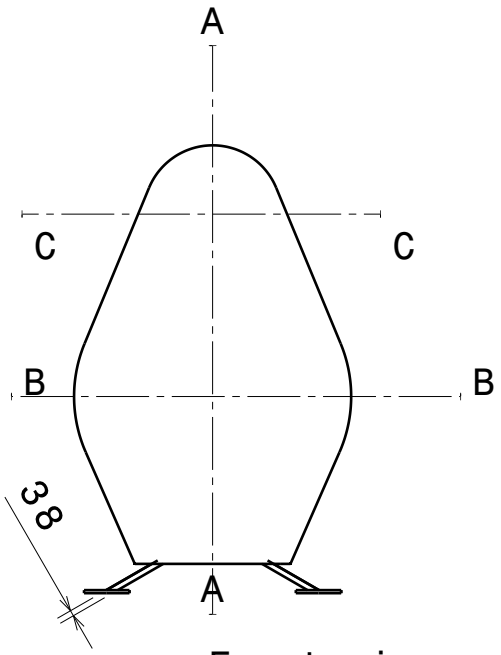

Front view
Scale: 1:50

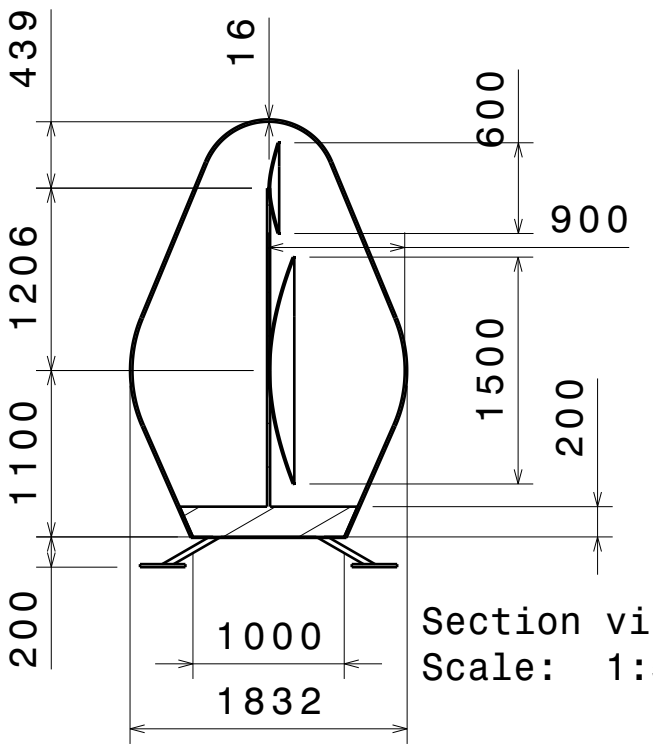

Section view A-A
Scale: 1:50

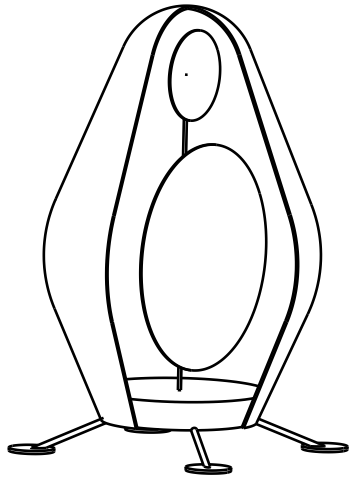

Isometric view
Scale: 1:50

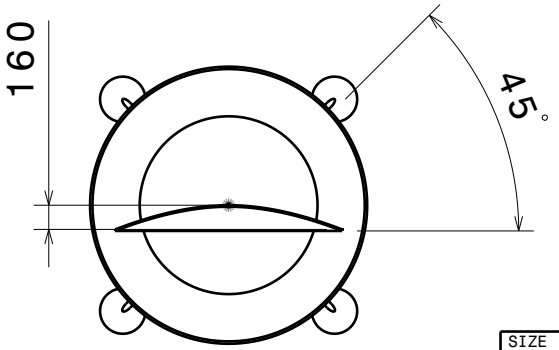

Section view B-B
Scale: 1:50

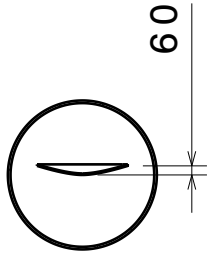

Section view C-C
Scale: 1:50

SIZE			Designed by
A4		T-WRAX	Date DSE Group 1 18-06-2014
SCALE	WEIGHT (kg)	DRAWING NUMBER	SHEET
1:50	132.4	Full system drawing	1/1